Assessment of Bio-jet Fuel Production through Alcohol-to-Jet Pathways from Lignocellulosic Biomass

By

Nusrat Fatema Nayan

A thesis submitted in partial fulfillment of the requirements for the degree of

Master of Science

in

Engineering management

Department of Mechanical Engineering

University of Alberta

Abstract

The aviation industry worldwide consumes approximately 1.5–1.7 billion barrels/year of conventional jet and 140 million litres/year of bio-jet fuel and it has been estimated that commercial aviation has contributed approximately 2-6% to global carbon emissions. Biomass-derived jet (bio-jet) fuel may be a promising solution for the aviation industry because of the fuel's potential to reduce CO_2 emissions over its life cycle. Bio-jet from edible, non-edible food crops and lignocellulosic biomasses compete with the cultivable lands, but algae-based biomass does not. When bio-jet fuel sourced from algae is used for aviation, GHG emissions can be reduced significantly relative to the conventional jet fuel. However, extensive research, development, and demonstration are being conducted to produce renewable jet fuels from a variety of feedstocks and pathways.

This thesis is focused on opportunities to produce alternative jet fuel components from different alcohols (the alcohol-to-jet [AJT] pathway). It also provides a brief overview of other conversion technologies (the oil-to-jet [OTJ], sugar-to-jet [STJ], and gas-to-jet [GTJ] pathways). The ATJ pathway consists of processes that convert platform alcohol molecules to an alternative jet fuel blend stock through catalytic reactions historically used by the petrochemical industry. For this study, a literature review was conducted for different alcohols and associated production processes. Further, selected variations of all the process pathways were evaluated.

For this study, process models were developed for ethanol-to-jet production processes. Techno-economic assessment was conducted. In addition, five scenarios, each with two cases were assessed. In Case 1 for all five scenarios, feedstock ethanol and hydrogen were sourced from an upstream process of a 2000 dry tonnes/day^{--1} production plant (using spruce wood chips). In Case 2, merchant ethanol was used. Two additional single-case scenarios were developed using n-butanol and isobutanol as feedstocks. In the best-case scenario, bio-jet production costs were \$1.43/kg (\$0.94/L) with a final yield of 47%. To understand the differences in bio-jet fuel production costs at different capacities, a wide range of production capacities (from 48 to 12,000 tonnes day^{-1}) was considered, and associated scale factors were developed for the individual units and the overall plants. The optimal size at which the cost of production is lowest is 12,000 dry tonnes/day^{-1} (50,000 kg/hr). With increasing capacity, feedstock cost significantly increases, while the capital cost per unit output decreases. The scale factor was determined through the developed process and techno-economic models for the overall plants, major units, and equipment.

A sensitivity analysis was conducted to estimate the impact of various process parameters on the final cost of bio-jet fuel. The results indicate that production cost is most sensitive to feedstock cost, followed by the plant lifetime, discount rate, and capital cost. A Monte Carlo simulation was used to assess a change the production cost of bio-jet fuel and generate mean and most likely prices for Cases 1 and 2 in both the base and best-case scenarios at a 95% confidence level.

The aviation industry is mainly interested in high-quality bio-jet fuel as it is nearly carbon neutral and could help provide energy independence. In short, low-carbon fuels are seen as both attractive and beneficial.

Dedication

Throughout the boundaries of a human capacity, I want to dedicate all my tiny efforts to continuous learning, striving to enlighten myself. The endless story of such a journey has been challenging, navigating through the chronicles of conflicts, yet the outcome should remain steadfast – a commitment to make a positive impact!

Impact on what? Air, water, and soil, from the north to the middle to the south of planet Earth! It seems there is no sun; maybe hope. I want to quote from Palestine's national poet:

"The war will end,

The leaders will shake hands,

The old woman will keep waiting for her martyred son,

The girl will wait for her beloved husband,

And those children will wait for their hero father,

I don't know who sold our homeland,

But I saw who paid the price" - Mahamoud Darwish

But the question is – when will the war end???

Acknowledgment

I express my sincere gratitude to Professor Amit Kumar, my supervisor, for his unwavering support during the unprecedented challenges of the pandemic. His unconditional support has been invaluable, and I am truly thankful for his guidance and encouragement. I want to add the NSERC/Cenovus/Alberta Innovates Associate Industrial Research Chair in Energy and Environmental Systems Engineering and the Cenovus Energy Endowed Chair in Environmental Engineering for providing financial support for this project. I extend my heartfelt gratitude to Dr. Maryam Akbari, Dr. Abhishek Dwivedi, and Dr. Olufemi Oni for their continuous support and technical guidance. Additionally, special thanks to Astrid Blodgett for her meticulous editing of this thesis. Finally, I would like to express my earnest appreciation to all my friends, colleagues, staff, and well-wishers.

Table of Contents

List of Figures

List of Tables

List of Acronyms

ABE - Acetone-butanol-ethanol

AC - Activated carbon

AFRL, US - Air Force Research Laboratory, US

AHFS - Ammonium hexa-fluorosilicate

AISAF - Australian Initiative for Sustainable Aviation Fuels

APR - Aqueous phase reforming

APEA – Aspen Process Economic Analyzer

ASTM - American Society for Testing Materials

ATJ - Alcohol-to-jet

BOCLE - Ball-on-Cylinder Lubricity Evaluator

BP - Boiling Point

CAAFI - Commercial Aviation Alternative Fuels Initiative

CAPEX - Capital expenditure

CLEEN - Continuous Lower Energy, Emissions, and Noise

CH - Catalytic hydro-thermolysis

C-HAP - Carbonated hydroxyapatite

COP - Cost of production

DEE - Diethyl ether (DEE)

DME - Dimethyl ether

DLA - Defense Logistics Agency

DSHC - Direct sugar-to-hydrocarbons

DFSTJ - Direct fermentation of sugar-to-jet

DTPA - Dodeca-tungstophosphoric acid

EDC - Ethylene dichloride

EU - European Union

FFAs - Free fatty acids

FAA - Federal Aviation Administration

FRL - Fuel readiness level

FT - Fischer-Tropsch

GIFT - Gevo Integrated Fermentation Technology

GHSV - Gas hourly space velocity

GTJ - Gas-to-jet

HEFA - Hydrotreated esters of fatty acids

HRJ - Hydro-processing renewable jet

HDO - Hydrodeoxygenation

HEFA - Hydrotreated esters of fatty acids

HRJ - Hydro-processing renewable jet

HSAG - High surface area graphite

HSBC - Hongkong and Shanghai Banking Corporation

IATA - International Air Transport Association

ICAO - International Civil Aviation Organization

ICI - Imperial Chemical Industries

INEOS - INspec Ethylene Oxide and Specialties

IRR - Internal Rate of Return

JFTOT - Jet fuel thermal oxidation testing

KOH - Potassium Hydroxide

LCA - Life cycle analysis

LHSV - Liquid hourly space velocity

MAO - Methyl-aluminoxane

MJ - Megajoule

MLY - Mega liter per year

MMT - Mega tonnes

MMT - Mega million tonnes

MPA - Molybdophosphoric acid

MLT-DTL - Military Details

MLT-T - Military Technology

NAWCWD - Navy/Naval Air Warfare Center Weapons Division

NCGs - Non-condensable gases

NER - Net energy ratio

NM - Not mentioned

NISA - Nordic Initiative for Sustainable Aviation

NREL - National Renewable Energy Laboratory

ODT - Oven Dry tonnes

OPEX - Operational expenditure

OTJ - Oil-to-jet

PNNL - Pacific Northwest National Laboratory

PSA - Pressure swing adsorption

RPM - Rotations per minute

RUST - Regression, Uncertainty, and Sensitivity Tool

SAPO - Si-Al-phosphate

SHOP - Shell higher olefin process

SIP - Synthesized iso-paraffins

SPA - Solid phosphoric acid

STA - Silicotungstic acid

STJ - Sugar-to-jet

TBD - To be determined

THF - Tetrahydrofuran

TPA - Tungstophosphoric acid

TRL - Technology readiness level

UCC - Union Carbide Corporation

USAF - United States Air Force

USEPA - US Environmental Protection Agency

WHSV - Weight hourly space velocity

ZSM-5 - Zeolite Socony Mobile-5

Chapter 1. Introduction

1.1 Background

In recent decades, the adverse impact of indiscriminate greenhouse gas (GHG) emissions have been observed through global warming which is a cause of climate change. The increase in global temperature has resulted in polar ice cap melting, weather pattern changes, and possibly the extinction of some animal species, etc. [1, 2]. CO_2 is the most important contributor to global warming among GHGs and accounted for 79% of the total greenhouse gas emissions in 2018, according to US Environmental Protection Agency (USEPA) [2, 3]. Atmospheric CO_2 levels increased by 2.2% annually between 2005 and 2021 [2, 4-6].

The aviation sector is a contributor to global warming through GHG emissions such as carbon dioxide (CO_2), hydrocarbons (HC), water vapor (H_2O), nitrogen oxides (NO_x or $NO + NO_2$), carbon monoxide (CO), sulfur oxides (SO_x), and nonvolatile black carbon (BC) or soot [7, 8]. The total CO_2 emissions from this sector account for approximately 4% of global GHG emissions and are expected to grow by around 4-5% per year [9, 10]. Since 1940, when it is thought that actual aviation travel began, GHG emissions from this sector have risen consistently and are predicted to keep growing [11]. According to the International Civil Aviation Organization (ICAO), if it remains unchecked (i.e., in the absence of any additional measures by 2050), GHG emissions could grow by over 300%, which would amount to about 43 metric gigatons of carbon dioxide because of the industry's continued expansion [1, 11, 12].

1.2 Technological progress

Research on bio-jet fuel started around 1960, and interest has grown steadily. Several review papers have been published on bio-jet or alternative aviation fuel production [13-19]. In 2016, Wang et al. reviewed scientific advancements in bio-jet fuel production and categorized them into four broad pathways: oil-to-jet (OTJ), alcohol-to-jet (ATJ), gas-to-jet (GTJ), and sugar-to-jet (STJ) [13]. In addition to the production pathways, Wang et al. comprehensively reviewed development of bio-refinery concepts, the industrial chain from the airplane manufacturer, ongoing R&D, the environmental impact of bio-aviation fuel, distribution, policy-making, and airline strategies in 2019 [17]. In a subsequent paper, Wang and Tao discussed each pathway in terms of conceptual process, design, and process economics, as well as through the life cycle analysis of GHG emissions [18]. Mawhood et al. also published a review paper in 2016 in which they cataloged the development and manufacturing efforts of six renewable jet fuel production pathways by evaluating their technological and commercial maturity [15]. Like Wang et al., Mawhood et al. determined the fuel readiness level (FRL) of different initiatives and partnerships in the aviation industry through a rapid evidence assessment [15, 18]. Gutiérrez-Antonio et al. published an overview of scientific and technological developments in 2017 regarding the available pathways for producing bio-jet fuel [1]. In 2018, Richter et al. published a review paper on alternative aviation fuels that highlights different pathways according to reaction chemistry along with the combustion properties of the produced jet fuel [16]. That same year, Wei et al. reviewed aviation biofuels by mapping the general outline of conversion technologies based on lignocellulosic and other carbohydrate-based materials [20]. Wei et al. and Why et al. focused on aspects related to economic assessment, environmental influence, the challenges and opportunities the aviation industry faces, and the development status of bio-jet fuels [19, 20]. Also in 2019, these authors reviewed in detail the scientific advancements of the hydro-processing method along with intermediate stages involved in producing bio-jet fuel from edible or non-edible vegetable oil, bio-oil, and lipids. The study also recapped the cases in which intermediate stages of hydro-processing (i.e., deoxygenation, cracking, isomerization, and separation) can be achieved instantaneously in a single step, thus reducing the production cost [19]. In 2019, Khan et al. wrote a comprehensive review of the deoxygenation of triglycerides-based feedstocks, one of the essential unit operations in the hydro-processing pathway [14]. In 2019, Ibarra-Gonzalez and Rong summarized the processing details of thermochemical conversion pathways from lignocellulosic biomass to jet fuel gasoline and diesel [13].

1.3 Jet fuel specifications and environmental aspects

Conventionally, aircraft is powered by liquid petroleum fuel with a carbon chain length of C_8-C_{16}, which is essentially a mixture of paraffin (C_nH_{2n+2}, 20%), iso-paraffin (C_nH_{2n+2}, 40%), naphthene or cycloparaffin (C_nH_{2n}, 20%), aromatics (C_nH_{2n-6}, 20%), and olefin (C_nH_{2n}) compounds known as jet fuel [10, 14, 17]. Due to safety issues, jet fuel has stricter requirements and regulations than other commonly used transportation fuels. Jet fuel must meet American Society for Testing and Materials (ASTM) standards: high energy density, good cold flow properties, good sealing capability, thermal stability, low freezing point, and compatibility with present engine design [14, 16, 21, 22]. Three standards are used to certify aviation fuels: ASTM (as of today, ASTM has certified five different alternative jet fuels), the International Air Transport Association Guidance Material, and the United Kingdom Ministry of Defense Standard [18]. Depending on the production route, bio-jet fuel is not always composed of aromatic compounds, which are required to expand the sealing components of aircraft engines (such as O-rings) to prevent fuel from leaking

[1, 23]. Therefore, ASTM D7566's specifications aim for a 10-50% mixture of biomass-based and conventional jet fuels as the alternative to 100% conventional fossil-based jet fuel [16, 18, 24]. Alternative aviation fuel candidates are fuels that can burn in existing aircraft without modifications to the engine and aviation sector infrastructure and are also termed "drop-in" fuels [18, 24]. Depending on the properties and specifications described above, jet fuels fit into one of five broad categories: Jet A, Jet A-1, JP-4, JP-5, or JP-8 [14, 20]. Jet A is commonly used in commercial flights in the USA, and Jet A-1 is for the same purpose in the rest of the world. Jet A and Jet A-1 have different freezing points, -40 °C and -47 °C, respectively. JP-4, JP-5, and JP-8 are conventionally used in military aircraft. **Table 1** shows the detailed specifications of different types of jet fuels [14,18, 19, 21].

Usually, 1 kg of jet fuel consumption produces 3.16 kg of CO_2; this ratio exists regardless of the phase of flight (i.e., take-off, flight, or landing) [25]. The upper troposphere (the lower atmospheric layer where weather patterns occur) and tropopause (the layer separating the troposphere and stratosphere) are where CO_2 is primarily emitted, at altitudes of 10 and 13 km, respectively [16]. At sufficiently cold and humid temperatures in these atmospheric layers, the emitted water vapor instantly freezes, and exhaust particulates from aircraft act as a nucleus for those ice crystals, which eventually turn into contrails. Cirrus clouds are created when contrails spread horizontally and vertically, changing the earth's atmosphere's radiation balance [16, 25]. Considerable increases in the concentration of GHGs (including CO_2 and water vapor) are responsible for recent climate change to a great extent [1]. There is no single solution for these complicated GHG emission problems; modifying aircraft designs and replacing conventional jet fuels with alternate advanced aviation fuels and technologies are considered promising solutions, the latter in particular [22]. In 2019, a report by ICAO included a materialistic goal to decrease climate impacts due to international aviation sector GHG emissions by improving fuel efficiency by 2% annually from 2020 to 2050 to ensure carbon-neutral growth [25]. In any vehicle, fuel efficiency is the effectiveness of a process that transforms the chemical potential energy of a carrier fuel into kinetic energy or work [26]. Fuel economy and fuel efficiency are often used interchangeably, yet efficiency is a broader term that covers fuel use in a specific type of vehicle. Both terms are significant in the developing stages of fuel to reduce worldwide GHG emissions and fuel consumption [26]. Apart from environmental concerns, the non-renewability of fossil fuels triggers the need for alternative renewable aviation fuels and a sustainable source [22]. Using biomass as a feedstock for jet fuel production is one of the most promising ways to address these issues. The European Union (EU) has launched the Biofuels Flight Path initiative with several airlines and partners to promote using biofuels to use two million tonnes of biofuel annually in Europe's aviation sector from 2020 onward [16, 27].

1.4 Types of biomass feedstocks and biofuel

According to its use or end use, biomass can be divided into three main categories: food-based, non-food-based, and lignocellulosic [28]. Generally, food-based biomass is of two types – sugar or starch-based and oil-based. First-generation biofuels can be produced by fermentation of sugar (or starch) or oil transesterification. However, using edible food crops for fuel production is challenging because of competition for cultivable lands [1]. Second-generation biofuels produced from lignocellulosic biomass came into light to address this problem. Algae (micro and macro)-based biomass feedstocks produce third-generation biofuels because algae contain lipids and lignocellulose [16, 22]. The biomass-to-jet fuel pathways are shown in **Figure 1.**

Table 1. Jet fuel types and specifications [14, 18, 19, 21]

Grade	**Jet A-1**				**Jet - A**	**JP-4**	**JP-5**	**JP-8**
Specifications	**ASTM D1655-04a**	**IATA**	**Def Stan 91–91**	**ASTM D7566**		**MIL-T-5624**	**MIL-T-5624**	**MIL-DTL-83,133E**
Compositions								
Acidity, total (mg KOH/g)	0.1*	0.015*	0.012*	0.1*	0.10	0.015	0.015	0.015
Aromatics (vol%/wt%)	25* (vol%)	25* (vol%)	25* (vol%)	8-25 (vol%)	25 (wt%)	25 (wt%)	20.36 (wt%)	25 (vol%)
Sulfur, total (wt%)	0.3*	0.3*	0.3*	0.3*	0.3*	-	-	0.3*
Naphthalene's (vol%)	3*	3*	3*	3*	3*	-	-	3*
Volatility								
Distillation temperature (°C)								
Initial boiling point	170	205	NM	NM	NM	145	240	152
10% recovery	205*	205*	205*	205*	205*	-	206	205*
50% recovery	-	-		15, min	-	-	-	-
90% recovery	-	-	-	40, min	-	-	-	-
Final BP	300*	300*	300*	300*	300*	270	300-330	300*
Flash point (°C), min	38	38	38	38	38	60–79	68	38
Density@15 °C (kg/m^3)	775-840	775-840	775-840	775-840	775-840	602–751	814	775-840
Fluidity								
Freezing point (°C), max	-47	-47	-47	-47	-47	-58	-50	-47
Viscosity @ 20 °C (cSt)	8*	8*	8*	8*	8*	-	8.5*	8*
BOCLE wear scar diameter (mm)	-	0.85*	0.85*	0.85*	-	-	-	-
Combustion properties								
Net heat of comb. (MJ/kg), min	42.8	42.8	42.8	42.8	43.28	42.8	43	42.8
Smoke point (mm), min	25	25	25	25	25	20	19	25

Thermal stability								
JFTOT DeltaP@260 °C (mmHg)	25*	25*	25*	25*	25*	25*	25*	25*
Tube deposit Rating (Visual)	< 3	< 3	< 3	< 3	< 3	< 3	< 3	< 3
Conductivity								
Conductivity (pS/m)	50-450	50-450	50-600	-	50-450	150-600	-	-

*: Maximum, NM: Not mentioned

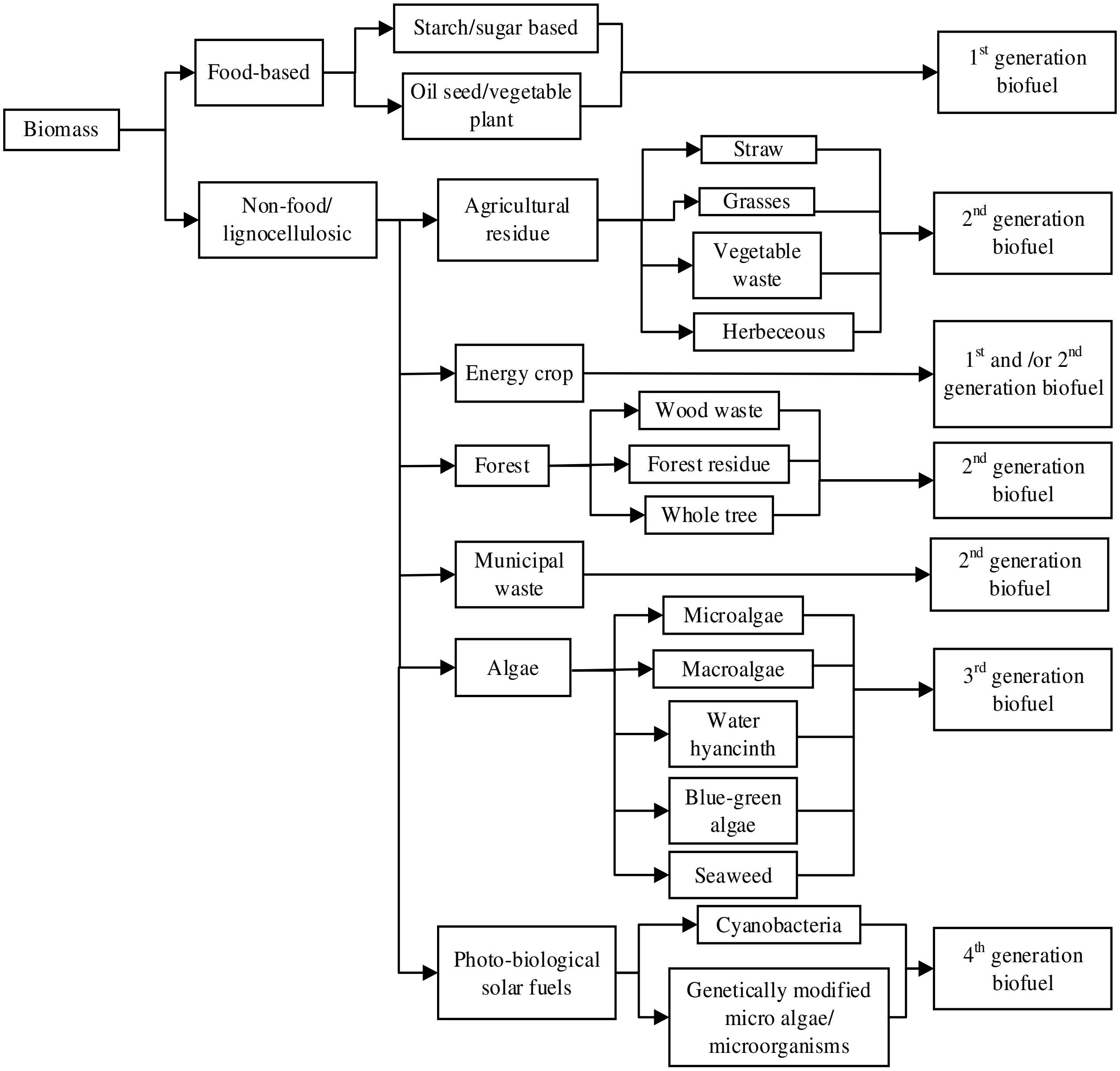

Figure 1. Classification of biofuels based on the feedstock [16, 28]

1.5 Overview of the bio-jet fuel production

Bio-jet fuel can be produced from the feedstocks shown in Figure 1 in several conversion pathways broadly segregated, as shown in **Figure 2**, as oil-to-jet, alcohol-to-jet, gas-to-jet, and sugar-to-jet.; Five pathways and/or sub-pathways are certified by ASTM are listed below [17, 18]: [29, 30]:

1. The production of hydrotreated esters of fatty acids (HEFA) in the oil-to-jet pathway,
2. Fischer-Tropsch (FT) synthesis in the gas-to-jet pathway,
3. The production of synthesized iso-paraffins (SIP) from hydro-processed fermented sugars in the sugar-to-jet pathway,
4. The use of iso-butanol as feedstock for jet fuel production in the alcohol-to jet-pathway, and,
5. Ethanol as feedstock for jet fuel production in the alcohol-to-jet pathway.

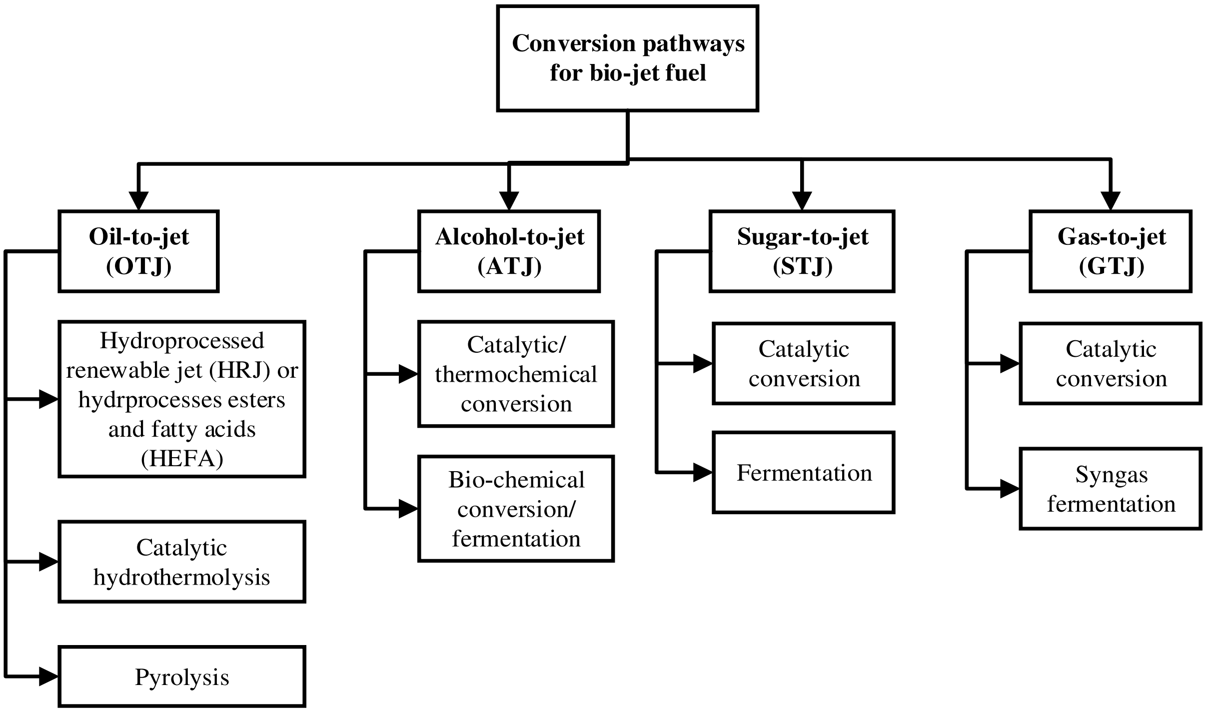

Figure 2. Classification of bio-jet fuel pathways [18]

Among these, HEFA from oil-to-jet and Fischer-Tropsch (FT) synthesis from the gas-to-jet are in industrial practice till recently [15].

Oil-to-jet

The oil-to-jet method comprises of three pathways: hydro-processing or HEFA (hydro-treated esters and fatty acids), catalytic hydro-thermolysis, and fast pyrolysis [18]. Hydro-processing is already certified by ASTM and is a less complex process than the two other oil-to-jet methods, as it uses low-quality triglyceride feedstocks and simpler product separation techniques [15, 18]. Hydro-processing uses oil from first-generation feedstocks such as edible and non-edible oils, whereas the other two methods use lignocellulosic biomasses.

The hydro-processing or HEFA pathway uses hydrodeoxygenation, hydro-isomerization, and hydrocracking to convert triglyceride feedstocks into bio-jet fuel. First, a triglyceride feedstock is deoxygenated and then decarbonylated with hydrogen and a solid catalyst at high temperature and pressure to produce direct long-chain hydrocarbons (with H_2O, CO, and CO_2 as by-products) [1, 31]. The second reactor fractures and isomerizes the linear long-chain hydrocarbons created in the first reactor. This technique produces light gases, naphtha, and green diesel with hydrocarbon chains between C_8 and C_{16}, equivalent to bio-jet fuel. Triglyceride feedstocks include different edible and non-edible vegetable oils, algal oil, animal fats, used cooking oils, pyrolysis, and bio-oil [1, 31].

Catalytic hydro-thermolysis (CH) or hydrothermal liquefaction comprises a series of reactions, including cracking, hydrolysis, decarboxylation, isomerization, and cyclization that turn triglyceride-based feedstocks into a mixture of branched, straight chain, and cyclic hydrocarbons (similar to the HEFA process). Applied Research Associates Inc. has created and patented a revolutionary method for creating drop-in fuels from plant or algae oils [18, 32]. The first stage of the CH process is carried out in the presence of water, with or without a catalyst, at a pressure of 210 bar and temperatures between 450 and 475 °C. Oxygenated species, carboxylic acids, and unsaturated molecules are the end products, and they are processed through decarboxylation and hydrotreating to remove the oxygen and reach saturation [18, 32]. The processed products, which range in carbon content from 6 to 28, comprise n-alkanes, iso-alkanes, aromatics, and cyclo-alkanes that need to be separated into naphtha, jet fuel, and diesel fuel, respectively, in a subsequent fractionation stage. This fuel satisfies ASTM and military (MIL) requirements, which include high-quality combustion, stability, and cold flow characteristics [18, 32].

Biochar, pyrolysis oil (also called bio-oil), and pyrolysis gas are the products of pyrolysis, which is the fast or slow heat decomposition of biomass in the absence of air (without oxygen) [18]. The mixture of oxygenated organic molecules with carbon atoms ranging from C_1 to C_{21} is known as bio-oil. If no further catalytic upgrading is necessary, this can be refined like vegetable and algal oil through a series of hydrotreating operations and subsequently fractionated to generate jet-range products [18].

Gas-to-jet

The GTJ pathway turns biogas, natural gas, or syngas produced from multiple sources, such as energy crops and agricultural, municipal, and industrial organic wastes, into bio-jet fuel through FT synthesis and fermentation [18]. FT synthesis is a well-developed set of catalytic processes for transforming syngas into liquid hydrocarbons and eventually to jet fuel, certified by ASTM [18]. It is also conceivable to ferment syngas to produce bio-jet fuel instead of catalytically upgrading

FT syngas. With an overall energy efficiency of 57%, gas fermentation may create more products than the conventional biochemical or thermochemical processes; the FT process has a relative overall energy efficiency of 45% [18].

Sugar-to-jet

In the sugar-to-jet (STJ) pathway, two processes generate jet fuel from sugar intermediates. The first uses aqueous phase reforming (APR), in which sugars and sugar intermediates are catalytically upgraded to hydrocarbons [18, 20]. APR, a thermochemical technology, turns soluble plant sugars into chemical intermediates such as alcohols, ketones, aldehydes, furans, acids, and other oxygenated hydrocarbons and transforms them into jet-range hydrocarbons [20]. The direct sugar-to-hydrocarbons (DSHC) process, also known as the direct fermentation of the sugar-to-jet (DFSTJ) process, is the second biological method for converting sugars and sugar intermediates to hydrocarbons [18, 20]. In this process, alkane-type fuels are produced directly from sugar feedstocks via fermentation. Here, the feedstocks are similar to the feedstock for first-generation bioethanol production, i.e., sugar cane, beets, and maize; lignocellulosic biomass needs some pre-treatment [20].

Alcohol-to-jet

The bio-jet fuel blend produced from alcohol-to-jet pathways and conventional fossil jet fuel started as a test run by the US Air Force in 2012 and is now certified by ASTM. [18, 19]. First-generation feedstocks like sugar or starches are directly fermented (a biochemical conversion) into alcohols and then converted to jet fuels [18, 33]. Lignocellulosic biomass feedstocks, on the other hand, can be converted into alcohols using both thermochemical and biochemical techniques. The thermochemical process refers to the conversion to fuel through pyrolysis, gasification, and upgrading. The thermal decomposition of biomass in the absence of air, known as pyrolysis, produces bio-oil and methane with other by-products [22]. Gasification is a process that uses limited amount of air or steam to treat pyrolysis products further to create syngas, a mixture of hydrogen and carbon monoxide [22]. The Fischer Tropsch (FT) process can improve syngas [22]. Biogas and syngas (from biomass feedstocks) can also be converted either thermochemically or biochemically (fermentation) to bio-jet fuel [18, 22, 33].

It is evident that bio-jet fuel production pathways have achieved a certain level of maturity, and a significant amount of review work has been done. Related research on production technology, policy-making, economics, environmental aspects, life cycle analysis (LCA), combustion chemistry, bio-aviation fuel properties, etc., is ongoing [15].

1.6 Problem statement

In the alcohol-to-jet pathway, alcohols act as the platform molecules to produce bio-jet, where alcohols can be generated from any fermentable biomass source. While the technology for producing alcohols from starch- and sugar-based feedstocks is relatively mature, that associated with lignocellulosic feedstock conversion to alcohol is still in the research and development stage [15, 33]. All the significant scientific advancements that led to jet fuel production from common alcohols such as methanol, ethanol, n-butanol, iso-butanol, higher degree alcohols, and cyclic alcohols are comprehensively compiled here along with existing limitations, research gaps, and recommendations for further study.

Applying more conversion technologies to a biorefinery to convert intermediate products and/or by-products into more value-added marketable products increases revenue and encourages the full use of the original feedstock such as lignocellulose [34-36]. This improves the overall rate of return that further protects the investors against market uncertainties [36-38]. Along with biochemical process, gasification and pyrolysis technologies are two most common thermochemical technologies for biomass valorization with the multi-product concept [36, 39].

Lignocellulose cannot be fermented directly without a series of pre-treatment and complex product separation stages to make the C_5 and C_6 sugars accessible for fermenting which is technologically more demanding [33]. Moreover, C_5 sugars (pentoses) from cellulose and hemicellulose necessitate genetically modified yeasts for further processing, since most of the commonly used yeasts can only convert C_6 sugars [33].

Lignocellulosic biomass (i.e. solid biofuels) can be gasified for syngas production before alcohol synthesis. However, due to the lower carbon content and some naturally occurring impurities from gasified solid biomass, an enhanced pre-treatment is necessary which is technologically demanding. Hence, biomass gasification is still under development, and fully commercial systems can hardly be found on the market until recently [33].

Slow pyrolysis primarily yields biochar, while fast pyrolysis produces bio-oil, biochar, and non-condensable gas in significant quantities [40]. Bio-oil, the major product of interest in the fast pyrolysis process is similar to crude oil and is subjected to further processing for the simultaneous production of gasoline, diesel, jet fuel and other valuable end products [36, 41]. The non-condensable gases are usually used to generate process heat and hydrogen depending on the composition [36]. Biochar is used for soil amendment [42], activated carbon production [43], and carbon nanomaterial production [44, 45] which are not strategically integrated into the biorefinery. Alcohol, specifically ethanol can be produced from biochar after gasification through syngas fermentation which can further processed to produce bio-jet fuel.

Therefore, starting from the lignocellulosic biomass as feedstock to get the bio-jet fuel as end product involves a complex biorefinery concept involving both biochemical and thermochemical process pathways. Apart from the conversion pathways, the extent of bio-jet fuel commercialization also depends on feedstock availability, GHG emissions reduction, and global socio-economic policy [18]. Ensuring a sustainable bio economy, prediction of a stable and secure supply of forest biomass as feedstock is also a vital fact [46]. The feedstock studied here is spruce wood chips (an important tree species globally) which make up about 47% of Canada's total forest inventory (21 M ODT/year, the annual national amount of available logging residues) [46, 47].

To the best of the author's knowledge, there is very limited research on the techno-economic assessment of conversion of lignocellulose-based jet fuel production via ATJ in Canada. This research assesses the fast pyrolysis of spruce wood chips, alcohol upgrading from syngas, and the subsequent bio-jet fuel production via ATJ conversion. By developing processes and techno-economic models, the aim is to address knowledge gaps and provide valuable insights into these processes.

1.7 Objectives of the research

The key objectives of this study are to:

- Conduct a comprehensive review of the historical data and literature to identify the significant scientific advancements in bio-jet fuel production from various common alcohols, such as methanol, ethanol, n-butanol, iso-butanol, higher-degree alcohols, and cyclic alcohol.
- Develop detailed process models for bio-jet fuel-focused facilities, with a specific focus on the use of bioethanol derived from lignocellulosic biomass, particularly spruce wood chips.
- Evaluate the net energy ratio of the developed pathways to understand the energy efficiency and sustainability of each bio-jet fuel production method.
- Develop techno-economic models to assess production costs, cost curves, and overall profitability of bio-jet fuel production under different scenarios.
- Establish scale factors for primary unit operations to understand the economies of scale benefits in the development of a large-scale plant.
- Perform sensitivity analysis to determine the impact of variations in input parameters on the production cost of bio-jet fuel.
- Conduct uncertainty analysis to understand the impact on the production cost of bio-jet fuel due to randomness in the input parameters.

1.8 Thesis outline

Chapter 1 outlines the background and goal of the present work. Chapter 2 includes a literature review on bio-jet fuel. The methodologies for development of process simulation and techno-economic models are described in Chapter 3. The results are discussed in Chapter 4. Finally, Chapter 5 summarizes the conclusions and recommendations for future work.

Chapter 2. Literature Review

2.1 Alcohol to Jet Pathways

In road transport, ethanol, and butanol are generally used as blending feedstocks in conventional fuels. However, methanol, ethanol, and butanol cannot be used directly as aviation fuel alternatives because of their high volatility, low flash point, and low energy density [22, 48]. If conventional jet fuel is blended with alcohols; in that case, it cannot be used without engine modifications because of the poor fuel properties of the mixture, which will cause adverse impacts during flight [22, 48].

Alcohol production pathways from first-generation feedstocks (starch- and sugar-based) have been practiced worldwide over the last hundred years [16, 33]. This is because feedstocks like starch and sugars contain readily fermentable C_6 sugar molecules that produce alcohols. Second-generation feedstocks like lignocellulosic biomass contain C_5 sugars that require complex microbial or catalytic processes to be converted to alcohol or platform molecules to produce bio-jet fuel. Jet fuel production via alcohol is done in two steps [33]:

1. The production of alcohols (platform molecules) from biogenic feedstocks, and
2. The manufacture of long-chain hydrocarbons from the alcohol(s)

Depending on the available feedstocks and other relevant factors, the alcohol-to-jet pathway can be a potential alternative for producing bio-jet fuel. Alcohols are chemically transformed into higher hydrocarbons, eventually leading to jet fuel. Theoretically, this transformation can be applied to all alcohols. However, methanol, ethanol, and butanol are commercially traded worldwide; fuel producers concentrate only on these alcohols to produce jet fuels [49].

2.2 Alcohol production routes

Bio-alcohols are produced biochemically or thermochemically by the following processes [20, 50]:

1. Sugar or starch fermentation with yeast or microbes,
2. Starch hydrolyzation-fermentation,
3. Enzymatic hydrolyzation-fermentation of lignocellulosic feedstock,
4. Thermochemical conversion of biogas or bio-based syngas,
5. Fermentation of syngas.

The yield of the produced alcohols depends on many factors, such as the composition of the feedstocks in terms of cellulose, hemicellulose, and lignin content, the selected microbes, the pretreatment method used and others [18]. Pretreatment methods were developed simultaneously with the primary process to produce alcohols. The pretreatment method for methanol production from lignocellulosic biomass has yet to be fully developed. Rather than directly producing methanol from lignocellulosic biomass, methanol can be produced from the oxidation of biomethane via methylotrophic bacteria; selecting microorganisms is the critical step [49]. Lignocellulosic biomass feedstocks are usually treated with dilute acid and alkali before producing ethanol, while pretreatment via autohydrolysis (steam explosion) has been shown to give the highest (~ 84%) bioethanol yield [49, 51]. Acid pretreatment and heat application are more effective because the hemicellulose part of lignocellulosic biomass can be easily converted into reducible sugars in the presence of acids [49]. Bio-jet fuel can be produced more economically from n-butanol and iso-butanol because butanol is similar to gasoline (it is closer to jet fuel) in terms of its physical and chemical features [49]. Bio-butanol, specifically n-butanol, is usually produced through a microbial process known as acetone-butanol-ethanol (ABE) fermentation in a typical molar ratio of 3:6:1 [18, 52]. Iso-butanol can be produced commercially from anaerobic (with a 100.0% theoretical yield) and aerobic fermentation [18, 53]. Several pretreatment methods have been developed for lignocellulosic materials to break down the complex structure of cellulose, lignocellulose, and lignin. However, enzymatic hydrolysis is the most efficient for bio-butanol production [53, 54].

2.3 Alcohol-to-jet process

The alcohol-to-jet (ATJ) method uses a sequence of reactions to produce alternative aviation fuel from alcohols such as methanol, ethanol, butanol, or higher alcohols employing dehydration, oligomerization, hydro-processing, and product separation methods through a distillation column [19, 55]. The process flow diagram of ATJ pathways (methanol, ethanol, and butanol to jet fuel) is depicted in **Figure 3**. The technical process routes under the ATJ pathway are mature and widely used in commercial petrochemical applications and the aviation sector [15, 56]. The major steps involved in this pathway are:

Dehydration: This is the first step in the ATJ pathway; it converts alcohols to olefins. In this process, alcohols are catalyzed by either zeolites or metal oxide catalysts [18, 33]. This chemical process removes the oxygen atom (within the hydroxyl group) from the alcohol molecule in the form of water, forming the olefin molecule [16]. This method converts C_{1-} to C_{4-} alcohols to C_{2-} to C_{5-} alkenes depending on the catalysts involved. It is comparatively easier to dehydrate tertiary alcohols than primary alcohols like methanol and ethanol. For small alcohols, strong acids and high temperatures of 170-200 °C are usually required; however, temperatures up to 538 °C have also been reported. Water and other impurities produced as by-products must be removed from the reaction mixture. Therefore, process design minimizes by-product formation, maximizing short-chain alkene production [16, 33, 57].

Oligomerization: During oligomerization, longer molecules are created from shorter alkene molecules in a gas or liquid phase reaction. Alkenes with a carbon number between 8 and 16 are formed by converting C_2 to C_4 alkenes, such as when six ethene molecules or three butene molecules combine to generate one dodecene molecule (C_{12} alkene) [33]. There are several developed catalytic procedures for oligomerizing alkenes, and the conditions of each reaction depend on the alkenes used as starting materials. Transition metals are most suitably used as catalysts for liquid phase oligomerization for shorter alkenes, while for other branched alkenes of higher carbon numbers, heterogeneous acid catalysts are used [16, 33, 58].

Hydrogenation: In this step, oligomers in the jet fuel range are first separated depending on the carbon number (chain length) and then saturated with hydrogen. Alkenes are chemically unstable molecules as they have unsaturated double bonds in their structure and hence cannot meet jet fuel specifications. Because the dissociation enthalpy is high during the reaction, this procedure often requires transition metal catalysts based on nickel, platinum, or palladium (dispersed on activated carbon) [33, 57, 59]. Pt-, Pd-, or PtO_{2-} catalysts can be used for reactions in standard conditions. However, sometimes high-temperature conditions might be required. Currently, in industry, inexpensive Raney nickel catalysts are popularly used if the feed contains some percentage of C_8-C_{15} range aromatics along with olefins [33, 60].

Distillation: This is the last process step; it delivers pure jet fuel and is done in conventionally developed ways [16]. Jet fuel production using the abovementioned steps is described below for specific alcohols.

2.4 Methanol-to-jet

Globally, methanol is one of the most highly synthesized chemicals. It is usually a by-product produced during the commercial production of other readily available alcohols [61]. Jet fuel production through the methanol pathway is still in the research and development stage except for a few attempts at commercialization from globally renowned companies such as ExxonMobil (i.e., its methanol-to-jet proprietary process technology and catalysts [30]).

Bio-methanol can be produced by catalytic (usually copper, zinc oxide, or chromium oxides) hydrogenation of biomass-derived syngas (carbon monoxide and carbon dioxide) or biogas (methane and carbon dioxide) [23]. Methanol can be produced through the following reactions [61]:

$$CO_2 + 3H_2 \rightleftharpoons CH_3OH + H_2O \ (\Delta H^{o} = -50 \text{ kJ/mol}) \tag{1}$$

$$CO_2 + H_2 \rightleftharpoons CO + H_2O \ (\Delta H^{o} = +41 \text{ kJ/mol}) \tag{2}$$

$$CO + 2H_2 \rightleftharpoons CH_3OH \ (\Delta H^{o} = -91 \text{ kJ/mol}) \tag{3}$$

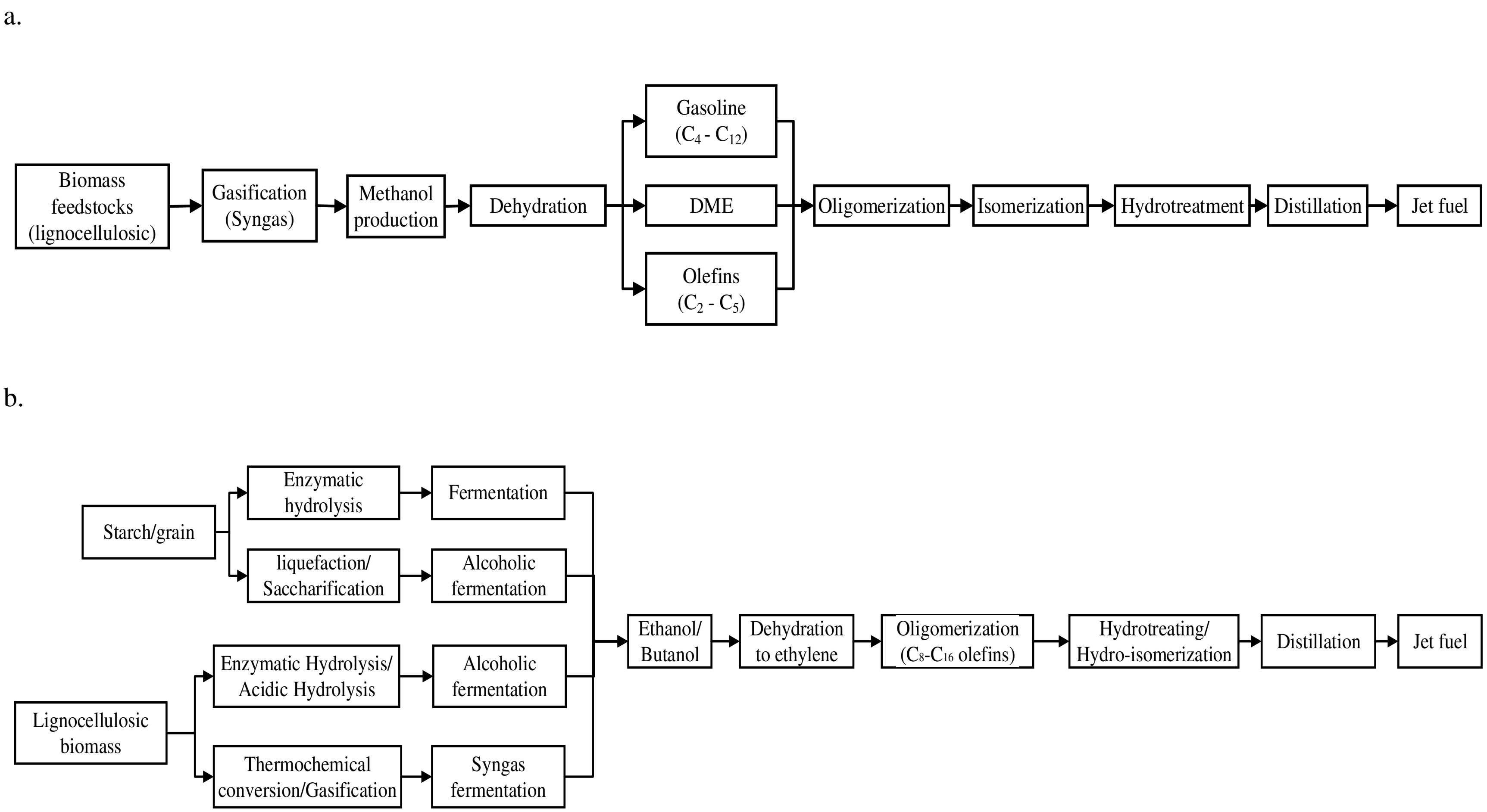

Figure 3. alcohol-to-jet production pathway: a. methanol-to-jet, b. ethanol- and butanol-to-jet [33]

The preferred temperature and pressure ranges for methanol production are 200-300 °C and 50-100 bar, respectively [23]. The unreacted gases need to be recycled, and the required cooling systems (due to the exothermic nature of the reaction) are responsible for the main costs of the synthesis process [23, 33].

Thus far, several patents are available describing the methanol-to-bio-jet process and some proprietary techniques, such as those used by ExxonMobil and Enerkem [30, 33, 47, 62]. However, the methanol-to-jet process is still in research and development and has yet to be commercialized. David Bradin describes the theoretical steps to produce bio-jet from methanol in a published patent [63]:

1. Syngas is produced from lignocellulosic biomass or other sources,
2. The produced syngas is transformed into methanol either thermochemically or biologically,
3. A portion of the generated methanol is converted to olefins (primarily ethylene and propylene with some butylene and higher olefins),
4. The remaining methanol is converted to dimethyl ether (DME) with a zeolite catalyst,
5. Hydrocarbons and aromatics are produced in the jet fuel range with a zeolite catalyst,
6. The olefins (ethylene, propylene, and the higher ones) are oligomerized to create higher olefins in the jet range.
7. Jet fuel-range paraffins are formed by isomerizing and/or hydrogenating the olefins in the presence of a zeolite catalyst, and
8. Commercial jet fuel is produced by combining one or more products from step (5) with one or more of the products of step (7).

The dehydration of alcohol removes the water molecule from alcohol's molecular structure to produce olefins. Different acidic catalysts such as SAPO-34, alumina, and zeolite are widely used to produce olefins from methanol, and ZSM-5 is the most commonly used. The superior performance and wide acceptance of ZSM-5 are primarily due to its high surface area, excellent resistance to deactivation by coke deposition, the acidic nature of its pores, and its well-defined porous structure [62]. Several research studies have reported different modifications to the ZSM-5 catalyst, which are applied to enhance product selectivity and yield, i.e., modifications with alkaline media (NaOH), phosphorus, ion exchange, metals (such as calcium), steam treatment, acid treatments or any other dealumination method, surface passivation by deposition of silica, and any combination of the above [62, 64, 65].

Theoretically, hydrocarbon yield from the alcohol dehydration process varies depending on the carbon number in alcohols or the carbon-to-oxygen ratio. With the increase in carbon number in the alcohol chain, the theoretical hydrocarbon yield also increases. The theoretical hydrocarbon yield for methanol is 44% (wt%), 61%, 70%, and 76%, respectively, for ethanol, 1-propanol, and 1-butanol [66]. Methanol dehydration produces dimethyl ether and other olefins such as ethylene, propylene, etc. To create jet fuel-range hydrocarbons yielding 80% C_{5+} hydrocarbon products, the DME produced, as mentioned above, is further dehydrated or oligomerized over a zeolite catalyst such as ZSM-5 [63]. The olefins produced from methanol undergo further oligomerization steps similar to those of other alcohol-to-jet processes and are discussed in the following sections. Then the produced olefins go through the usual jet fuel production processes, i.e., hydrogenation, isomerization, and fractionation.

Methanol is the least preferred alcohol to produce fuel-range hydrocarbons using a ZSM-5 catalyst. This is because methanol produces high amounts of durene (i.e., 1,2,4,5- tetramethyl benzene) and benzene during the catalytic conversion with ZSM-5. Durene's higher melting point makes it solid at room temperature, and benzene is a carcinogenic chemical not accepted as fuel in either transportation or aviation [66].

2.5 Ethanol-to-jet

Usually, ethanol is made from sugar under anaerobic conditions through alcoholic fermentation, in which various microorganisms or biocatalysts catalyze sugars. Because of their durability, effectiveness, and ease of cultivation, both yeasts (such as *Saccharomyces cerevisiae*, *S. uvarum*, and *Candida utilis*) and bacteria (*Z. mobilis*) are used [67]. It is necessary to continuously monitor and manage variables like temperature, pH level, and nutrient supply to give microorganisms the best circumstances for fermentation [33]. Yeast cannot directly ferment polysaccharide starches because they only contain glucose building blocks. Hence, a two-step biochemical procedure is used: starch is first liquefied by α-amylase and then saccharified by gluco-amylase, transforming the starch into maltose and glucose that yeasts can ferment [33]. To make the sugar accessible in the case of lignocellulosic biomass, a pretreatment (chemical and/or biological degrading process) is required; this pretreatment is energy intensive. In lignocellulosic biomass, sugars are effectively incorporated into the hemicellulose, cellulose, and lignin macromolecules. Hemicellulose is hydrolyzed using various methods to produce C_5 sugars (pentoses), which must then be processed using genetically altered yeast [33, 68]. The conversion of lignocellulosic biomass to sugar has been explored intensively in many countries and is characterized by low efficiencies and high processing costs. Therefore, this pathway is far from commercialization.

The significant steps of the ethanol-to-jet fuel conversion pathway are dehydration, oligomerization, hydrotreating, and fractionation, as described below:

Ethanol Dehydration

The first step in the ethanol-to-jet pathway is catalytic ethanol dehydration, which has been practiced industrially since 1913 [69]. Water in the ethanol feed is detrimental to the dehydration reaction of ethanol [70]. The product profile of the catalytic ethanol dehydration reaction mainly depends on the reaction temperature. The dehydration of ethanol can be represented by two reactions, a primary reaction (Equation 4) and a side reaction (Equation 5).

$$C_2H_5OH \rightleftharpoons C_2H_2 + H_2O \ (\Delta H^o = 44.9 \text{ kJ/mol}) \quad (4)$$

$$2C_2H_5OH \rightleftharpoons C_2H_5OC_2 H_5 + H_2O \ (\Delta H^o = -25.1 \text{ kJ/mol}) \quad (5)$$

Equation 4 is an endothermic intramolecular dehydration reaction that produces ethylene and is favored at high temperatures (>300 °C). Equation 5 is favored at low temperatures (<230-300 °C) and is an intermolecular exothermic dehydration reaction that leads to the production of diethyl ether (DEE) [71-74]. In addition to diethyl ether, there are other by-products such as acetaldehyde, a few hydrocarbons up to C_4 (methane, ethane, propylene, butylene), and some common light base groups (CO_2, CO, H_2, etc.) [74]. However, besides ethylene and diethyl ether, the production of other by-products is negligible [74].

Three reaction routes are considered for the dehydration of ethanol: (i) the parallel production of ethylene and diethyl ether from ethanol, (ii) a series of reactions in which diethyl ether is first produced (from ethanol) and subsequently converted to ethylene, and (iii) a combination of the two. Apart from the temperature, the reaction route or mechanism controlling ethylene production from ethanol depends on the type of catalyst, ethanol concentration, and other factors. Ethylene is the desired product from ethanol to produce jet fuel and is produced mainly in two types of reactors, fixed bed and fluidized bed reactors [74, 75]. Fixed bed reactors are of two kinds, isothermal tubular and adiabatic reactors; the first is seldom used because of several limitations (poor temperature control ability, complex regeneration, and replacement of catalysts, etc.), and the other is popular in industrial practice to produce ethylene from ethanol [74, 76, 77]. Using a fluidized bed for the dehydration reaction is recent and promising. It is still in the research and development stage and has several advantages (high heat and mass transfer rate, the ability to control the temperature, large capacity, and stable operation) and some disadvantages (friction and collision of catalyst particles with each other and the reactor body) [74, 78]. Ethanol dehydration to ethylene is an acid-catalyzed reaction, and the catalysts are of one of four categories [74]:

1. Phosphoric acid,
2. Metallic oxides,
3. Miscellaneous acid catalysts/heteropoly acid catalysts, and
4. Molecular sieves.

Phosphoric acids were first used industrially in the 1930s as catalysts to dehydrate ethanol to ethylene after British Imperial Chemical Industries (ICI) developed them by loading phosphate on coke or clay. The produced ethylene was highly pure; however, because of the easier deactivation by coke deposition and the long regeneration cycle (about a month), they have not been in use since the 1950s [74, 79].

Metal oxides have Brønsted and Lewis acidity on their surface, which drives their catalytic activities [80]. Among the metallic oxides, the industry most widely uses activated alumina-based compounds as a catalyst or catalyst carrier for the dehydration of ethanol to ethylene and other chemical reactions such as isomerization, catalytic cracking, alkylation, etc. Activated alumina-based catalysts are highly stable, and the ethylene's purity is also high. However, high ethanol concentration in the feed is a prerequisite for these catalysts; otherwise, high temperatures and low space velocity are required, leading to higher energy consumption [74]. If γ-Al_2O_3 is used as the catalyst, the achievable conversion rate for the ethanol and ethylene selectivity is up to 99% and 94%, respectively. Apart from alumina, other transition metal oxides are also widely used separately or in different combination ratios with alumina (γ-Al_2O_3 or Al_2O_3) and/or silicon oxides. Transition metal oxides include titanium oxides (TiO_2/γ-Al_2O_3), magnesium oxides (MgO, $A1_2O_3-MgO/SiO_2$), cobalt oxides, chromium oxide ($Al_2O_3-Cr_2O_3$), iron oxides (Fe_2O_3, Fe_2O_3/Al_2O_3, FeO_x/Al_2O_3) and NiO/clay, iron ion-exchanged mordenite, Na_2O-doped Mn_2O_3/Al_2O_3, calcium oxide (CaO), and zinc oxide (ZnO) [74, 81].

Oxygen-containing multi-acids are generally called heteropolyacids and are formed by the central atom (i.e., P, Ge, Si, Fe, and Co) through the oxygen atom bridging with the ligand atoms (i.e., Mo, W, V, and Nb, etc.). Heteropolyacid catalysts for ethanol dehydration to ethylene are advantageous because of the low reaction temperature requirement. However, the ethanol conversion rate is comparatively low, and the preparation cost is high because of the loading requirement in a carrier. These catalysts are currently in research and development [74, 82, 83]. Keggin-type phosphor-molybdate and phosphor-tungstic acid (TPA/HPW) loaded on SiO_2, phosphotungstic salts, $K_xH_{3-x}PW_{12}O_{40}$, and $Ag_xH_{3-x}PW_{12}O_{40}$ loaded on SiO_2, silicotungstic acid (STA), and molybdophosphoric acid (MPA) are the most promising examples of this type of catalyst [74].

Molecular sieves are used as catalysts and adsorbent or ion exchange materials in many engineering fields and have a regular pore structure, large specific surface area, and unique acid-base properties [74, 84]. Since the 1980s, four molecular sieves have dehydrated ethanol to ethylene: A, AM-11, Zeolite Socony Mobile-5 (ZSM-5), and the Si-Al-phosphate (SAPO). The last two have been studied the most [74, 85]. Surface acidity and the pore size of molecular sieves have an essential role in the performance of these catalysts. Some researchers have found that modified molecular sieves can dehydrate ethanol to ethylene at lower temperatures and lower concentrations of ethanol than regular molecular sieves [18, 20, 74]. However, molecular sieves can be costly depending on their preparation steps, and given their higher acidity, they can be easily deactivated by coke deposition. Research is ongoing on catalysts to overcome these limitations and make the sieves industrially more acceptable [74].

In the 1970s, Argauer and Landolt and Dwyer and Jenkins synthesized the most critical molecular sieve, ZSM-5 ($Na_nAl_nSi_{96-n}O_{192} \cdot 16H_2O$, n<8), which has a two-dimensional 10-

membered ring structure (0.53-0.56 nm × 0.51-0.55 nm) with very good shape-selective catalysis and adsorbent properties [86-89]. Steam-treated zeolites like H-ZSM-5 ($Si_{95.68}Al_{0.32}H_{0.32}O_{192}$) show a reversible phase transition exhibiting monoclinic symmetry below 67 ºC and orthorhombic symmetry above this transition temperature, while ZSM-5 is orthorhombic as synthesized [89, 90]. The HZSM-5 zeolite is more active and stable for the selective conversion to ethylene than the commonly used γ-Al_2O_3, with delayed deactivation by coke deposition, mitigated by treatments to moderate acid strength [91]. To achieve complete conversion of ethanol to ethylene with 100% selectivity and to lower the acidity (which facilitates their regeneration), researchers have modified both the ZSM-5 and HZSM-5 zeolites with several methods such as hot water treatment, ion exchange, impregnation, etc. [74]. Among these modifications, impregnation and ion exchange with different metals (single or bimetallic) such as Cu, La, V, Zn, Mn, Mg, alkaline-earth metals, etc., and/or with phosphorus (P) are the most promising [71, 92]. Different studies have found that a low-temperature range of 270-320 ºC favors the ethanol dehydration reaction, while high temperatures (350-450 ºC) prohibit the reaction. At high reaction temperatures, the formation of higher hydrocarbons such as C_3–C_{9+} aliphatic and aromatics occurs to a significant extent [93]. Another molecular sieve, the SAPO series (Si-Al-phosphate, SAPO-n), was developed by Union Carbide Corporation (UCC) in the US in 1984. The "n" represents the compositional range in the anhydrous form, which depends on the synthesis conditions. In the SAPO series, SAPO-34 is widely used for ethanol dehydration and performs better than ZSM-5 catalysts under certain reaction conditions [74]. The performance of this catalyst has been improved by the insertion of metals such as Ni [94]. The notable scientific research work and recent outputs on these catalysts are summarized in **Table 2, Table 3, and Table 4**.

Table 2. Scientific advancements in phosphoric acid and metal oxides catalysts for the dehydration of ethanol to ethylene

Ethanol (%)	Catalyst	P (atm)	Temp (°C)	WHSV /LHSV(h^{-1}) /RPM	Reactor type	Conversion (max% @°C)	Selectivity (max% @ °C) of ethylene	Remarks	Ref
80-100 wt%	Liquid Polyphosphoric Acid (PPA)	1	160-300	2020 RPM	-	100.0%	97.0-99.0%	• Product separation is more straightforward as ethylene is in the gas phase.	[79]
7.9 vol% ethanol in N_2	γ. Al_2O_3	1	150-450	1.43-2.9	Tubular	100.0% @ 450 °C	100.0% @ 350 °C	• Produces trace amounts of butene and ethane. • Diethyl ether selectivity is 100.0% @150-200 °C. • Higher conversion at a lower space velocity (low T). • In most cases, ethylene selectivity decreases with the increase in temperature after reaching maximum selectivity.	[95]
	γ. AlOOH			1.43		99.8% @ 400 °C	99.4% @ 400 °C		
	θ. Al_2O_3			1.43		100.0% @ 350 °C	99.6% @ 400 °C		
	δ. Al_2O_3			1.43-1.66		100.0% @ 450 °C	99.9% @ 350 °C		
	Si-AL			1.43-4.95		100.0% @ 400 °C	100.0% @ 350 °C		
-	$A1_2O_3$-MgO /SiO_2 (syndol)	1	550	-	Fixed bed	97% – 99.98%	98.7%	• One cycle of the catalyst activity is 8-12 months. • Ethylene selectivity increases with increasing temperature.	[74, 96]
100.0 vol%	Al_2O_3-Cr_2O_3	1	280-350	0.006 - 0.012	Flow reactor	13% @ 400 °C	100.0% @ 450 °C	• The produced ethylene is in the gas phase, so product separation is easier. • By-products include acetaldehyde and acetone.	[97, 98]
Ethanol vapor in H_2	CoO-bentonite	1	250-400	0.67	Pulse micro-reactor	100.0%	77.0% @ 400 °C	• Selectivity of diethyl ether and ethyne is the same at 325 °C for CoO and NiO. • Fe_2O_3 can produce ethylene at low temperatures.	[99]
	Nio-bentonite						98.3% @ 400 °C		
	Fe_2O_3-bentonite						88.0% @ 400 °C		
99 wt%	Fe_2O_3	1	200-500	2.85	Fixed bed	97.0% @ 500 °C	65.4% @ 500 °C		[81]

Ethanol (%)	**Catalyst**	**P (atm)**	**Temp (°C)**	**WHSV /LHSV(h^{-1}) /RPM**	**Reactor type**	**Conversion (max% @°C)**	**Selectivity (max% @ °C) of ethylene**	**Remarks**	**Ref**
	Mn_2O_3					90.1% @ 500 °C	58.0% @ 500 °C	• Total conversion increases steadily with an increase in temperature. • Acetaldehyde and ethane are non-dominant by-products. • Because of the reducibility of the iron active species, iron-manganese oxide and iron-manganese-silica oxide catalysts had the highest selectivity.	
	Mn_2O_3-Fe_2O_3 (50:50)					94.3% @ 500 °C	63.4% @ 400 °C		
	Mn_2O_3-Fe_2O_3-Al_2O_3 (45:45:10)					95.3% @ 500 °C	57.0% @ 450 °C		
	Mn_2O_3-Fe_2O_3-SiO_2 (45:45:10)					99.7% @ 500 °C	63.4% @ 400 °C		
	Mn_2O_3-Fe_2O_3-Al_2O_3-SiO_2 (31:53:6:10)					96.0% @ 500 °C	65.4% @ 500 °C		
100.0 vol%	Na_2O doped Mn_2O_3/Al_2O_3	1	200-350	-	Pulse micro-reactor	97.0% @ 350 °C	-	• 3 mol% Na_2O gives the best result.	[100]
100.0 vol%	γ-irradiated Co_3O_4/MgO	1	250-400	-	Pulse micro-reactor	Temperature and γ-ray dependent (80%)	100.0%	• MgO acts as catalyst support. Conversion increases with increases in Co_3O_4, γ-irradiation, and temperature.	[101]
100.0 vol%	Al_2O_3-TiO_2 (50:50)	1	300-500	-	Pulse micro-reactor	Temperature dependent	Temperature dependent	• 50:50 ratio of alumina to TiO_2 gives the highest activity.	[80]
100.0 vol%	ZnO doped Co_3O_4-Al_2O_3	1	300	-	Pulse micro-reactor	Temperature and dopant dependent (20%)	Temperature and dopant dependent (90%)	• Depending on temperature and dopant, selectivity switches from dehydration to dehydrogenation (max@ 400 °C and 2.33% of ZnO).	[102]
2 vol% ethanol in N_2	FeO*x*/Al2O3	1	200-350	1.67	Fixed bed	Temperature -dependent (60%)	Temperature and Fe_2O_3 dependent (68%)	• Dehydration to diethyl ether $(C_2H_5)_2O$ is highest at <210 °C. • Ethylene selectivity is greatest with 10% Fe_3O_4.	[103]
12-100.0 wt%	TiO_2 - γ. Al_2O_3	1	300-500	26-234	Micro channel reactor	100.0% @ 460 °C	98.7% @ 430 °C	• Both ethanol conversion and ethylene selectivity are highest with 10 wt% TiO_2 dopants.	[104]

Ethanol (%)	Catalyst	P (atm)	Temp (°C)	WHSV /LHSV(h^{-1}) /RPM	Reactor type	Conversion (max% @°C)	Selectivity (max% @ °C) of ethylene	Remarks	Ref
								• A high temperature is required to enhance the reaction rate at high LHSVs.	
-	NC1301 (alumina)	3	350-440	0.3-0.6	-	99.53-100.0%	99.57-100.0%	• The life cycle of the catalyst is nearly 12-18 months.	[105]
50-100.0 vol%	Activated alumina	-	410-440		Tubular -fixed bed	88%-98%	98% +	• With the feed flow rate decrease, selectivity increases to 100.0%, but the conversion rate decreases.	[106]
7.9 vol% in N_2	SiO_2	1	150-500	1.43	Tubular	33.4% @ 500 °C	81.0% @ 500 °C	• Al_2O_3> TiO_2> ZrO_2> MgO-Al_2O_3> SiO_2 is the trend of ethanol conversion over metal oxides without WO_3 doping, and this can be attributed to the strength of the Lewis acid sites and the polarizing power of ethanol. • Small amounts of other products (2% ethane + C_4 hydrocarbons) are also formed at 100.0% conversion. • The addition of WO_3 enhances catalytic activity; however, in some cases, the selectivity is lower because of the formation of the oligomer.	[107]
	MgO-Al_2O_3					100.0% @ 500 °C	56.4% @ 450 °C		
	ZrO_2					100.0% @ 400 °C	87.3% @ 500 °C		
	TiO_2					100.0% @ 400 °C	65.1% @ 500 °C		
	Al_2O_3					100.0% @ 350 °C	99.0% @ 450 °C		
	WO_3/SiO_2					100.0% @ 450 °C	92.6% @ 400 °C		
	WO_3/ZrO_2					100.0% @ 350 °C	99.0% @ 350 °C		
	WO_3/TiO_2 (H)					100.0% @ 300 °C	98.3% @ 350 °C		
	WO_3/TiO_2 (C)					100.0% @ 250 °C	92.7% @ 250 °C		
	WO_3/MgO-Al_2O_3					100.0% @ 500 °C	45.7% @ 450 °C		

Table 3. Scientific advancements in hetero-poly acids catalysts for the dehydration of ethanol to ethylene

Ethanol %	**Catalyst**	**P (atm)**	**Temp (°C)**	**WHSV /LHSV (h^{-1}) /RPM**	**Reactor type**	**Conversion (max % @ °C)**	**Selectivity (max% @ °C) of ethylene**	**Remarks**	**Ref**
48 vol% in He	Silicotungstic acid (STA), $H_4SiW_{12}O_{40}$	1	140-250	1.08 s.g/cm^3	Tubular	70.0% @ 250 °C	61.0% @ 250 °C	• The ethanol conversion trend follows STA>TPA>MPA, while the ethylene selectivity trend follows TPA>STA>MPA. • Diethyl ether and ethylene production follow parallel reaction routes. • The presence of water in the feed stream reduces ethanol conversion.	[108]
	Molybdophosphoric acid (MPA)					10.0% @ 250 °C	25.0% @ 250 °C		
48 vol% in He	Silica-supported tungstophosphoric acid (TPA), $H_3PW_{12}O_{40}.6H_2O$					53.0% @ 250 °C	74.0% @ 250 °C		
5 vol% in He						88.0% @ 250 °C	77.0% @ 250 °C		
5.7 mol% in He	Potassium dodecatungstophosphoric acid (HPW) salts K_xH_{3-x} $PW_{12}O_{40}/SiO_2$,	1	125-500	-	Flow-type	98.0% @ 470 °C, X = 1	-	• The samples with the lowest potassium levels show the highest catalytic activity for the monolayer Kx/SiO_2 series. Samples other than monolayer K_x/SiO_2, showed higher activity. • The Ag^{2+} salt activity is significantly higher than pure heteropolyacids activity. • The catalytic reaction occurs on the surface of the catalysts, which contain both Brønsted acid sites and redox centers.	[109]
	Silver dodecatungstophosphoric acid (HPW) salts Ag_xH_{3-x} $PW_{12}O_{40}/SiO_2$					95.0% @ 445 °C, X = 2	70.0% @ 400° C		
	Dodecatungstophosphoric acid (HPW) 30% $H_3PW_{12}O_{40}/SiO_2$					99.0% @ 475 °C	-		

Ethanol %	**Catalyst**	**P (atm)**	**Temp (°C)**	**WHSV /LHSV (h^{-1}) /RPM**	**Reactor type**	**Conversion (max % @ °C)**	**Selectivity (max% @ °C) of ethylene**	**Remarks**	**Ref**
80 wt%	Dodecatungstophosphoric acid $[H_3PO_4 \cdot 12WO_3 \cdot xH_2O]$ (DTPA)/montmorillonite	1	150-350	1.0	Fixed bed	74.0% @ 250 °C	92.0% @ 250 °C	• An increase in acidity favors the conversion and selectivity of ethylene. • Montmorillonite acts as a weak catalyst. • 30% m/m DTPA/montmorillonite shows the highest conversion and selectivity at 250 °C. • For very long spacetimes, the conversion of ethanol accelerates significantly.	[110]
	Dodecamolybedo-phosphoric acid $[H_3PO_4 \cdot 12MoO_3 \cdot 24H_2O]$ (PMA)/ montmorillonite					32.0% @ 250 °C	78.0% @ 250 °C		
	Sodium tungstate (hydrated purified) $[Na_{12}WO_4 \cdot 2H_2O]$ (STH)/ montmorillonite					45.0% @ 250 °C	89.0% @ 250 °C		
50 vol% in He	W-silicate-based mesoporous nanocomposite (TRC-92)	-	180-400	0.27 s.g/ cm^3	Fixed bed	85.0% @ 350 °C, calcination @ 400°C	100.0% @ 350 °C, calcination @ 400 °C	• At 350 and 400 °C, calcined catalysts demonstrate incredibly high activity. • By-product acetaldehyde was observed at low temperatures.	[111]
vapor in He	12-tungstophosphoric acid ($H_3PW_{12}O_{40}$, HPW) supported on 16.3 - 44.7% ceria-zirconia mixed oxide ($Ce_{0.8}Zr_{0.2}O_2$, CZ)	0.95	250-400	17	Programmed reaction temperature system	100.0% @ 250 °C, 26.4% HPW	100.0% @ 200 °C, 46.4% HPW	• As the HPW concentration increases, ethylene selectivity increases at lower temperatures. • At low temperatures (200-300 °C), a combination of catalyst compositions results in the simultaneous conversion of 100.0% ethanol and selectivity for ethylene.	[112]
99.8 wt%,	$GaPW_{12}O_{40}$ (GaPW)	0.013	110-250	-		80.0% @ 220 °C	100.0% @ 250 °C		[113]

Ethanol %	**Catalyst**	**P (atm)**	**Temp (°C)**	**WHSV /LHSV (h^{-1}) /RPM**	**Reactor type**	**Conversion (max % @ °C)**	**Selectivity (max% @ °C) of ethylene**	**Remarks**	**Ref**
	$AlPW_{12}O_{40}$ (AlPW)				Batch and differential flow reactors	-	100.0% @ 270 °C	• The specific surface area size does not significantly affect catalytic activity. Acid strengths influence the catalyst activity. • Compared to mono-cationic salts, bi-cationic catalysts with Cs doping have better catalytic activity.	
	$CsGa_{0.5}H_{0.5}PW_{12}O_{40}$ (CsGaHPW)					-	100.0% @ 250 °C		
	$CsAl_{0.5}H_{0.5}PW_{12}O_{40}$ (CsAlHPW)					-	100.0% @ 250 °C		
31 vol% in He	Tungstophosphoric acid (TPA, $H_3O_{40}PW_{12}{\cdot}nH_2O$) / AC	1	200-300	5 cm^3 min^{-1}	Fixed bed microreactor	90.0% @ 250 °C	100.0% @ 250 °C	• HPAs containing tungsten have better catalytic activity and stronger acidity than HPAs containing molybdenum because of their superior heat stability. • When the reaction temperature increases, ethylene production increases, but DEE production decreases. • Acetaldehyde and ethane are observed as by-products catalyzed by PMA because of the presence of some primary sites. • Acidity and activity follow the trend of TPA ≥ STA > PMA.	[114]
	Silicotungstic acid (STA, $H_4O_{40}SiW_{12}{\cdot}nH_2O$) / AC					55.0% @ 250 °C	100.0% @ 250 °C		
	Phosphomolybdic acid (PMA, $H_3Mo_{12}O_{40}P{\cdot}nH_2O$) / AC					10.0% @ 250 °C	26.0% @ 250 °C		
	Tungstophosphoric acid (TPA, $H_3O_{40}PW_{12}{\cdot}nH_2O$) / HSAG					90.0% @ 250 °C	97.0% @ 250 °C		
	Silicotungstic acid (STA, $H_4O_{40}SiW_{12}{\cdot}nH_2O$) / HSAG					55.0% @ 250 °C	85.0% @ 250 °C		
	Phosphomolybdic acid (PMA, $H_3Mo_{12}O_{40}P{\cdot}nH_2O$) / HSAG					10.0% @ 250 °C	23.0% @ 250 °C		

AC: Activated carbon

HSAG: High surface area graphite

Table 4. Scientific advancements in molecular sieve catalysts for the dehydration of ethanol to ethylene

Ethanol %	**Catalyst**	**P (atm)**	**Temp (°C)**	**WHSV /LHSV (h^{-1}) /RPM**	**Reactor type**	**Conversion (max % @ °C)**	**Selectivity (max% @ °C) of ethylene**	**Remarks**	**Ref**
Zeolite Socony Mobile-5 (ZSM-5) type									
20 vol%	ZSM-5	1	399	-	-	99.0% @ 399 °C	80.0% @ 399 °C	• At 298 °C, the ethanol conversion rate falls to 42%, with ethylene selectivity of 72%.	[115]
10 wt%	H-ZSM 5/TFA (Si/ Al - 10:1)	1	170-205	0.9-4.5	Flow-type reactor	99.2% @ 205 °C	99.9% @ 200 °C	• The highest conversion is at 200 °C but the highest selectivity is at 205 °C. • The conversion rate increases with WHSV but does not affect selectivity. • The best result is achieved at a WHSV of 1 h^{-1} at all temperatures and Si/Al ratios.	[70]
	H-ZSM 5/TFA (Si/ Al - 21:1)		200-285			95.8% @ 200 °C	99.3% @ 285 °C		
	H-ZSM 5/TFA (Si/ Al - 54:1)		200			72.0% @ 200 °C	98.1% @ 200 °C		
20 wt%	ZSM-5 (Si/Al - 25:1)	< 0.7	140-220	4	Differential packed-bed reactor	62.2% @ 220 °C	60.0% @ 140 °C	• Diethyl ether is formed in substantial amounts at low temperatures (<230 °C), and ethylene is the main product at high temperatures (>300 °C). • The rate constant is quite sensitive to the variations in the Si/Al ratio, and this sensitivity is more significant in the silica-rich H-ZSM-5 samples (Si/Al > 140) than in the samples with lower ratios.	[116]
	H-ZSM-5 (Si/Al - 37.5:1)					22.0% @ 140 °C	20.0% @ 140 °C		
2-19 vol%	ZSM-5 modified with	1	300-450	2.5	Fixed bed microreactor	99.0% @ 400 °C	82.0% @ 400 °C	• The amount of ethanol in the feed has a linear	[117]

Ethanol %	**Catalyst**	**P (atm)**	**Temp (°C)**	**WHSV /LHSV (h^{-1}) /RPM**	**Reactor type**	**Conversion (max % @ °C)**	**Selectivity (max% @ °C) of ethylene**	**Remarks**	**Ref**
	Zn and Mn (Si/Al - 29:1)							relationship with ethylene yield. • Selectivity to ethylene rises in the order: ZSM-5 ≤ ZSM-5/Zn ≤ ZSM-5/Zn-Mn.	
100.0 wt%	HZSM-5	0.13	450	-	Fixed bed micro-reactor	-	99.0% @ 277 °C	• Acetaldehyde and diethyl ether are produced as minor by-products at a low temperature. • The Cu-ZSM-5 zeolite undergoes a thorough oxidation of ethanol to produce CO_2 and CO.	[118]
	H-NaZSM-5					-	90.0% @ 327 °C		
	NaZSM-5					-	90.0% @ 577 °C		
	K-HZSM-5					-	90.0% @ 427 °C		
	Ca-HZSM-5					-	90.0% @ 527 °C		
	Cu-NaZSM-5					-	100.0% @ 327 °C		
	Co-NaZSM-5					-	100.0% @ 277 °C		
99.5 wt%	H-mordenites (HM20) - JRC-Z-HM20 (4), (Si/Al - 18.9:1)	1	180-300	-	Fixed bed flow-type	100.0% @ 180 °C	99.8% @ 180 °C	• Diethyl ether, trace amounts of ethane, acetaldehyde, propene, and butenes are the by-products of dehydration. • Catalyst activity decreases in this order: HM20 > HM90 > ZSM5-25 > HB25 > ZSM5-90 > HY5.5 > SA. • The amount of potent Brønsted acid sites may be associated with the catalyst activity during dehydration.	[119]
	H-mordenites (HM90) - JRC-Z-HM90 (2), (Si/Al - 90:1)					100.0% @ 180 °C	99.9% @ 180 °C		
	Zeolites (HZSM5-25) - JRC-Z5-25H, (Si/Al - 25:1)					100.0% @ 180 °C	95.9% @ 180 °C		
	Zeolites (HZSM5-90) - JRC-Z5-90H, (Si/Al - 90:1)					100.0% @ 200 °C	31.9% @ 200 °C		

Ethanol %	**Catalyst**	**P (atm)**	**Temp (°C)**	**WHSV /LHSV (h^{-1}) /RPM**	**Reactor type**	**Conversion (max % @ °C)**	**Selectivity (max% @ °C) of ethylene**	**Remarks**	**Ref**
	H-beta-zeolite (HB25) - JRC-Z-HB25 (1), (Si/Al - 25:1)					100.0% @ 180 °C	57.5% @ 180 °C	• For HM20, HM90, ZSM5-25, ZSM5-90, HB25, HY5.5, and SA, the proportion of Brønsted acid sites was calculated to be 83%, 95%, 94%, 92%, 33%, and 50%.	
	H-Y zeolite (HY5.5) - JRC-ZHY5.5, (Si/Al - 5.6:1)					100.0% @ 250 °C	71.3% @ 250 °C		
	Silica-alumina(SA) - JRC-SAL-2, (Si/Al - 9.2:1)					100.0% @ 300 °C	76.7% @ 300 °C		
≥99.9 wt%	HZSM-5 (SiO_2/Al_2O_3 - 25:1)	1	280-440	3	Fixed bed (continuous flow)	100.0% @ 280 °C	98.3% @ 280 °C	• The HZSM-5 framework's dealumination causes the catalyst's acidity to decrease as P loading increases significantly. This decrease in acidity increases ethylene selectivity by up to 3.6%. • Higher hydrocarbons are also found at high temperatures. • A high reaction temperature is required for ethanol dehydration to ethylene because the P concentration is higher than 3.4 wt%. • Because of the shape-selective effect brought on by the narrow channel size of the catalyst, where higher hydrocarbons cannot pass through the pores: the ethylene selectivity is very high (99.4%) between 300 and 440 °C, whereas that of higher hydrocarbons is	[93]
	PZ-1.9 (SiO_2/Al_2O_3 - 25:1, P-1.9%)					100.0% @ 300 °C	97.1% @ 280 °C		
	PZ-3.2 (SiO_2/Al_2O_3 - 25:1, P-3.2%)					100.0% @ 340 °C	99.0% @ 300 °C		
	PZ-3.4 (SiO_2/Al_2O_3 - 25:1, P-3.4%)					100.0% @ 340 °C	99.8% @ 300 °C		
	PZ-3.6 (SiO_2/Al_2O_3 - 25:1, P-3.6%)					100.0% @ 340 °C	99.6% @ 400 °C		
	PZ-5.1 (SiO_2/Al_2O_3 - 25:1, P-5.1%)					100.0% @ 400 °C	99.6% @ 440 °C		

Ethanol %	**Catalyst**	**P (atm)**	**Temp (°C)**	**WHSV /LHSV (h^{-1}) /RPM**	**Reactor type**	**Conversion (max % @ °C)**	**Selectivity (max% @ °C) of ethylene**	**Remarks**	**Ref**
								relatively low, even at high temperatures.	
50 wt%	3 wt% La-modified HZSM-5	≤ 0.5	200-300	1.1	Tubular reactor	98.5% @ 260 °C	99.5% @ 260 °C	• An LHSV below 2.5 h^{-1} could result in 99% ethanol conversion. • The ethanol dehydration process is more favorable at higher reaction temperatures.	[71]
90 wt%	H-ZSM-5 (Si/Al -14:1)	1	245-260	1.2-2.0	Fixed bed micro-reactor	99.0% @ 260 °C	87.0% @ 260 °C	• The ethanol conversion and ethylene selectivity increase with a lower Si/Al. • Higher conversion ought to result from increased acidic density (Brønsted acid) caused by increased aluminum in the zeolite framework. • Regardless of the WHSV, the rise in temperature leads to increased ethanol conversion. • The conversion at low temperature increases as the WHSV decreases.	[120]
	H-ZSM-5 (Si/Al - 23:1)					96.0% @ 250 °C	98.0% @ 250 °C		
	H-ZSM-5 (Si/Al - 30:1)					95.0% @ 250 °C	98.0% @ 250 °C		
	H-ZSM-5 (Si/Al - 50:1)					92.0% @ 250 °C	97.0% @ 250 °C		
	H-ZSM-5 (Si/Al - 80:1)					90.0% @ 250 °C	96.0% @ 250 °C		
	H-ZSM-5 (Si/Al - 280:1)					60.0% @ 250 °C	18.0% @ 250 °C		
	H-ZSM-5 treated with NaOH (Si/Al - 12:1)					99.0% @ 260 °C	87.0% @ 260 °C		
	H-ZSM-5 treated with ammonium hexafluorosilicate (AHFS) (Si/Al -15:1)					99.0% @ 260 °C	85.0% @ 260 °C		
	H-ZSM-5 treated with pseudomorphic synthesis (Si/Al - 10:1)					99.0% @ 260 °C	80.0% @ 260 °C		
20 vol%	HZSM-5, without Hydrothermal treatment	1	220-290	2.37	Tubular-Fixed bed reactor	100.0% @ 260 °C	100.0% @ 250 °C	• When the temperature rises, ethylene production's	[120, 121]

Ethanol %	**Catalyst**	**P (atm)**	**Temp (°C)**	**WHSV /LHSV (h^{-1}) /RPM**	**Reactor type**	**Conversion (max % @ °C)**	**Selectivity (max% @ °C) of ethylene**	**Remarks**	**Ref**
	(Si/Al - 25.5:1)							selectivity increases, and diethyl ether's selectivity drops. • The selectivity to ethylene over the parent HZSM-5 decreases at relatively high temperatures (255-270 °C) because of the formation of higher hydrocarbons. In contrast, the selectivity of ethylene over steam-treated catalysts increases because of the abrupt reduction of strong acidic sites in steam-treated HZSM-5.	
	HZSM-5, Hydrothermal treatment at 400 °C (Si/Al – 28.5:1)					100.0% @ 270 °C	95.0% @ 270 °C		
	HZSM-5, Hydrothermal treatment at 450 °C (Si/Al – 29.4:1)					97.0% @ 270 °C	98.0% @ 275 °C		
	HZSM-5, Hydrothermal treatment at 500 °C (Si/Al – 28.5:1)					97.0% @ 270 °C	98.0% @ 275 °C		
	HZSM-5, Hydrothermal treatment at 550 °C (Si/Al – 28.9:1)					94.0% @ 290 °C	98.0% @ 290 °C		
95 vol%	Nanoscale HZSM-5 (SiO_2/Al_2O_3 – 26:1)	1	240	1	Fixed bed (vertical, downflow)	100.0% @ 240 °C	98.7% @ 240 °C	• The nanoscale HZSM-5 zeolite catalyst shows high coke resistance and stability compared to the microscale HZSM-5 zeolite. • The nanoscale HZSM-5 catalyst's product distribution is similar to that of the microscale HZSM-5.	[122]
	microscale HZSM-5 (SiO_2/Al_2O_3 - 25:1)					99.0% @ 240 °C	98.0% @ 240 °C		
45 vol%	Nanoscale HZSM-5 (SiO_2/Al_2O_3 - 26:1)			0.8		98.0% @ 240 °C	97.6% @ 240 °C		
	microscale HZSM-5 (SiO_2/Al_2O_3 - 25:1)					97.5% @ 240 °C	95.6% @ 240 °C		
-	ZSM-5	1	160-220	2.4	Fixed bed micro-reactor	90.0% @ 220 °C	88.0% @ 220 °C	• The formation of diethyl ether is favored at a low-temperature range (e.g., between 180 and 200 °C) over Cu-loaded ZSM-5 catalysts, and ethylene is favored at temperatures above 200 °C over pure ZSM-5 or Fe/ZSM-5.	[123]
	Cu_5/ZSM-5 (Cu - 5%)					88.0% @ 220 °C	28.0% @ 220 °C		
	Cu_2/ZSM-5 (Cu - 2.5%)					83.0% @ 220 °C	43.0% @ 220 °C		
	Fe_2Cu_2/Z (Cu - 2.5%, Fe - 2.5%)					75.0% @ 220 °C	50.0% @ 220 °C		

Ethanol %	Catalyst	P (atm)	Temp (°C)	WHSV /LHSV (h^{-1}) /RPM	Reactor type	Conversion (max % @ °C)	Selectivity (max% @ °C) of ethylene	Remarks	Ref
	Fe_5/Z (Fe - 2.5%)					63.0% @ 220 °C	83.0% @ 220 °C		
50 wt%	HZSM-5 (SiO_2/Al_2O_3 - 50:1)	1	200-300	2.0	Fixed bed	100.0% @ 200 °C	98.2% @ 200 °C	• Adding some lanthanum to the 2% PHZSM-5 catalyst increases the catalytic performance. • The selectivity of ethylene increases markedly at relatively high temperatures (240-260 °C).	[4]
	2% PHZSM-5					100.0.0% @ 260 °C	97.4% @ 260 °C		
	0.25% La - 2% PHZSM-5					100.0.0% @ 260 °C	99.9% @ 260 °C		
	0.5% La - 2% PHZSM-5					100.0% @ 240 °C	99.9% @ 240 °C		
	1% La - 2% PHZSM-5					100.0% @ 260 °C	99.9% @ 240 °C		
	0.5% LaHZSM-5					100.0% @ 240 °C	99.8% @ 240 °C		
-	H-ZSM-5 (NH4-ZSM-5 zeolite, Zeolyst CBV, Si/Al - 30:1)	1	250-450	-	Fixed bed micro-reactor (continuous Flow)	100.0% @ 400 °C	10.0% @ 400 °C	• With an increase in H_3PO_4, the selectivity towards ethylene rises noticeably, i.e., over 98% on the 20HPZSM-5. • With an increase in temperature, both conversion and ethylene selectivity rise. • Catalysts treated with H_3PO_4 demonstrate substantially higher stability; deactivation is not noticed until 110 hours of operation. • High selectivity towards ethylene by defeating other products (i.e., higher olefins and aromatics) is seen after the phosphorus modification, which can be attributed to modifying the	[124]
	5HP-ZSM-5 (NH4-ZSM-5 zeolite, Zeolyst CBV, Si/Al - 30:1 with 5% H_3PO_4)					100.0% @ 400 °C	38.0% @ 400 °C		
	10HPZSM-5 (NH4-ZSM-5 zeolite, Zeolyst CBV, Si/Al - 30:1 with 10% H_3PO_4)					100.0% @ 400 °C	90.0% @ 400 °C		
	15HPZSM-5 (NH4-ZSM-5 zeolite, Zeolyst CBV, Si/Al - 30:1 with 15% H_3PO_4)					100.0% @ 400 °C	95.0% @ 400 °C		
	20HP-ZSM-5 (NH4-ZSM-5 zeolite, Zeolyst CBV, Si/Al -					100.0% @ 400 °C	99.0% @ 400 °C		

Ethanol %	**Catalyst**	**P (atm)**	**Temp (°C)**	**WHSV /LHSV (h^{-1}) /RPM**	**Reactor type**	**Conversion (max % @ °C)**	**Selectivity (max% @ °C) of ethylene**	**Remarks**	**Ref**
	30:1 with 20% H_3PO_4)							acid strength distribution by selectively reducing the number of strong acid sites.	
95 wt%	ZSM-5 (Zeolyst)	1	250-450	1.5	Fixed bed (U-type)	92.0% @ 280 °C	97.1% @ 280 °C	• Modifying the ZSM-5 catalyst through dealumination improves its catalytic performance and anti-coking ability to dehydrate ethanol to ethylene at a low temperature.	[125]
	ZSM-5-deAl-1/25					99.9% @ 280 °C	94.8% @ 240 °C		
	ZSM-5-deAl-1/50					98.5% @ 280 °C	100.0% @ 280 °C		
	ZSM-5-deAl-1/100.0					98.9% @ 280 °C	100.0% @ 280 °C		
	ZSM-5-P					99.8% @ 240 °C	94.4% @ 240 °C		
	ZSM-5-La					97.7% @ 240 °C	93.3% @ 240 °C		
Silico-alumino-phosphate materials SAPO-n type									
≥99.9 wt%	ZSM-5	1	400	2.37	Fixed bed (continuous flow)	81.9% @ 400 °C	58.0% @ 400 °C	• At 400 °C, both the SAPO-34 and SAPO-34@ZSM-5 composite demonstrate a comparatively high ethanol conversion. • The overall selectivity towards ethylene increases from 74% over ZSM-5 to 80 and 99% over SAPO-34@ZSM-5 and silicalite-1@ZSM-5, respectively.	[126]
	SAPO-34					89.8% @ 400 °C	96.0% @ 400 °C		
	SAPO-34@ silicalite-1 (composite)					65.8% @ 400 °C	65.0% @ 400 °C		
	SAPO-34@ZSM-5 (composite)					84.5% @ 400 °C	99.5% @ 400 °C		
	SAPO-34/ZSM-5 (mechanically mixed)					86.6% @ 400 °C	60.0% @ 400 °C		
(≥99.9 wt%	NiAPSO-34	0.7	240-440	3	Fixed bed	97.0% @ 380 °C	98.0% @ 340 °C	• With the increase in temperature, an increase in ethanol conversion was observed.	[94]
	SAPO-34					92.0% @ 380 °C	94.0% @ 340 °C		
≥99.9 wt%	SAPO-11, $(Si_{2.54}Al_{19.4}P_{18.1})O_{80}$	1	240-440	2	Fixed bed micro-reactor	97.0% @ 340 °C	92.0% @ 240 °C		[72]

Ethanol %	**Catalyst**	**P (atm)**	**Temp (°C)**	**WHSV /LHSV (h^{-1}) /RPM**	**Reactor type**	**Conversion (max % @ °C)**	**Selectivity (max% @ °C) of ethylene**	**Remarks**	**Ref**
	SAPO-34, $(Si_{5.68}Al_{33.48}P_{27.28})O_{130}$					55.0% @ 340 °C	65.0% @ 340 °C	- The SAPO-11 surface is unfavourable for catalytic processes when Mn^{2+} or Zn^{2+} are present. - Mn^{2+} or Zn^{2+} modified SAPO-34, on the other hand, perform better than SAPO-34. - In the following order, ethanol conversion and ethylene selectivity decrease: Mn-SAPO-34 > Zn-SAPO-34 > SAPO-11 > Mn-SAPO-11 > Zn-SAPO-11 > SAPO-34.	
	Mn-SAPO-11					94.0% @ 340 °C	77.0% @ 340 °C		
	Zn-SAPO-11					85.0% @ 340 °C	70.0% @ 340 °C		
	Mn-SAPO-34					99.0% @ 340 °C	98.0% @ 340 °C		
	Zn-SAPO-34					97.0% @ 340 °C	94.0% @ 340 °C		

Ethylene oligomerization

After the dehydration process, the produced ethylene can be turned into linear and branched higher olefins through the catalytic oligomerization reaction, which is as follows [69, 127]:

$nC_2H_4 \rightarrow C_{2n}H_{4n}$; n=2, 3 (6)

The catalytic oligomerization of ethylene to C_8-C_{16} olefins is essential for jet fuel production because the rest depends on this step. Several catalytic methods have been devised for the oligomerization of ethene to produce straight-chain alkenes. The relevant reaction conditions are influenced by the catalyst and starting material [33].

Current commercial processes in producing higher-range olefins by ethylene oligomerization use homogeneous and heterogeneous catalysts. When products, reactants, and catalysts are all in the same phase and all dissolved in the same solvent, homogeneous catalysis occurs [29]. The Shell higher olefin process (SHOP), created by Shell Oil Company, the Ziegler one-step process, used by Chevron Phillips (with a capacity of 680,000 metric tonnes/year in 2002); and the Ziegler two-step process, used by Ethyl Corporation are the three most popular commercial homogeneous catalytic technologies for ethylene oligomerization (now under INEOS Corporation, with a capacity of 470,000 metric tonnes per year as of 2002)[18].

The catalyst used in SHOP belongs to homogeneous transition metal catalysts (i.e., complexes of Ni, Ti, Cr, Zr, Ta, Co, Fe, Hf, W, etc.). Light olefins such as ethylene monomers are oligomerized through the chain growth in the electropositive transition sites of metals such as V, Zr, Ti, and Ni [128]. The SHOP catalyst has two parts: the Ni atom, the primary active metal, and the PO- group, which acts as a ligand and 1,4-butanediol as a solvent. The reaction happens at 90 °C-100 °C and 80-100 bar [69, 129]. The homogeneous nickel/phosphorous ligand, where PO- is near the Ni atom, allows the control of carbon number distribution in the oligomerization reaction [129].

The Ziegler one-step and two-step oligomerization procedures use the same tri-ethyl-aluminum catalyst but have different reaction parameters (i.e., pressure, temperature, and catalyst feed ratio). In the one-step Ziegler reaction, which takes place at 200 °C and 250 bar, 1×10^{-4} moles of catalyst are needed for every mole of ethylene, whereas in the two-step Ziegler reaction, which takes place at 90 °C and 120 °C and 100 bar, the stoichiometric catalyst is needed for the products [69]. Following the Schultz-Flory distribution, the single-step Ziegler reaction and SHOP both result in linear α-olefins with chain growth propagation (also known as a K-value) values of 0.75-0.8 and 0.5-0.75, respectively. On the other hand, the two-step Ziegler reaction produces olefins in the jet range with a Poisson distribution rather than the Schulz-Flory distribution [69]. Homogeneous catalysts typically have more activity and selectivity than heterogeneous ones, allowing them to specifically target more suitable olefins for the jet range, including hexene and octene, rather than creating a diverse range of products [29, 128]. Catalysts must be added in minimal amounts and have a high turnover frequency to be economically viable for industrial operations, and the catalyst and product separation should be convenient.

Heterogeneous catalysts are created by connecting the organometallic complexes to specific catalytic supports, such as MCM-41, a mesoporous aluminosilicate, or silica. Ni-containing porous materials have been characterized as effective catalyst systems for the oligomerization of ethylene, including Ni-exchanged amorphous silica-alumina, Ni-zeolites, Ni-AlMCM-41, Ni/sulfated alumina, and Ni-AlSBA-15 [127]. The amount of accessible Ni sites in these Ni-based catalysts for converting ethylene to olefins justifies their catalytic activity [127]. Over the years, researchers have investigated Ni-exchanged catalysts with large pores that are very active and resistant to deactivation, such as Ni- AlSBA-15, Ni-AlMCM-41, Ni-SiO_2-Al_2O_3, and Ni-AlMCM-48 [127, 130]. Andrei et al. reported that Ni-AlSBA-15 is the most active and stable Ni-exchanged catalyst for ethylene oligomerization in batch and continuous processes [86]. This is due to their larger interconnected mesopores, which allow movement of the heavier oligomer, leading to a lower deactivation rate. Improvements in different catalytic systems are listed in **Table 5** [127, 130].

Pathways other than ethylene oligomerization

Several pathways are available for the production of jet fuel from ethanol. As discussed, one of those is the intermediate product, ethylene. However, direct oligomerization from ethylene to jet-range paraffins is challenging, given the lower yield and selectivity and higher demand for the recycling and separation processes. Hence, there are several alternative pathways in which either ethanol or the intermediate product ethylene is converted to another intermediate olefin (such as butene or hexene), a range of intermediate olefins, or other intermediates before further oligomerization to produce jet range olefins [29]. These pathways are:

1. The conversion of ethylene to butene/hexene intermediate,
2. The conversion of ethanol to propylene,
3. The conversion of ethanol to a higher alcohol intermediate (Guerbet reaction), and
4. The conversion of ethylene to a carbonyl intermediate.

Table 5. Scientific advancements in catalysts for the oligomerization of ethylene to olefins

Ethylene (%)	**Catalyst**	**P (bar)**	**Temp (°C)**	**WHSV /LHSV (h^{-1}) /RPM**	**Reactor type**	**Conversion (max % @ °C)**	**Selectivity (max% @ °C) of Jet range olefins**	**Remarks**	**Ref**
Homogeneous catalysts – SHOP process									
99 vol%	Nickel/ phosphorous ligand catalyst with 1,4-butanediol as a solvent	80-100	90-100	-	Coil-tubed reactors	-	-	• The chain growth propagation (also known as a K-value) values of the linear α-olefins produced by the SHOP method range from 0.75 to 0.8, following the Schultz-Flory distribution. .	[69]
Homogeneous catalysts – Ziegler one-step process									
99 vol%	Triethylaluminium catalyst	250	200	-	Tubular	-	61.0%	• The triethylaluminium catalyst is used in the one- and two-step Ziegler oligomerization procedures; however, the reaction environment (temperature, pressure, and catalyst feed ratio) varies.	[69]
Homogeneous catalysts – Ziegler two-step process									
99 vol%	Triethylaluminium catalyst	100	90-120	1.9	Tubular	100.0%	95.0%	• Unlike the olefins from the Schulz-Flory distribution, the two-step Ziegler process produces a primarily Poisson distribution of jet-range olefins,	[69]

Ethylene (%)	**Catalyst**	**P (bar)**	**Temp (°C)**	**WHSV /LHSV (h^{-1}) /RPM**	**Reactor type**	**Conversion (max % @ °C)**	**Selectivity (max% @ °C) of Jet range olefins**	**Remarks**	**Ref**
								• The two-step Ziegler method requires few reactions to produce jet-range hydrocarbons and regenerate the catalyst.	
Other homogeneous reactors									
4:1, H_2:C_2H_4	Cr-SIM-NU-100.00	30-50	80-110	2	Parr reactor	20.0% @ 25 °C, 5 bar	79.0% @ -25 °C, 5 bar	• At low pressure and ambient temperature, Cr-SIM-NU-100 demonstrated high ethylene oligomerization activity with noticeably less cocatalyst additions.	[131]
Heterogeneous catalysts									
99.9 vol%	Ni/SIRAL-30, (SiO_2:Al_2O_3 - 30:70)	10	200-550	0.250-0.750	Fixed bed reactor	71.0% @ 200 °	38.0% @ 200 °C	• Because of the greater surface acidity brought on by a high Al/Si ratio, the amount of C_{10+} products formed over Ni (4 wt%)/SIRAL-30 was noticeably larger than that produced by Ni-AlSBA-15	[132]
						99.0% @ 550 °C	39.0% @ 550 °C		
						99.0% @ 550 °C	36.0% @ 550 °C		
99 vol%	Ni-AlSBA-15, (1.9 wt% Ni and Si/Al - 9:1)	5-15	150-200	0.375-0.899	Fixed bed	99.0% @ 200 °C	69.0% @ 100.0 °C	• This process integrates the oligomerization of ethylene over Ni-AlSBA-15 and the co-oligomerization of the oligomeric mixture over Amberlyst 35 dry ion-exchange resin.	[127]
	Amberlyst 35	30	100	0.375	Autoclave	98.0% @ 100.0 °C	82.0% @ 100.0 °C		
99 vol%	Ni/Siral-30, (SiO_2/Al_2O_3 -	10	200-350	0.375		89.0% @ 250 °C	42.0% @ 250 °C		[133]

Ethylene (%)	**Catalyst**	**P (bar)**	**Temp (°C)**	**WHSV /LHSV (h^{-1}) /RPM**	**Reactor type**	**Conversion (max % @ °C)**	**Selectivity (max% @ °C) of Jet range olefins**	**Remarks**	**Ref**
	30:70)				Fixed bed micro-reactor			• For catalysts, liquid product conversion rate and yield decrease with increased temperature. Although the selectivity to C_{10+} and the proportion of $C_{10\sim19}$ are both low at low temperatures; 250 °C is considered ideal.	
	Ni/Siral-30 + H-ZSM-5A					95.0% @ 250 °C	62.0% @ 250 °C		
	Ni/Siral-30 + H-ZSM-5B					80.0% @ 250 °C	73.0% @ 250 °C		
99 vol%	Ni-Hβ, (CP814E, SiO_2/Al_2O_3 - 25:1	11.2-22.4	120	5.5	Packed bed	100.0% @ 120 °C, 22.4 bar	28.0% @ 120 °C, 11.2 bar	• The transition from subcritical (120 °C and 11.2/22.4 bar) to supercritical (at 120 °C and 52.5 bar) conditions impact the products' conversion and selectivity.	[134]
	Ni-Al-SBA-15	42-53.2				98.0% @ 120 °C, 53.2 bar	7.0% @ 120 °C, 42 bar		
99 vol%	NiAlKIT-6	1-20	250-350	0.28-1.12	Fixed bed (continuous flow)	95.9% @ 300 °C, 20 bar	56.6% @ 300 °C, 20 bar	• The acidic content and Ni % greatly influence the catalytic activity and selectivity for C_{8+}. • A significant portion of aromatic hydrocarbons is produced via aromatization due to high acid strength. • Ni active sites either start the dimers' dimerization or further oligomerization. A high Al concentration alters	[135]
	2NiAlKIT-6 (10), (Si/Al - 10:1, 2% Nickel)					58.1% @ 300 °C, 20 bar	33.6% @ 300 °C, 20 bar		
	4NiAlKIT-6 (5) (Si/Al - 5:1, 4% Nickel)					68.4% @ 300 °C, 20 bar	39.7% @ 300 °C, 20 bar		
	4NiAlKIT-6 (10) (Si/Al - 10:1, 4% Nickel)					84.3% @ 300 °C, 20 bar	46.9% @ 300 °C, 20 bar		
	4NiAlKIT-6 (15) (Si/Al - 15:1, 4% Nickel)					73.6% @ 300 °C, 20 bar	35.6% @ 300 °C, 20 bar		

Ethylene (%)	**Catalyst**	**P (bar)**	**Temp (°C)**	**WHSV /LHSV (h^{-1}) /RPM**	**Reactor type**	**Conversion (max % @ °C)**	**Selectivity (max% @ °C) of Jet range olefins**	**Remarks**	**Ref**
	6NiAlKIT-6 (10) (Si/Al=10:1, 6% Nickel)					89.4% @ 300 °C, 20 bar	45.3% @ 300 °C, 20 bar	the mother catalyst's structure, reducing its catalytic activity.	
99 vol%	Platelet Ni-AlSBA-15 (15 mesoporous silica)	1-20	150-350	0.56-4.5 h^{-1}	Fixed bed	100.0% @ 300 °C, 20 bar	34.0% @ 300 °C, 20 bar	• The ideal reaction condition: temperature of 275-300 °C, pressure of 20 bar, and a WHSV of 0.56 h^{-1}. • Using non-Schulz-Flory type hydrocarbon distribution, ethylene conversion of 98-99 mol% was accomplished under the optimal reaction conditions.	[136]
90 vol% (10% Ar)	Ni/Al-HMS (mesoporous silica, prepared by sol-gel reaction)	10	200	-	Fixed bed	96.3% @ 200 °C	33.1% @ 200 °C	• Ni sites are the primary active sites in ethylene oligomerization.	[137]
	Ni/Al-HMS (prepared by post-modification)					45.0% @ 200 °C	45.5% @ 200 °C		
	Ni/Al-MCM-41					95.2% @ 200 °C	22.5% @ 200 °C		
99.95 vol%	NiO_x/SA-001 (Si/Al=0.01:1, Ni=3.81 wt%)	10	200	0.375 h^{-1}	Fixed bed (continuous flow)	60.0% @ 200 °C	28.0% @ 200 °C	• The average ethylene conversion drops in the following order: NiO_x/SA-047> NiO_x/SA-028> NiO_x/SA-007 > NiO_x/SA-001> NiOx/SA-386,	[138]
	NiO_x/SA-007 (Si/Al =0.07:1, Ni =3.41 wt%)					74.0% @ 200 °C	52.0% @ 200 °C		
	NiO_x/SA-028 (Si/Al =0.28:1, Ni =3.94 wt%)					85.0% @ 200 °C	36.0% @ 200 °C		

Ethylene (%)	**Catalyst**	**P (bar)**	**Temp (°C)**	**WHSV /LHSV (h^{-1}) /RPM**	**Reactor type**	**Conversion (max % @ °C)**	**Selectivity (max% @ °C) of Jet range olefins**	**Remarks**	**Ref**
	NiO_x/SA047 (Si/Al =0.47:1, Ni =3.85 wt%)					95.0% @ 200 °C	55.0% @ 200 °C	• In addition to having the lowest ethylene conversion, NiO_x/SA-386:1 also has the lowest selectivity to C_{10+}. • Despite having many acid sites, NiO_x/SA-386:1 has a poor metal oxide-support interaction and little catalytic activity because of the buildup of NiO_x particles on the surface.	
	NiO_x/SA-386 (Si/Al =3.86:1, Ni =3.80 wt%)					48.0% @ 200 °C	7.0% @ 200 °C		
99.95 vol%	Ni-SiO_2-Al_2O_3 (Ni:Si =25:1, Ni =1.36 wt%)	35	200-400	2 h^{-1}	Fixed bed micro-reactor	98.0% @ 200 °C	35.0% @ 300 °C	• A low Si/Al ratio and high aging and activation temperature can improve catalytic performance to produce more C_{10+} products. • Higher C_{10+} generation depends more on high Ni loading than surface area or acid concentration.	[139]
	Ni-SiO_2-Al_2O_3 (Ni:Si =15.2:1, Ni =1.45 wt%)					98.0% @ 200 °C	43.0% @ 300 °C		
	Ni-SiO_2-Al_2O_3 (Ni:Si =7.7:1, Ni =1.94 wt%)					98.0% @ 200 °C	55.0% @ 300 °C		
99.99 vol%	8Ni_2P/SiO_2, (Ni=8.5 wt%, P=9.9 wt%)	10-35	230	-	Batch reactor (Parr Instruments)	-	29.5% @ 230 °C	• The Ni_2P/SiO_2 with the lowest particle size performed best. • The Brønsted acid sites created by PO-H groups on the catalyst surface impacted oligomerization activity	[129]
	8Ni_2P/SiO_2-Al_2O_3 (Ni=7.3 wt%, P=12.3 wt%)						31.1% @ 230 °C		
	8Ni_2P/Al_2O_3, (Ni=7.2 wt%, P=13 wt%)						15.1% @ 230 °C		

Ethylene (%)	**Catalyst**	**P (bar)**	**Temp (°C)**	**WHSV /LHSV (h^{-1}) /RPM**	**Reactor type**	**Conversion (max % @ °C)**	**Selectivity (max% @ °C) of Jet range olefins**	**Remarks**	**Ref**
	8NiO/SiO_2 (Ni=9.2 wt%)						26.3% @ 230 °C	because the acidity encouraged cationic oligomerization and the isomerization of terminal olefins.	
	16P_xO_y/SiO_2, (P=11.7 wt%)						27.2% @ 230 °C		

Industrially viable full-scale conversion technologies exist for turning ethylene into butene and then butene into higher hydrocarbons in the jet range. Heterogeneous or homogeneous catalysts can convert ethylene to olefins, primarily in the C_4 and C_6 range. In the ethylene-to-butene process, heterogeneous nickel-exchanged AlMCM-41 works at 150 °C, 3.5 MPa, and 1 h^{-1}, which produces linear and branched olefins. Commercially available homogeneous catalysts with product selectivity principally towards butene (80%) and hexene (18%) are used with ethylene conversions greater than 95%. Butenes are further selectively oligomerized to form jet-range oligomers. The next stage, similar to the direct ethylene conversion method, is to hydrotreat the α-olefins to produce the final product [29].

With a homogeneous Cp_2ZrCl_2/methylaluminoxane (MAO) catalyst, 1-hexene can be created as an intermediate and fully converted (100%) to jet fuel with higher than 80% selectivity to a mixture of the dimers [29, 140]. The by-product trimer can be separated into diesel fuels. 1-hexene technology is extensively developed and has a turnover frequency of more than 17,000, making it cheap for industrial applications [29]. The notable scientific research work and outputs of these processes are summarized in **Table 6**.

Propylene is more easily oligomerized than ethylene; however, the dehydration of ethanol to propylene produces lower yields, requiring higher recycles of unconverted ethanol. With an increase in temperature, the conversion of ethanol to propylene increases, but selectivity towards ethylene also increases because of the dominance of the ethanol dehydration reaction at higher temperatures [29, 141]. The HZSM-5 zeolite is usually used to produce propylene from ethanol. Alkaline earth metals, Sc, and La, and the dealumination of the HZSM-5 zeolite have all been described as modifications that can be made to increase propylene production [29, 141]. Despite these changes, these procedures produce lower molecular weight alkanes that are less suitable for producing jet fuel [141, 142]. However, the suggested reaction process incorporates dimerization to butene as a primary by-product equally appropriate for conversion to jet fuel, resulting in higher conversion and propylene yield at 400 °C [143].

The Guerbet reaction, named after its creator Marcel Guerbet, is a term used to describe the binding of alcohol molecules with their carbon atoms, which involves the dehydration of two molecules of alcohol to produce a dimer [29, 144]. When ethanol is subjected to the Guerbet reaction, butanol is produced (Equation 7) [29].

$$2CH_3CH_2OH \rightarrow CH_3\,CH_2CH_2CH_2OH + H_2O \tag{7}$$

Direct condensation of two alcohol molecules, the predominant approach, is one of several methods that have been postulated for the mechanism of the Guerbet reaction. Alcohols such as butanol can be converted to higher alcohols via the Guerbet reaction with other butanol molecules or ethanol [29, 144]. Butanol and/or higher alcohols can then be dehydrated and oligomerized to make jet-range fuel. Higher alcohols are more susceptible to the Guerbet reaction, but ethanol is more resistant to the dehydrogenation reaction, so more research is being done in this area [145, 146]. Various catalyst systems, i.e., homogeneous, heterogeneous, and homogeneous/heterogeneous, have been studied for the Guerbet reaction [144, 147, 148].

Jet fuel can also be made from alcohols using the hydroformylation or "oxo synthesis" process, which starts with readily available alkenes created during dehydration [29]. In the hydroformylation step, alkenes are reacted with syngas (CO and H_2) to produce aldehydes in a homogeneously catalyzed industrial process. The aldehydes produced are then hydrogenated into a higher alcohol and dehydrated to higher olefins for further processing into final fuels. As ethylene is already available as the starting molecule, this method produces olefins higher than ethylene, which oligomerizes more readily than ethylene. This method's drawback is that the hydroformylation stage needs a supply of low-cost, renewable syngas (produced from biomass or waste gas); others have noted that still more research is needed in this area [29, 149].

The processes described above should be assessed for implementation at an industrial level based on parameters such as the fraction of ethanol converted to jet fuel, the selectivity of the desired range of intermediates and final jet range products, feedstock type and availability, process simplicity, the cost of the feedstocks and catalyst, the technology readiness level (TRL), etc.[29]. Details about these processes are listed in **Table 6**.

Table 6. Scientific advancements in catalysts for the oligomerization of ethylene to C_4-C_{16} range alkenes through intermediate olefins

Feed (%)	Catalyst	P (atm)	Temp (°C)	WHSV /LHSV (h-1) /RPM	Reactor type	Conversion (max % @ °C)	Selectivity (max% @ °C) of Jet range alkenes	Remarks	Ref
Conversion of ethylene to butene intermediate									
Ethylene	NiMSA10	35	150	800 rpm	Well-mixed gas-slurry reactor	max % @ 150 °C	99.0% @ 150 °C	• The selectivity for 1-butene is increased by a greater Si/Al ratio (lower acid site density). • At rising temperatures, the selectivity for 1-butene significantly declines.	[150]
	NiMSA20						98.0% @ 150 °C		
	NiMSA30						99.0% @ 150 °C		
	NiMSA50						98.0% @ 150 °C		
	NiMSA80						97.0% @ 150 °C		
	NH4MSA50						99.0% @ 150 °C		
Conversion of ethylene to hexene intermediate									
Ethylene	NiMSA10	35	150		Well-mixed gas-slurry reactor	max % @ 150 °C	75.7% @ 150 °C	• The development of thermodynamically stable internal alkene products results from the higher double-bond rate, which could result in hexene-1 being the initial trimer product. • The major 3-methyl-C_5 chain structure was found in the reaction products, consistent with the composition of branching C_6 isomers.	[150]
	NiMSA20						69.9% @ 150 °C		
	NiMSA30						68.3% @ 150 °C		
	NiMSA50						64.3% @ 150 °C		
	NiMSA80						65.5% @ 150 °C		
	NiMSA50						78.3% @ 50 °C		
	NiMSA50						71.6% @ 100 °C		
	NiMSA50						63.6% @ 200 °C		

Feed (%)	**Catalyst**	**P (atm)**	**Temp (°C)**	**WHSV /LHSV (h-1) /RPM**	**Reactor type**	**Conversion (max % @ °C)**	**Selectivity (max% @ °C) of Jet range alkenes**	**Remarks**	**Ref**
	NH4MSA50						68.1% @ 150 °C		
-	Chevron Phillips Chemical's proprietary homogeneous chromium-based catalyst	-	-	**-**	-	-	93%	• Proprietary catalyst; not much information available.	**[29]**
-	Proprietary chromium-based catalyst system	44	115	**-**	-	93.0% @ 115 °C	95-99% @ 115 °C	• Solid product formation is negligible. • Proprietary catalyst; not much information available.	[11]
Conversion of ethylene to hexene and butene intermediate									
-	Titanium tetrabutoxide and triethylaluminum	-	-	**-**	-	95.0% @ 150 °C	80.0% @ 150 °C C_4+ 16.0~18.0% @ 150 °C C_6	• Butenes have a higher yield than hexene; they can be selectively oligomerized to produce oligomers in the jet fuel range.	[29, 151]
Conversion of ethanol to propylene intermediate									
Ethanol (>99.5 wt%)	HZSM-5 with SiO_2/Al_2O_3=52	1	400-600	0.0025-0.04 gcat/ml /min	Quartz reactor	-	28% @ 500 °C	The greatest performance was obtained with Sr-HZSM-5, Sr/Al=0.1 at 500 °C. The C_3H_6 yield and the catalytic stability of this zeolite depend considerably on the alkaline earth metals/Al and SiO_2/Al_2O_3 ratios and	[141]
	HZSM-5 with SiO_2/Al_2O_3=76					-	25% @ 500 °C		
	HZSM-5 with SiO_2/Al_2O_3=184					-	20% @ 500 °C		
	Sr-HZSM-5, Sr/Al=0.1					-	32% @ 500 °C		

Feed (%)	**Catalyst**	**P (atm)**	**Temp (°C)**	**WHSV /LHSV (h-1) /RPM**	**Reactor type**	**Conversion (max % @ °C)**	**Selectivity (max% @ °C) of Jet range alkenes**	**Remarks**	**Ref**
								the reaction circumstances.	
Ethanol (>99.5 wt%)	H-ZSM-5 (Si/Al=30)	1	250	0.63	Fixed bed	73% @ 550 °C	10% @ 550 °C	• La-modified H-ZSM-5 was highly efficient, with 31% selectivity and a Si/Al ratio 280.	[142]
	H-ZSM-5 (Si/Al=280)					90% @ 550 °C	28% @ 550 °C		
	H-ZSM-5 (Si/Al=400)					95% @ 550 °C	30% @ 550 °C		
	H-ZSM-5 (La/Al=2.2, Si/Al=280)					95% @ 550 °C	31% @ 550 °C		
Oligomerization reactions									
Propene	HZSM-5	40	200	0.125	Fixed bed	-	-	• The ultimate yields of jet and diesel fuel are reported to be significantly higher for the silica-modified catalysts.	[152]
50 wt% propane + 50 wt% propene	Silica gel-phosphotungstic acid	40	150	1.0	Fixed bed	60.0% @ 150 °C	80.0% @ 150 °C	• The ideal oligomerization reaction conditions were 170 ° C, 45 atm of pressure, and 1.0 h^{-1} of space velocity.	[153]
						78.0% @ 160 °C	93.0% @ 160 °C		
						60.0% @ 170 °C	92.0% @ 170 °C		
						60.0% @ 180 °C	94.0% @ 180 °C		
						60.0% @ 190 °C	94.0% @ 190 °C		
1-hexene	Cp_2ZrCl_2/ 10% MAO	1	25		Standard Schlenk techniques	100.0% @ 25 °C	>80% @ 25 °C	• A low Al/Zr ratio can eliminate greater molecular weight oligomers.	[140]

Hydrotreating and product purification

After oligomerization, a hydrotreating/hydrogenation step is required to saturate the unsaturated double bonds using transition metal catalysts such as cobalt molybdenum (CoMo), palladium (Pd), or platinum (Pt) on an activated carbon catalyst. Research showed that a Pd or Pt catalyst is more suitable for hydrotreating the α-olefins [69]. Noble metals, such as Pt and Pd, are robust hydrogenation catalysts that balance the acidity of catalyst supports such as Al_2O_3 or SiO_2-Al_2O_3, resulting in high selectivity to isomerized products, a significant component of jet fuel. According to research, the amounts of isomerized and regular alkanes produced during n-alkane hydrotreating rely on the relative potencies of the metal catalyst for hydrogenation and the acidic support materials. Pt-promoted zeolites have been used as n-alkane hydrotreating catalysts for the past 20 years, and they have demonstrated strong selectivity to iso-alkanes and increased resistance to heteroatom impurities [69].

Hydrotreating and hydro-isomerization are two processes used to convert olefins into jet-range fuel blend stock. To saturate the olefins, compressed hydrogen (purchased or produced on-site)is delivered in excess into the hydrotreating reactor [69, 154]. The hydrotreating reactor is operated at 350 ^{o}C, and its hot product streams are fed to the waste heat recovery unit to improve the energy efficiency of the process. After hydrotreating, a similar hydro-isomerization step is required to convert normal paraffins into their isomers. A hydro-isomerization catalyst’s lifetime is usually three or more years, during which a hydrogen atmosphere minimizes carbon depositions on the catalysts, keeping hydrogen consumption insignificant [69, 154].

After the hydrotreater, the entire product stream enters a gas/liquid separation unit with a pressure swing adsorption unit that separates, purifies, and recycles hydrogen from alkanes. The resulting alkanes are distilled into several hydrocarbon fractions in gasoline, diesel, and jet ranges. The hydrocarbon fraction containing C_2-C_4 are light paraffins recycled back to the oligomerization step or separated as by-products. Another separated hydrocarbon fraction is in the carbon range of C_5-C_8 belongs to the gasoline range. The third hydrocarbon fraction contains carbon numbers in the range of C_8-C_{16}, belonging to the jet range to produce bio-jet fuel blend stocks. The hydrocarbon fraction beyond the jet range with carbon numbers from C_{16}-C_{22} is considered diesel fuel blend stocks. [16, 69]. The established technologies for hydrotreating olefins are summarized in **Table 7**.

Table 7. Scientific advancements in catalysts for hydrotreating olefins to jet-range alkanes

Feed olefins (%)	**Catalyst**	**P (atm/ bar)**	**Temp (°C)**	**WHSV /LHSV (h^{-1})**	**Reactor type**	**Conversion (max % @ °C)**	**Selectivity (max% @ °C) of Jet range alkanes**	**Remarks**	**Ref**
Hydrotreating reaction									
-	Cobalt molybdenum (CoMo)	525 psig	350	3	Fixed bed	100.0% @ 350 °C	**-**	• Following hydrotreating, the product stream is directed into the pressure swing adsorption cycle, where the hydrogen is separated, purified, and recycled.	[12, 69]
Hydro-isomerization reaction									
n-C$_9$	Pt (0.5%)/HY Methanol on Platinum catalyst	32 psi	275-300	1	Fixed bed	76.4% @ 275 °C	Yield$_{iso}$ (%) = 67.1, S$_{iso}$(%) = 87.8 @ 275 °C	• Both bulk and supported catalysts deactivated rapidly without Pt. • Compared to bulk Pt/WZ catalysts, silica-supported catalysts have higher hydrogenating activity.	[155]
n-C$_8$	Pt (0.3%)/ H-MOR	29.8 psi				67.9% @ 300 °C	Yield$_{iso}$ (%) = 16.4 S$_{iso}$(%) = 24.2 @ 300 °C		
n-C$_9$	Pt (0.5%)/ HZSM-5	2.8 psi				98.5% @ 280 °C	Yield$_{iso}$ (%) = 18.6 S$_{iso}$(%) = 18.9 @ 280 °C		
n-C$_8$	Pt (0.5%) W$_{7.5}$Z$_{1.0}$Si	4 psi				96.7% @ 300 °C	Yield$_{iso}$ (%) = 18.6 S$_{iso}$(%) = 73.9 @ 300 °C		

2.6 Butanol to jet

Biobutanol can be produced by the same pathway (from grain- and lignocellulosic-based feedstocks) as bioethanol, shown in **Figure 3**. **Figure 3b** illustrates the production pathways of biobutanol. Usually, the conventional pathway for biobutanol (n-butanol and iso-butanol) production is acetone-butanol-ethanol (ABE) fermentation using the microorganism *Clostridium acetobutylicum* from sugars where butanol is the main product [156]. The acetone, butanol, and ethanol ratio is approximately 3:6:1, which requires the same feedstock as that used in ethanol production [33, 157]. The pathways that produce biobutanol from lignocellulosic biomass differ from those that use sugars and starches. As illustrated in **Figure 3b**, two major pathways produce biobutanol from lignocellulosic biomass. One gasifies the lignocellulosic biomass to produce syngas. Syngas is then fermented anaerobically to biobutanol via the reductive acetyl-coenzyme A (acetyl-CoA) pathway, also known as the Wood-Ljungdahl pathway [33]. Although this process has several technological and financial limitations, butanol production from biogenic material has received considerable attention because it has a smaller carbon impact than other non-biogenic processes [33]. The other pathway involves a pretreatment step, such as enzymatic hydrolysis or acid-catalyzed hydrolysis, making the sugars accessible for further processing. Both types of hydrolysis yield C_5 sugars (pentoses) and hexose (C_6 sugars) from the hemicellulosic part of the biomass. C_5 sugars specifically demand genetically modified yeasts for further processing, and most of the commonly used micro-organisms can only convert C_6 sugars, such as *E. coli* and *Z. mobilis*. The major steps of the butanol-to-jet pathway are dehydration, oligomerization, hydrotreating, and fractionation, described below [33].

Butanol dehydration

The dehydration of butanol produces a range of butene isomers. 1-butene, cis- and trans-2-butene can be produced from the n-butanol (1-butanol) dehydration reaction. The dehydration of iso- and tert-butanol produces iso-butene. Equation 8 describes the general dehydration reaction of butanol [33].

$$C_4H_9OH \rightarrow C_4H_8 + H_2O \qquad (8)$$

Alcohol dehydration reactions over solid catalysts such as alumina, Rh, Amberlyst acidic resins, and ZSM-5 zeolites under high/normal pressure have been studied and reported in the literature for the last 100 years [158, 159]. N-butanol can be dehydrated using these catalysts with different reaction conditions. Zeolite, zirconia, solid acid catalysts, HPW ($H_3PW_{12}O_{40}$), and the mesoporous silica group are the most popular catalysts for the dehydration of butanol [20].

Similar research has been done over the years on iso-butanol dehydration using a variety of catalysts, including metal oxides, inorganic acids, acidic resins, zeolites, and many more. The most notable is a slightly acidic gamma-alumina catalyst [20]. The two-step mechanism proposed by Makarova et al. for the dehydration of n-butanol involves the rapid production of dibutyl ether ($C_8H_{18}O$) and the delayed breakdown of this ether. This discovery suggests that higher temperatures are needed to guarantee good olefin selectivity [158, 160]. The investigation by Lee et al. supports this notion, showing that at temperatures above 250 °C, butanol dehydration predominates over ether production. According to the same study's findings on product selectivity, the kind of butene product depends on the butanol isomer that goes through dehydration [158, 161]. Selecting the suitable catalyst will determine how selective isobutene is compared to other butenes. In addition, butene oligomerization can eventually be started by powerful acidic catalysts like Amberlyst 35 and ZSM-5. However, compared to the isomers created when the two reactions occur separately in sequence, those made in one step of oligomerization and dehydration have lower fuel/chemical characteristics. The butenes created can go through oligomerization to form jet-range alkenes after dehydration [159]. The reaction conditions of different catalytic processes for butanol dehydration, their conversion rate, and selectivity are summarized in **Table 8**.

Butene oligomerization

After dehydration, carbon atoms in the chain increase by the following reaction:

$$nC_4H_8 \rightarrow C_{4n}H_{8n}; \ n=2, 3 \qquad (9)$$

Unsaturated alkene molecules undergo a procedure known as oligomerization in which the relevant oligomers, such as dimers, trimers, and even tetramers, are created. The process occurs selectively in the liquid phase inside the stirred reactors in the presence of particular catalysts that support the creation of oligomers in opposition to other undesirable reactions (i.e., cracking, dehydrogenation, and polymerization).

Table 8. Scientific advancements in the dehydration of butanol to butylene

Feed butanol %	**Catalyst**	**P (atm)**	**Temp (°C)**	**WHSV /LHSV (h^{-1}) /RPM (ms)**	**Reactor type**	**Conversion (max % @ °C)**	**Selectivity (max% @ °C) of butene**	**Remarks**	**Ref**
				n-butanol					
Varying	Rh/Al_2O_3	1	460-500	25 ms	Stainless steel cylinder quartz reactor	42.0% @ <500 °C	94.0% @ <500 °C	• The order of selectivity:blank alumina foam>Rh/ γ-alumina foam>γ-alumina-coated alumina foam.	[161]
	γ-alumina-coated alumina foam					58.0% @ <500 °C	88.0% @ <500 °C		
	Blank alumina monolith foam					80.0% @ <500 °C	40.0% @ <500 °C		
Varying	γ-Al_2O_3 top layer supported on a tubular α-Al_2O_3 membrane	1	200-350		Porous inorganic membrane reactors	95.0% @ 250 °C	100.0% @ 350 °C	• The 1-butanol conversion decreases with rising membrane calcining temperature under the same reaction conditions, but the selectivity of 1-butene remains constant.	[162]
-	Silane-modified γ-alumina	2.06	380	0.01~1	-	98.0% @ 380 °C	95.0% @ 380 °C	• 95% selectivity is for 1-butene. The other product is 2-butene, which is produced via the isomerization of 1-butene.	[69]
				2-butanol					
Varying	Rh/Al_2O_3	1	460-500	25 ms	Stainless steel cylinder quartz reactor	76.0% @ <500 °C	98.0% @ <500 °C	• The γ-alumina coating's selectivity increase for 2-butanol is negligible.	[161]
	γ-alumina-coated alumina foam					78.0% @ <500 °C	90.0% @ <500 °C		
	Blank alumina monolith foam					83.0% @ <500 °C	40.0% @ <500 °C		
	MCM-41,	1	150-350	40.4	Tubular	30.0% @ <350 °C	5.0% @ <500 °C		[163]

Feed butanol %	**Catalyst**	**P (atm)**	**Temp (°C)**	**WHSV /LHSV (h^{-1}) /RPM (ms)**	**Reactor type**	**Conversion (max % @ °C)**	**Selectivity (max% @ °C) of butene**	**Remarks**	**Ref**
2-butanol (0.25–1.00 mol%)	(20 wt% SiO_2, Na/Si - 0.5:1)							• The application of selectivity for 1-butene over MMZ-FER catalysts in bio-butanol dehydration appears promising. • In essence, the product yield or conversion does not dramatically decline with time, indicating that the catalyst's deactivation is not severe.	
	MMZ-FER (0.67), NaOH/ (Si + Al) - 0.67:1					96.0% @ <350 °C	87.0% @ <250 °C		
	MMZ-FER (1.0), NaOH/ (Si + Al) - 1.0:1					85.0% @ <500 °C	52.0% @ <250 °C		
	MMZ-FER (1.33) NaOH/ (Si + Al) - 1.33:1					8.0% @ <250 °C	9.0% @ <250 °C		
	Ferrierite					95.0% @ <350 °C	61.0% @ <250 °C		
					Isobutanol				
Varying	Rh/Al_2O_3	1	460-500	25 ms	Stainless steel cylinder quartz reactor	65.0% @ <500 °C	96.0% @ <500 °C	• The alumina foam is given a covering of γ -alumina to increase butene selectivity.	[161]
	γ-alumina-coated alumina foam					81.0% @ <500 °C	100.0% @ <500 °C		
	Blank alumina monolith foam					100.0% @ <500 °C	46.0% @ <500 °C		
99.5 vol%	BASF AL3996, (γ-alumina)	1	250-400	5	Fixed bed	100.0% @ 325 °C	96.0% @ 325 °C	• Both water content and pressure negatively impact conversion and selectivity.	[159]
-	ZSM-5	4.08	325	2	-	99.1% @ 325 °C	95.1% @ 325 °C	• A blend of 1.6% 1-butene, 95.1% isobutene, 1.9% cis-2-butene, and 0.5% trans-2-butene makes the product.	[69]
-	γ-alumina	1	310		-	98.0% @ 310 °C	92.0% @ 310 °C	• It is possible to create oligomers, trimers, and tetramers from isobutene.	[69]

Phosphoric acid soaked on solid supports was a pioneering industrial catalyst for the oligomerization of light olefins. More catalysts have since been studied, including sulfonic acid resins, acid solids like sulfated titania and zirconia, nickel-doped zeolites, nickel supported on sulfated zirconia, and NiO-W_2O_3/Al_2O_3, etc. Zeolites are intriguing stable acid catalysts with both Lewis and Brønsted acid sites. As they are strong acid catalysts, rapid deactivation is a problem; it is responsible for the poor regeneration efficiency of catalysts. However, researchers continuously try to modify this catalyst to improve its catalytic and regeneration properties [20]. Significantly branching, chiral compounds with dimer-containing chiral carbon centers are produced by the oligomerization reaction, which is also highly selective [33].

1-butene is subjected to the oligomerization process at ambient temperature over group IV transition-metal catalysts such as Cp_2ZrCl_2 in the presence of methyl aluminoxane (Cp_2ZrCl_2/MAO) as a co-catalyst to produce olefins ranging from C_8-C_{32} with a conversion rate of 97%. The product distributions of these olefins are 26.46% C_8, 25.48% C_{12}, 17.64% C_{16}, 11.76% C_{20}, 7.84% C_{24}, 4.9% C_{28}, and 3.92% C_{32} [18, 69, 164]. 2-butenes, i.e., cis-and trans-2-butenes, remain unreacted and separated by temperature-controlled distillation. C_8 olefins, i.e., 2-ethyl-1-hexene, are distilled and further sent to the dimerization reactor operated at 116 °C for 2 h over a Nafion/bimetallic catalyst with 100.0% conversion and a yield of 90% $C_{16}H_{32}$. Alternatively, C_8 olefins can be reacted with butenes to produce C_{12} olefins, increasing the C_{12} in jet-range chemicals [18, 69, 165].

Amberlyst 15, a cationic ion-exchange resin, is used as the catalyst in the widely studied process of isobutene oligomerization. It exhibits high conversion rates (over 90%) and excellent selectivity on dimers (di-isobutylene), trimers (tri-isobutylene), and tetramers (tetra-isobutylene) [18, 69]. Zeolites, an alternative, are also used and exhibit extremely strong performance, although they deactivate quickly, as seen with other butenes [158]. The reaction conditions of different catalytic processes for butene oligomerization with their conversion rates and selectivity are summarized in **Table 9**.

Hydrogenation and distillation

After oligomerization, the resulting products are hydrotreated and hydro-isomerized to saturate carbon double bonds and then sent to distillation for product separation. C_{12} to C_{32} olefins produced by 1-butene oligomerization and C_{16} olefins produced by dimerization are transported to the hydrogenation process over 0.08 wt% PtO_2 or 5 wt% palladium alloy catalysts or platinum on an activated carbon catalyst with up to 90% yield at relatively high pressure (>20 bar) and 200-350 °C [1, 158]. The hydrogenation reaction is as follows:

$$C_nH_{2n} + H_2 \rightarrow C_{2n}H_{2n+2};\ n=8,\ 12,\ 16 \qquad (10)$$

The resulting C_{12}-C_{16} paraffins can be blended with jet fuel, and the remaining C_{20}-C_{32} alkanes are separated and traded as lubricants [18]. These two-unit operations are similar to the ethanol-to-jet method discussed earlier. The reaction conditions of different catalytic processes for olefin hydrogenation with their conversion rates and selectivity are summarized in **Table 10**.

Table 9. Scientific advancements in the oligomerization of butenes to olefins

Feed Butene %	**Catalyst**	**P (atm)**	**Temp (°C)**	**WHSV /LHSV /GHSV (h^{-1})**	**Reactor type**	**Conversion (max % @ °C)**	**Selectivity (max% @ °C) of jet range olefins**	**Remarks**	**Ref**
1-butene	Group IV transition-metal catalysts with methyl aluminoxane (Cp_2ZrCl_2/MAO)	1	25	-	Stainless steel Parr reactor	97.0% @ 25 °C	52.0% @ 25 °C	• Product distributions of mixed olefins: 26.46% C_8, 25.48% C_{12}, 17.64% C_{16}, 11.76% C_{20}, 7.84% C_{24}, 4.9% C_{28}, and 3.92% C_{32}.	[166]
1-butene	Amberlyst 35	16.77	170	0.9	Tubular	99.0% @ 170 °C	71.0% @ 170 °C	• A low space velocity and a high separator temperature are favorable for higher oligomerization.	[167]
Isobutene	Amberlyst 35	1	100	2	Fixed bed (continuous flow)	96.0% @ 100.0 °C	90.0% @ 100.0 °C	• C_8 olefins can be refined, transported to a different dimerization procedure, and then recycled to the oligomerization reactor to boost the jet-range yields.	[168]
1-butene, 2% cis-2-butene, and 3% trans-2-butene	Ziegler-Natta catalyst	-	-	-	-	95.0%	72.0%	• The mixed olefin product's distribution: 27% C_8, 26% C_{12}, 18% C_{16}, 12% C_{20}, 8% C_{24}, 5% C_{28}, and 4% C_{32}.	[166]
Isobutene	MSU-S/WBEA (Si/Al - 44:1, mesoporous	1	60	32.8	Fixed bed (glass)	55.0% @ 60 °C	100.0% @ 60 °C	• By changing the feed composition, product	[169]

Feed Butene %	Catalyst	P (atm)	Temp (°C)	WHSV /LHSV /GHSV (h^{-1})	Reactor type	Conversion (max % @ °C)	Selectivity (max% @ °C) of jet range olefins	Remarks	Ref
	aluminosilicate with a wormhole motif)							selectivity can be regulated to create primarily C_8 or C_{12} products while preventing the creation of unwanted high molecular weight oligomers. • A higher GHSV results in higher conversion rates.	
	MSU-S/SBEA (Si/Al - 44:1, non mesostructured analogue)					52.0% @ 60 °C	100.0% @ 60 °C		
	BEA (Si/Al - 45:1, commercial zeolite)					48.0% @ 60 °C	100.0% @ 60 °C		
	USY (Si/Al - 2.5:1, Commercial zeolite)					44.0% @ 60 °C	100.0% @ 60 °C		
1-butanol (99%)	NH_4-ZSM-5/ H-ZSM-5 (Zeolyst, Si/Al - 15:1, CBV 3024E)	1	150-250	13.5	Fixed bed (continuous flow)	16.0% @ 200 °C	90.0% @ 200 °C	• With the rising temperature, partial pressure, and contact time, catalytic activity rises.	[170]
Varying	Borate-Containing alumina (γ-Al2O3)	79	150-200	0.5 ~- 1.0	Fixed bed (continuous flow)	85.0% @ 200 °C	90.0% @ 200 °C	• Catalyst activity in butene isomer conversion can be controlled by adjusting the boron oxide level.	[171]
isobutene (99%)	Amberlyst 35	14.8	30-110	50	Fixed bed (continuous flow)	96.0% @ 70 °C	66.0% @ 70 °C	• At high temperatures and low space velocities, conversion and selectivity are high. • The conversion increases with the increase in the acid capacities in the following order Amberlyst 35 ≥ Amberlyst 15 > Amberlyst DT.	[172]
	Amberlyst 15					90.0% @ 70 °C	64.0% @ 70 °C		
	Amberlyst DT					71.0% @ 70 °C	50.0% @ 70 °C		
	Amberlyst 31					5.0% @ 70 °C	36.0% @ 70 °C		
	WK-40					1.0% @ 70 °C	- *		
	Zeolite mordenite (Zeocat, ammonium					70.0% @ 70 °C	16.0% @ 70 °C		

Feed Butene %	Catalyst	P (atm)	Temp (°C)	WHSV /LHSV /GHSV (h^{-1})	Reactor type	Conversion (max % @ °C)	Selectivity (max% @ °C) of jet range olefins	Remarks	Ref
	form, SiO_2/Al_2O_3 - 25:1)								

*No information

Table 10. Scientific advancements in catalysts for the hydrogenation of olefins to jet-range alkanes

Feed olefins (%)	Catalyst	P (atm)	Temp (°C)	WHSV /LHSV	Reactor type	Conversion (max % @ °C)	Selectivity (max% @ °C) of Jet range alkanes	Remarks	Ref
Olefins (C_9–C_{16})	5 wt% palladium or platinum on an activated carbon catalyst	1	370	3 h^{-1}	Trickle-bed	99.0% @ 150 °C	90.0% @ 150 °C	• After the fractionation of hydrocarbons, an isolated blend of roughly 20% dimers, 40% trimers, and 40% tetramers (and trace amounts of higher oligomers) is produced. This blend stock is used to make jet fuel.	[168]

2.7 Cyclic and higher alcohols to jet fuel

20% of jet fuel consists of naphthene, and 20% is aromatic compounds needed for elastomer compatibility [173]. To meet the consistency of jet fuels, cyclic alcohols/polyols are converted to aromatics with desired traits. Higher carbon or cyclic alcohols are not readily available, unlike the smaller alcohols. Higher alcohols or polyols can be produced directly from grains by hydrolysis and fermentation reactions and from lignocellulosic biomass by hydrolysis and fermentation or thermochemical pathways. As smaller alcohol molecules need multiple steps to produce jet fuel, research is ongoing to produce the desired range of alkanes from higher alcohols. Because of the lower yield and conversion rates, they are produced via various kinds of C-C coupling reactions, such as aldol condensation through ketones (i.e., cyclo-pentanone, cyclo-hexanone), furanic aldehydes, and isophorone, reductive coupling/rearrangement reactions through ketones, hydroxy-alkylation/alkylation through 2-methyl furan with ketones, and oligomerization/rearrangement through cyclo-pentanol [174]. Generally, after the production of the platform molecules (higher alcohols or polyols), one-step catalytic conversion is the next step which is merely a dehydration step with catalysts such as HZSM-5 and MCM-41 [175]. Since the reaction occurs in the aqueous phase and the produced alkanes are hydrophobic, the alkanes can automatically be separated from the aqueous phase, which saves energy without distillation [175]. In these synthetic procedures, biomass platform alcohols must be transformed into monocyclic, bicyclic, or multicyclic intermediates to increase jet fuel density. Normal expectations for high-density fuels include bicyclic and multicyclic structures. Still, their low-temperature characteristics frequently need to catch up to what is required for actual jet fuel applications. Some monocyclic or bicyclic alkanes with branched chains have relatively low freezing points that can improve the fuels' cryogenic properties [174]. The reaction conditions and the catalysts involved are summarized in **Table 11**.

Table 11. Scientific advancements in catalysts for the dehydration/oligomerization reaction from higher/cyclic alcohols

Alcohols (%)	**Catalyst**	**P (atm)**	**Temp (°C)**	**WHSV /LHSV (h^{-1}) /RPM**	**Reactor type**	**Conversion (max % @ °C)**	**Selectivity (max% @ °C) of jet-range aromatics/alkanes**	**Remarks**	**Ref**
Higher/cyclic alcohol dehydration reactions									
Glucose	10%Ni (Ni(NO$_3$)$_2$·6H$_2$O) @HZSM-5 (80-100.0 mesh, Si/Al - 38:1)/ 40%MCM-41 (pure silica)	39.5	500	1.25	Tubular	93.0% @ 300 °C	78.7% @ 300 °C	• The methanol, ethanol, iso-sorbitol, and glycol present in the aqueous phase residue can be further processed into aromatic fuels by refeeding the reactor with fresh reactants. • This method uses cellulosic and traditional plant sugars, offering an affordable way to produce sustainable aromatics for bio-jet.	[175]
Sorbitol						98.0% @ 300 °C	81.6% @ 300 °C		
Polyol (40% xylitol+60% sorbitol)						96.0% @ 300 °C	89.0% @ 300 °C		
Menthol (Sigma-Aldrich, >99wt%)	No catalyst	20	110-190	0.05 mol L^{-1}	Autoclave (semi-batch)	9.0% @ 190 °C	-	• Pd and Pt, which yield almost 90%, are the most efficient metal catalysts investigated. Ru has a lower hydrogenation activity. • As the cascade reaction continues, cycloalkane is produced by acid-catalyzed menthol dehydration, metal-catalyzed cycloalkene hydrogenation, and metal-catalyzed cycloalkene hydrogenation. • The primary factors impacting catalyst	[176]
	Nb$_2$O$_5$ (only support)					100.0% @ 190 °C	3.0 @ 190 °C		
	Ru/Nb$_2$O$_5$					71.0% @ 190 °C	54.0% @ 190 °C		
	Ru/SiO$_2$					12.0% @ 190 °C	17.0% @ 190 °C		
	Pd/Nb$_2$O$_5$					100.0%@ 190 °C	88.0% @ 190 °C		
	Pd/SiO$_2$					18.0% @ 190 °C	59.0% @ 190 °C		
	Pt/Nb$_2$O$_5$					100.0% @ 190 °C	86.0% @ 190 °C		
	Pt/Nb$_2$O$_5$ lower catalyst					100.0% @ 190 °C	86.0% @ 190 °C		

Alcohols (%)	**Catalyst**	**P (atm)**	**Temp (°C)**	**WHSV /LHSV (h^{-1}) /RPM**	**Reactor type**	**Conversion (max % @ °C)**	**Selectivity (max% @ °C) of jet-range aromatics/alkanes**	**Remarks**	**Ref**
	dispersion (44%),					99.0% @ 170 °C	95.0% @ 170 °C	performance are reaction temperature and the equilibrium between the acid and metal sites.	
						18.0% @ 150 °C	57.0% @ 150 °C		
						2.0% @ 110 °C	-		
Benzene: propene (mol/mol = 6:1)	C84-3 solid phosphoric acid (SPA)	38	160-240	-	Stainless steel autoclave batch reactors	3.1% @ 160 °C	88.6% @ 160 °C	• Alkylation and oligomerization are favorable processes operating at low aromatic-to-olefin ratios. • Temperature and variations in the aromatic-to-olefin ratio have varied effects on benzene alkylation and propene oligomerization rates. • Both the alkylation rate and the oligomerization rate increase when the aromatic-to-olefin ratio increases from 6:1 to 1:1. • For this range of aromatic-to-olefin molar ratios, the alkylation rate is consistently higher than the oligomerization rate. • The trend of the catalyst's activity is similar for benzene alkylation and toluene alkylation.	[173]
Benzene: propene (mol/mol = 1:1)						11.9% @ 160 °C	84.2% @ 160 °C		
Benzene: propene (mol/mol = 1:6)						10.1% @ 160 °C	53.1% @ 160 °C		
Benzene: propene (mol/mol = 6:1)						11.7% @ 180 °C	84.2% @ 180 °C		
Benzene: propene (mol/mol = 1:1)						13.6% @ 180 °C	82.3% @ 180 °C		
Benzene: propene (mol/mol = 1:6)						14.2% @ 180 °C	49.7% @ 180 °C		
Benzene: propene (mol/mol = 6:1)						11.6% @ 200 °C	96.3% @ 200 °C		

Alcohols (%)	**Catalyst**	**P (atm)**	**Temp (°C)**	**WHSV /LHSV (h^{-1}) /RPM**	**Reactor type**	**Conversion (max % @ °C)**	**Selectivity (max% @ °C) of jet-range aromatics/alkanes**	**Remarks**	**Ref**
Benzene: propene (mol/mol = 1:1)						13.2% @ 200 °C	83.4% @ 200 °C		
Benzene: propene (mol/mol = 1:6)						9.0% @ 200 °C	59.4% @ 200 °C		
Benzene: propene (mol/mol = 6:1)						12.8% @ 220 °C	91.2% @ 200 °C		
Benzene: propene (mol/mol = 1:1)						10.3% @ 220 °C	83.4% @ 200 °C		
Benzene: propene (mol/mol = 1:6)						9.0% @ 220 °C	60.7% @ 200 °C		
Benzene: propene (mol/mol = 1:1)						10.5% @ 240 °C	88.0% @ 240 °C		
Toluene: propene (mol/mol = 5:1)						4.5% @ 160 °C	44.5% @ 160 °C		
Toluene: propene (mol/mol = 1:1)						9.1% @ 160 °C	83.6% @ 160 °C		
Toluene:						6.3% @ 160 °C	53.4% @ 160 °C		

Alcohols (%)	**Catalyst**	**P (atm)**	**Temp (°C)**	**WHSV /LHSV (h^{-1}) /RPM**	**Reactor type**	**Conversion (max % @ °C)**	**Selectivity (max% @ °C) of jet-range aromatics/alkanes**	**Remarks**	**Ref**
propene (mol/mol = 1:6)									
Toluene: propene (mol/mol = 1:1)						9.7% @ 180 °C	85.8% @ 180 °C		
Toluene: propene (mol/mol = 5:1)						8.8% @ 220 °C	90.5% @ 220 °C		
Toluene: propene (mol/mol = 1:1)						8.4% @ 220 °C	83.4% @ 220 °C		
Toluene: propene (mol/mol = 1:6)						10.3% @ 220 °C	59.3% @ 220 °C		
20 wt% sorbitol	1%Ni @ HZSM-5/MCM-41	39.5	500	1.5	Tubular	100.0% @ 300 °C	-	• The reaction temperature ranges from 240 °C to 320 °C and impacts the product distribution. Lower carbon alcohol molecules from the aqueous phase can be further converted into aromatic fuels by refeeding the reactor with fresh reactants.	[175]
	3%Ni @ HZSM-5/MCM-41					100.0% @ 300 °C	49.5% @ 300 °C		
	5%Ni @ HZSM-5/MCM-41					100.0% @ 300 °C	26.3% @ 300 °C		
	10%Ni @ HZSM-5/MCM-41					100.0% @ 300 °C	30.7% @ 300 °C		
	20%Ni @ HZSM-5/MCM-41					100.0% @ 300 °C	7.6% @ 300 °C		
C_{10} and C_{15} oxygenates derived from	5 wt% Ni-SiO2-DP	59	230	0.04 mL min^{-1}	Tubular	98.9% @ 230 °C	-	• The activity of several Ni catalysts is in the following order: 30 wt% Ni-SiO_2-DP	[177]
	20 wt% Ni-SiO_2-DP					98.9% @ 230 °C	20.0% @ 230 °C		

Alcohols (%)	**Catalyst**	**P (atm)**	**Temp (°C)**	**WHSV /LHSV (h^{-1}) /RPM**	**Reactor type**	**Conversion (max % @ °C)**	**Selectivity (max% @ °C) of jet-range aromatics/alkanes**	**Remarks**	**Ref**
cycle-pentanol	30 wt% Ni-SiO_2-DP					98.9% @ 230 °C	55.0% @ 230 °C	> 30 wt% Ni/SiO_2-CIM > 30 wt% Ni/SiO_2-IM. • At a Ni level of 35 wt%, the Ni-SiO_2-DP catalyst's activity reaches its peak value. • The process of hydrodeoxygenation (HDO) over a Ni catalyst followed by the solvent-free Guerbet reaction of cyclo-pentanol with Raney metal and a solid base can yield cyclopentane.	
	35 wt% Ni-SiO_2-DP					98.9% @ 230 °C	100.0% @ 230 °C		
	30 wt% Ni/SiO_2-CIM					98.9% @ 230 °C	30.0% @ 230 °C		
	30 wt% Ni/SiO_2-IM					98.9% @ 230 °C	10.0% @ 230 °C		
2-benzyl-4-ethylphenol and 3-benzyl-4-ethylphenol (mono-alkylated products)	A mixture of HZSM-5 and Pd/C as catalyst (3%) and cyclohexane as solvent	60	180	-	Autoclave	99.6%	100.0	• The 4-ethylphenol/phenyl methanol ratio is 2, and the reaction temperature is 110 °C. The 4-ethylphenol/phenyl methanol alkylation reaction occurs first, and the conversion of the phenyl methanol is 100.0% with 71% selectivity of the monoalkylated products (2-benzyl-4-ethylphenol and 3-benzyl-4-ethylphenol).	[174]
2-Methyl-2,4-pentanediol	Nafion	1	170	-	-	100.0% @ 170 °C	77.7% @ 170 °C	• In the synthetic route, first diacetone alcohol (a self-aldol condensation product of acetone) is hydrogenated to 2-methyl-2,4-pentanediol.	[178]
	Amberlyst 45					100.0% @ 170 °C	68.6% @ 170 °C		
	Amberlite IRC 76CRF					51.0% @ 170 °C	3.1% @ 170 °C		

Alcohols (%)	**Catalyst**	**P (atm)**	**Temp (°C)**	**WHSV /LHSV (h^{-1}) /RPM**	**Reactor type**	**Conversion (max % @ °C)**	**Selectivity (max% @ °C) of jet-range aromatics/alkanes**	**Remarks**	**Ref**
	H_2SO_4					100.0% @ 170 °C	72.1% @ 170 °C	• By dehydrating and undergoing a Diels-Alder reaction over acidic catalysts, 2-methyl-2,4-pentanediol is transformed into C_{10} and C_{12} cycloalkenes. • Because of its strong acid strength, Nafion resin shows the highest activity. • The Pd/C catalyst further hydrogenates C_{10}-C_{12} cycloalkenes to C_{10}–C_{12} cycloalkanes at low temperatures (170 °C and 0.1 Mpa H_2).	
	H_3PO_4					93.0% @ 170 °C	17.5% @ 170 °C		
	Acetic acid					17.5% @ 170 °C	0.0% @ 170 °C		

2.8 Commercial status of the ATJ pathway

The ATJ pathway's key strength is its flexibility in processing alcohols manufactured by many methods and feedstocks [15]. Several companies have been developing bio-jet through the ATJ pathway and aiming toward commercialization. Gevo, Inc., and LanzaTech have contributed significantly to sophisticated biochemically engineered fermentation systems for regulatory approval of ATJ-derived fuel [154]. The Gevo Integrated Fermentation Technology (GIFT) process is a proprietary isobutanol fermentation method that uses a designed yeast strain and a cutting-edge integrated separation system [154]. The fermentation of gas feedstocks from steel mills is a specialty of LanzaTech. Partnerships exist between companies that produce alcohol platform molecules and those that convert them into bio-jet, particularly Cobalt Technologies/Albemarle Corporation/NREL (not currently in operation), BioChemtex/Gevo, LanzaTech/Swedish Biofuels, etc. Collaborations also exist between these fuel developers and aviation operators [15]. In most cases, the jet fuel conversion processes have fuel readiness levels (FRLs) of 7, fuel that meets international standards, and technology readiness levels ranging from 6 to 7 [15, 179]. The lower TRLs indicate system/subsystem models or prototype demonstrations in a simulated/relevant environment (an industrially relevant one for key enabling technologies), and the upper ends correspond to prototypes ready for demonstration in an appropriate operational environment [15, 179-181]. More than 3000 flight tests have been conducted using a 50% blend of bio-jet and conventional jet fuel bio-jet [182]. Globally, some groups are working together to deploy bio-jet fuels instead of fossil jet fuel, including the Commercial Aviation Alternative Fuels Initiative (CAAFI, US) (a coalition of airlines, aircraft, and engine manufacturers), BioFuelNet (Canada), Plan de Vuelo (Mexico), Ubrabio (Brazil), the Aviation Initiative for Renewable Energy in Germany (or aireg), Bioqueroseno (Spain), Sustainable Aviation (UK), Bioport Holland (The

Netherlands), the Nordic Initiative for Sustainable Aviation (NISA), and the Australian Initiative for Sustainable Aviation Fuels (AISAF), as well as in other countries (i.e., China, the UAE, Qatar, Israel, and Japan) [20, 182]. Relevant information related to the commercialization of the pathways is listed in **Table 12**.

Figure 4 shows supply chain for the pathways, specifically alcohol-to-jet pathways focusing on Canada. The color codes used in this figure are explained below:

- Blue boxes with solid lines indicate pathways from first-generation oil-based feedstocks.
- Pink boxes with solid lines indicate pathways from first-generation grain-based feedstocks.
- Green boxes with solid lines indicate pathways that start from the 2nd generation i.e. lignocellulosic biomasses.
- Grey boxes with solid lines indicate pathways from 3rd and 4th generation feedstocks.
- Red boxes with red dotted lines indicate pathways related to this study.
- Violet texts indicate ASTM-certified processes and pathways.
- Pink texts indicate alcohol sourced from the open market.
- Orange dotted lines indicate final products ready to go to the market. Black boxes with black dotted lines indicate the flow of the supply chain.
- Green dotted rectangles highlight the segment of the processes and pathways we followed.

Table 12. Scientific advancements in ATJ pathways

Conversion pathway	**Companies**	**International agencies/partners**	**Feedstock**	**Bio-jet content**	**Year (flight tests)**	**Aircraft**	**Commercial airline**	**Ref**
Ethanol-to-jet	Terrabon/MixAlco; Lanza Tech/Swedish Biofuels; Coskata, Freedom Pines Biorefinery	Defense Advanced Research Projects Agency, Federal Aviation Administration (FAA)	Miscellaneous	-			Boeing, Virgin Atlantic	[18]
Ethanol-to-jet	LanzaTech/PNNL, Vertimass		Sugar					[154]
Ethanol-to-jet	LanzaTech/PNNL		Syngas					[154]
Ethanol-to-jet	PNNL	-	Catalytic (thermochemical) conversion of syngas to ethanol	-	-	-	-	[154]
Ethanol-to-jet	Byogy	Avianca Brazil's Continuous Lower Energy, Emissions, and Noise (CLEEN) program through the Federal Aviation Administration (FAA) Rolls Royce, Pratt & Whitney	Agave, sugarcane, corn, sweet sorghum, cassava, sugar beet			-	Qatar Airways	[15]
Ethanol-to-jet	LanzaTech/Beijing Shougang, LanzaTech, Blue Scope Steel Mill, LanzaTech, Swedish Biofuels	Hongkong and Shanghai Banking Corporation Limited (HSBC) and GE aviation	Flue gas from steel plants		2014	-	Virgin Atlantic, Boeing	[15]
Ethanol-to-jet	Swedish Biofuels	Abengoa Bioenergy, Lufthansa, SkyNRG, SCA	MSW, biogas, grain crops, agricultural and forest residues		2019	-		[15]

Conversion pathway	**Companies**	**International agencies/partners**	**Feedstock**	**Bio-jet content**	**Year (flight tests)**	**Aircraft**	**Commercial airline**	**Ref**
		Energy, 4Tech, Remeski Keskus, the Institute for European Studies						
Butanol-to-jet	Gevo; Byogy; Albemarle/Colbalt; Solazyme	Navy/Naval Air Warfare Center Weapons Division (NAWCWD), Air Force Research Laboratory (AFRL, US), Defense Logistics Agency (DLA), United States Air Force (USAF)	Miscellaneous	-			Continental Airlines, United Airlines	[18]
Isobutanol-to jet	Gevo	Luverne, Minnesota and USA Bio-refinery: Demonstration Silsbee, Texas	Sugary feedstocks (maize, grains, sugar cane)		2016		Alaska Airlines, United Airlines	[15]
Alcohols-to-jet	Solazyme,	United Airlines	Algae, sugarcane	-	2011	B737-800	Continental Airlines	[18]
Alcohols-to-jet	Gevo	U.S. Air Force	Cellulose-derived alcohol	-	2012	A-10C		[18]
Alcohols-to-jet	Swedish Biofuels	U.S. Air Force	Biomass-derived sugar	100%	TBD	TBD	U.S. Air Force	[18]
Alcohols-to-jet	Gevo	U.S. Army	Cellulose-derived alcohol	50%	2013		Sikorsky UH-60 Black Hawk helicopter	[18]

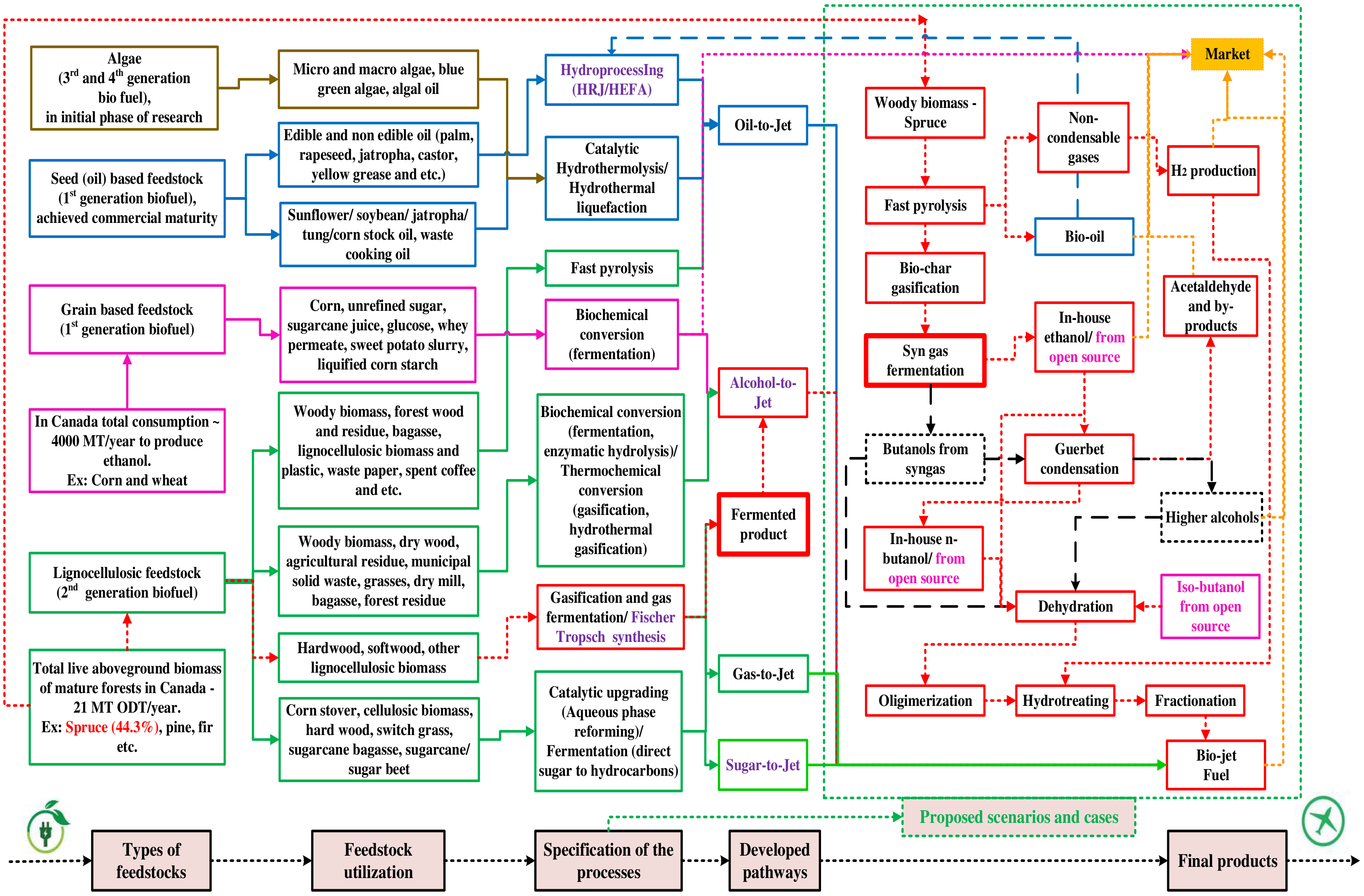

Figure 4. The proposed supply chain of bio-jet fuel production [13-19, 36, 183-185]

Chapter 3. Methodology

3.1 Analytical approach and case development

The study has two main parts: modeling process scenarios to establish material and energy balances and estimating the production costs of bio-jet fuel through development of a techno-economic model. The Aspen Plus® process simulator was used to simulate process scenarios with PENG-ROB as the property method [186, 212]. To validate the model, the process outlined by Brooks et al. was simulated [29]. The model was calibrated by thoroughly exploring individual process conditions and unit operations tailored to this study, taken from a wide range of published sources. The model was further validated by comparing outputs with bio-jet production data obtained from relevant sources [29, 69]. Process yield, relative to biomass and ethanol feed, along with the final recovery after fractionation column loss and isomer content, are evaluated through the material balance given by Aspen Plus (formulas included in ***Appendix B***). Following this, a techno-economic analysis was conducted through a spreadsheet-based model. The capital costs of the equipment were derived by extracting data from both the Aspen Process Economic Analyzer and relevant publications. The techno-economic model included capital costs, operating costs, and the cost of bio-jet fuel production. Following this, a sensitivity analysis was conducted to explore the impact of various parameters on production costs. The framework of the study is highlighted in **Figure 5**.

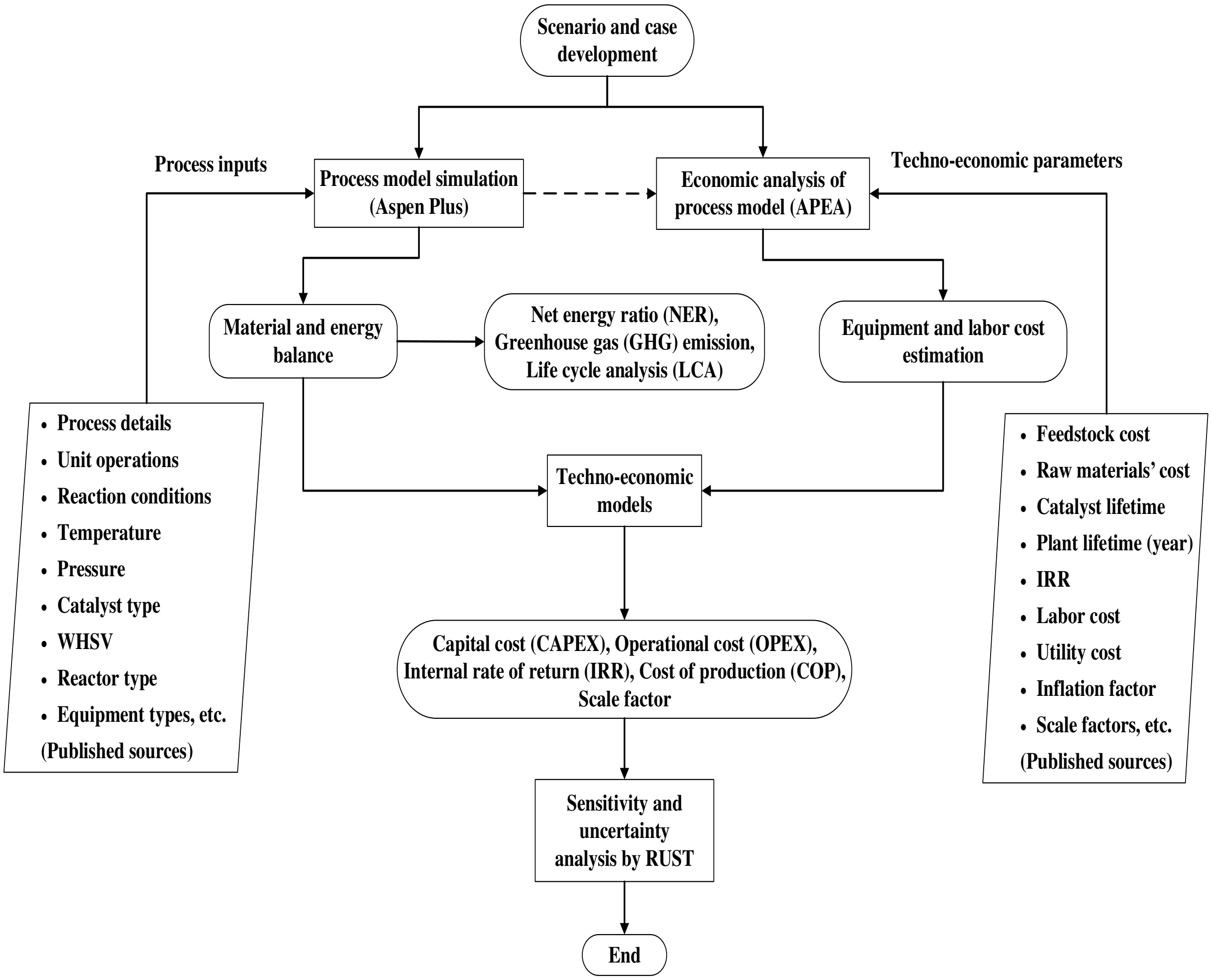

Figure 1. The framework of this study

3.2 Scenario descriptions

Seven unique process scenarios were created, shown in **Figure 6** and described in **Table 13**; in five of them, two cases are featured. In Case 1, it was assumed that bio-jet fuel is produced from ethanol as a platform molecule which originally came from the pyrolysis of spruce wood chips, as per the study by Giwa et al., who used the process conditions from a study by Medeiros et al. [36, 187]. In this initial segment, the pyrolysis of spruce wood, following drying and grinding, yields bio-oil, biochar, and non-condensable gases (NCGs). Ethanol is derived from the char through gasification followed by syngas fermentation. Hydrogen is generated from the NCGs [27].

In Case 2, the production of bio-jet fuel begins with either merchant ethanol or alternative sources. For the techno-economic analysis, a uniform cost assumption was applied to ethanol. The baseline scenario involved simulating the conventional ethanol-to-jet process via the single-step oligomerization of ethylene [29, 69].

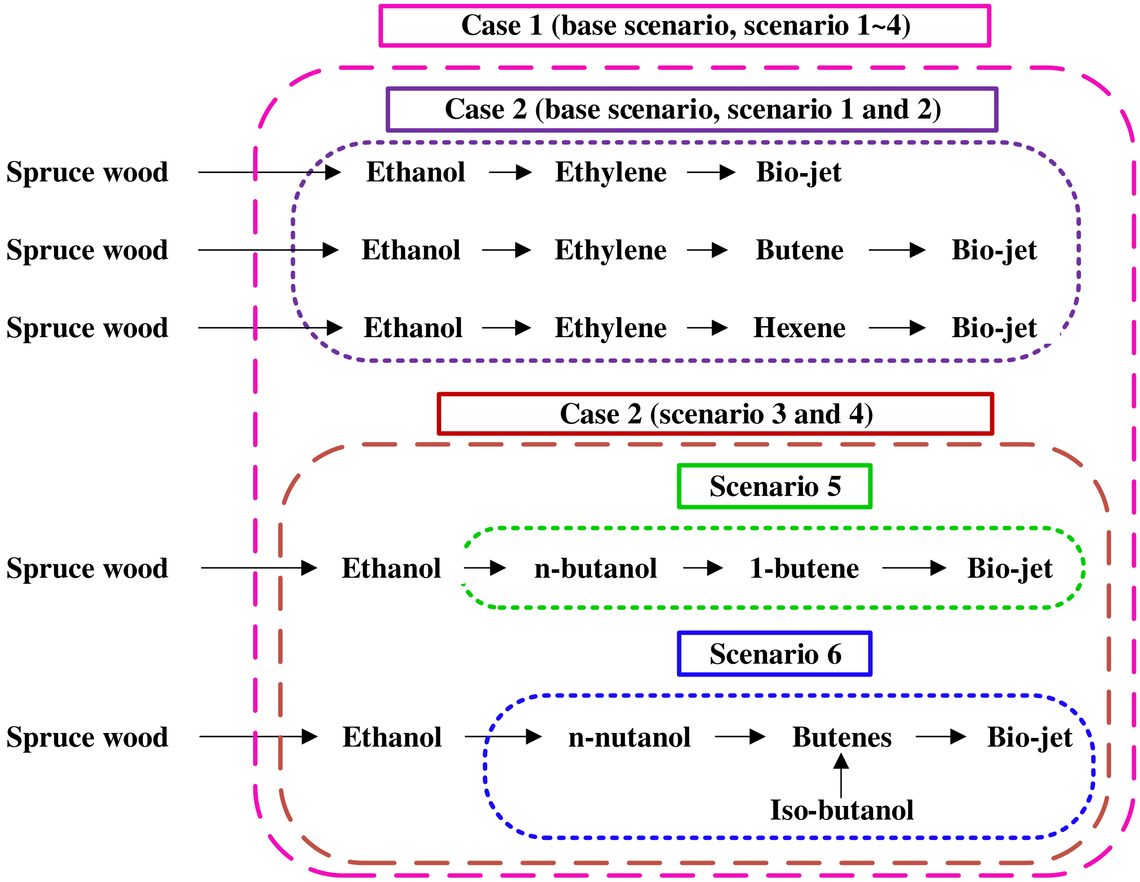

Figure 6. Proposed and developed scenarios for this study

In addition to the five scenarios, two single-case scenarios were established, incorporating n-butanol and iso-butanol in varying combinations of feedstock quantities.

Table 13. Scenario descriptions and the capacities considered for the techno-economic analysis

Scenario description			**Capacity**
Case 1	**Base Scenario**	Spruce wood to ethanol, then direct ethanol to bio-jet	50000, 40000, 30000, 20000, 10000, 5000, 2000 kg/hr or 48, 120, 240, 480, 720, 960, 1200 tonnes/day
	Scenario 1	Spruce wood to ethanol, then butene intermediate to bio-jet	
	Scenario 2	Spruce wood to ethanol, then hexene intermediate to bio-jet	
	Scenario 3	Spruce wood to ethanol, ethanol to Guerbet condensation, then n-butene to bio-jet	
	Scenario 4	Spruce wood to ethanol, ethanol to Guerbet condensation, then n-butene and iso-butene to bio-jet	
Case 2	**Base Scenario**	Ethanol to bio-jet	~ 14000 kg/hr or 336 tonnes/day
	Scenario 1	Ethanol to butene intermediate, then butene to bio-jet	
	Scenario 2	Ethanol to hexene intermediate, and hexene to bio-jet	
	Scenario 3	Ethanol to Guerbet condensation, then n-butene to bio-jet	
	Scenario 4	Ethanol to Guerbet condensation, then n-butene and iso-butene to bio-jet	
Scenario 5		Butanol to bio-jet	All the above-mentioned capacities
Scenario 6		n-butanol and iso-butanol to bio-jet at a ratio of 13:7	

The maximum and minimum bio-ethanol availability in Canada as feedstock was determined by crosschecking the ethanol production statistics across Canada [188]. As of today, there is no established reference point for the commercial production of bio-jet fuel in Canada, as no such commercial-scale production has taken place. However, reference points have been given for all the scenarios developed for this study in **Table 14**. using existing data.

Table 14. Recent statistics of ethanol, butanol (input), and bio-jet fuel (output) production in Canada

<table>
<tr><th></th><th colspan="2">Market size (Demand and supply)</th></tr>
<tr><td rowspan="5">Input</td><td colspan="2">Ethanol [188]</td></tr>
<tr><td>Maximum</td><td>Minimum</td></tr>
<tr><td>57152 kg/hr or 1737 tonnes/day</td><td>2378 kg/hr or 72 tonnes/day</td></tr>
<tr><td>Suncor - St. Clair Ethanol Plant, Ontario, Canada</td><td>Northwest Pure Alcohol & Spirits, Saskatchewan, Canada</td></tr>
<tr><td colspan="2">Butanol (mega million tonnes [MMT] per year) [91, 116]
- Mostly sourced from outside of Canada.
- In 2022, the global market value was 5.45 MMT.
- The global market value was $3.1 billion in 2020 and is estimated to be $4 billion by 2025.
- Major players: BASF SE and OQ chemicals (Germany), The Dow Chemical Company, Eastman, and OXO Corporation (US), Sasol Ltd (South Africa), Petro China and SINOPAC (China), Mitsubishi Chemical Company (Japan).</td></tr>
<tr><td rowspan="3">Output</td><td colspan="2">Bio-jet fuel from ethanol-to-jet
(mega litres per year [MLY]) [29]</td></tr>
<tr><td>Maximum</td><td>Minimum</td></tr>
<tr><td>340 MLY (Lanzajet, USA)</td><td>38 MLY (Lanzajet, Freedom Pines, USA)</td></tr>
</table>

3.3 Base scenario development

Merchant ethanol or ethanol from an upstream process (93 wt%) is directly introduced into the system, with the aim of an optimal concentration of 50-99 wt% to enhance performance in the dehydration reactor. Observing the ethanol dehydration processes listed in **Table 2**, **Table 3** and **Table 4**, this optimum range of concentration of ethanol feed might be selected, though in industry 90~100% conversion is already achieved even from a lower concentration of ethanol as this is already an established technology for a long time [69, 74]. To avoid the azeotrope formation (at 95.5 wt%) during the purification process, 93 wt% ethanol is considered as our upstream process ended up at this concentration and 100% conversion is also achievable [36, 69, 189]. Given the energy-intensive nature of the purification process, catalysts and reactor configurations have been improved over the years to reduce the need for higher ethanol purity [69, 74, 190, 191]. A catalyst of 0.5% LaHZSM-5 was used at a temperature of 250 °C and 1 atm pressure, with a WHSV (weight hourly space velocity) of 2.0 h^{-1}. Under these conditions, the conversion rate reached 100%, and ethylene selectivity was 99.8 wt%, accompanied by a minor by-product, diethyl ether, at 0.2 wt% [69, 192]. After the dehydrated products are cooled, they are sent to a distillation column to separate ethylene from water and the diethyl ether by-product. The wastewater from both the reactor and the distillation column is combined and sent to the wastewater treatment plant [29].

The purified ethylene is pressurized for oligomerization through the two-step Ziegler process with a homogeneous triethylaluminium catalyst [193]. In the first step, ethylene undergoes oligomerization by bonding with stoichiometric quantities of recycled and fresh triethylaluminium catalyst at temperatures of ~90-120°C and a pressure of 100 bar. In the second stage, the oligomers are detached from the catalyst surfaces using new ethylene at temperatures of ~200-300°C and a pressure of 10 bar [69, 193, 194]. After oligomerization, olefins are sent to the hydrotreater where double bonds are saturated with H_2 [24, 34-36]. H_2 at a 3:1 molar ratio reacts with olefins with a cobalt molybdenum (CoMo) catalyst under conditions of 525 psig, 340 °C, and a WHSV of 3 h^{-1} [24, 34-36]. Assuming complete conversion in the hydrotreater because of excess H_2, the resulting alkanes and any remaining unconverted H_2 are sent to the isomerization reactor along with fresh H_2. In this step, the final H_2-to-feed ratio is set at 350:1 to ensure complete isomerization, along with some cracking reactions with a Pt/AlSBA-15 catalyst at 340 °C, 5 MPa, and 3.5 h^{-1} WHSV

[154, 195, 196]. Following the isomerization reaction, the vapor-liquid is separated in a flash separator at 50 °C and 3 MPa.

Recovered H_2 undergoes separation in a PSA unit and is then recycled through a compressor and a heater at the process specifications of the reactors. Following the heater in the splitter, a 2% supplementary purge stream is introduced along with the H_2 feeds to eliminate impurities. This purge stream may be used as boiler fuel to reclaim its energy [29, 191, 197]. A mixture of alkanes, comprising the liquid fraction from the flash separator and the vapor stream from the PSA unit, is introduced into a fractionation tower to facilitate the separation of alkanes within the jet fuel range.

Conventional jet fuel includes a defined volume of aromatics, up to 25 wt%. Aromatics can be produced directly from ethanol or through olefinic intermediates. However, since an excess of aromatics results in suboptimal combustion characteristics and conventional jet fuel already contains sufficient aromatics, the additional aromatic content as a blending agent is not desirable [26]. The paraffinic hydrocarbons generated through the alcohol-to-jet pathways alone may not satisfy all jet fuel specifications. However, they can be blended with conventional jet fuel to achieve a 100% replacement fuel, known as an SKA-type fuel, with a maximum ratio of 50:50 [26]. **Figure 7** is the process flow diagram of the base case along with Scenarios 1 and 2, and all the process conditions are listed in **Table 22** in ***Appendix A***. The dotted line in the figures shows the system boundary started from feed ethanol to bio-jet which was modeled in this study.

3.4 Developing other scenarios

In Scenarios 1 and 2, merchant ethanol or ethanol from the upstream process (93 wt%) undergoes two-step oligomerizations to form butene or hexene after dehydration. In Scenario 1, a homogeneous catalyst, triethyl aluminum (Ti(iv)/Al/THF/EDC molar ratios = 1:4:4:5), is used at 55 °C and 30 bar. The conversion rate is 97%, with 1-butene selectivity reaching approximately 82% [45].

The second oligomerization reaction occurs at room temperature and pressure with a zirconium-based methyl aluminoxane (MAO) homogeneous catalyst with an approximately 100% conversion with a selectivity of 71% for olefins within the jet range (C_8, C_{12}, and C_{16}) [69]. The second oligomerization is similar for n-butene in Scenarios 3-6 after the dehydration of n-butanol.

In Scenario 2, ethylene is transformed into hexene in the first step of oligomerization. This oligomerization reaction uses a proprietary chromium-based catalyst system, characterized by milder process conditions at 110 °C and 40 bar [43]. The process converts ethylene gas into an olefinic product primarily composed of approximately 93 wt% 1-hexene, along with minor coproducts like 1-octene and 1-decene [43]. In the second oligomerization reactor, 1-hexene can be transformed into jet fuel using a homogeneous Cp_2ZrCl_2/methyl aluminoxane catalyst at ambient temperature and pressure. This process leads to a complete conversion of 1-hexene, with over 80% selectivity towards a mixture of the dimer and trimer. The dimer is suitable for jet fuel, while the trimer is desirable for diesel applications due to its high cetane number [44].

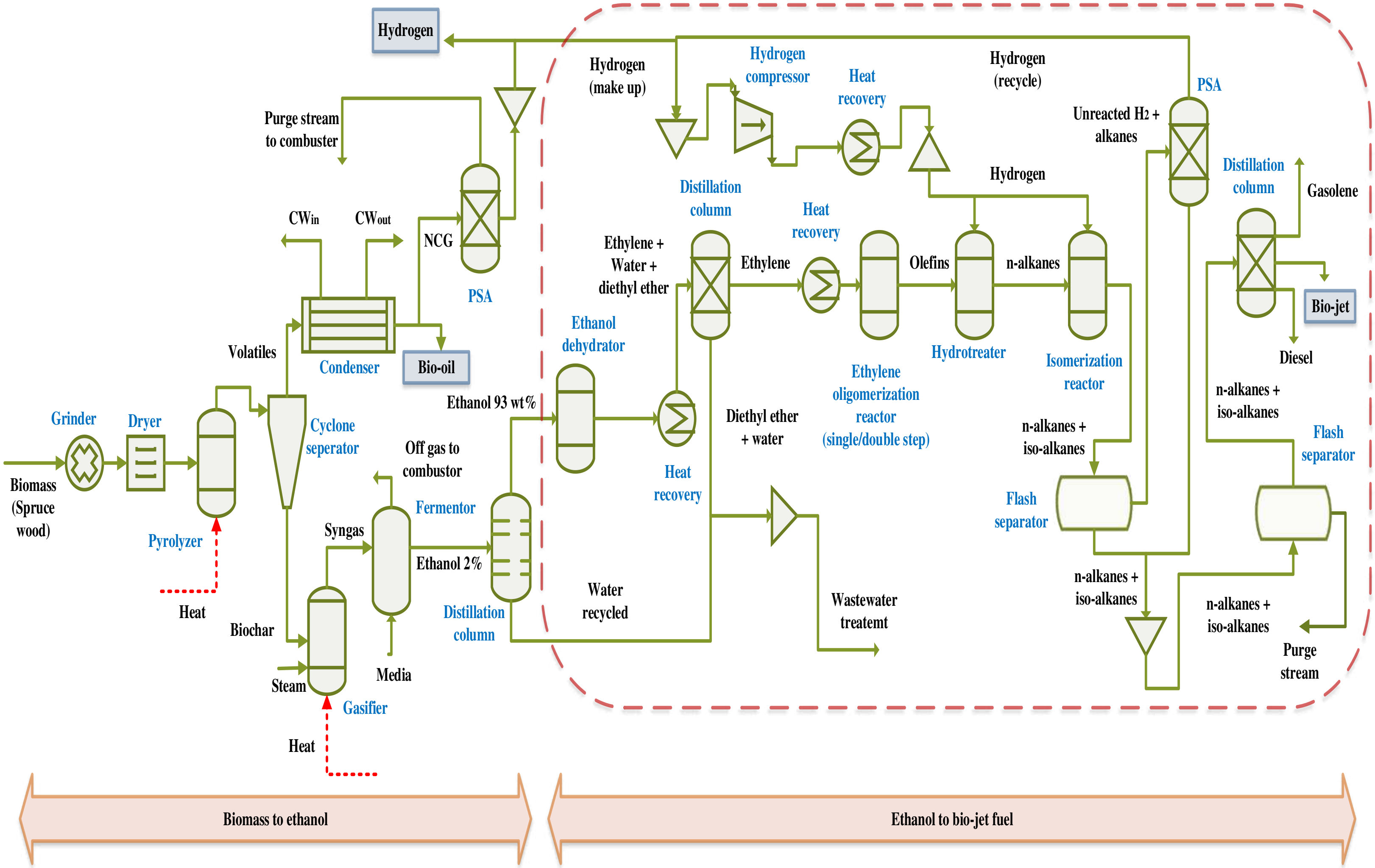

Figure 7. Bio-jet fuel production from ethanol.

Note: The dotted line in the figures shows the system boundary which was modeled in this study.

In Scenario 3, ethanol undergoes a Guerbet condensation reaction to produce n-butanol, which is subsequently converted to jet fuel. The conversion of ethanol to n-butanol occurs on a C-HAP catalyst in a fixed-bed reactor operating at a temperature of 400 °C, pressure of 1 atm, and a WHSV of 1 h^{-1}. The selectivity and yield for n-butanol are 73.2% and 21.1%, respectively. To be economically competitive, efficient separation is crucial because of low conversion, by-product formation, and the formation of an ethanol-water azeotrope solution. A study by Peters and Timmerhaus suggests that 99.9% wt% butanol separation is achievable [47]. **Figure 8** shows the flow diagram of all the butanol processes and **Table 23** in ***Appendix A*** lists the process conditions. The dotted line in the figures shows the system boundary started from feed ethanol to bio-jet which was modeled in this study. All the yield data and final composition of jet range alkanes are given in **Table 15** (**Table 24** and **Table 25** in ***Appendix B*** includes the chemical formulas)**.**

In Scenario 5, n-butanol from an open source is transformed into jet fuel as in Scenario 3 after the condensation stage. N-butanol undergoes dehydration to produce 1-butene at 300 °C and 1 atm pressure in the presence of γ-Al_2O_3, with the top layer supported on a tubular α-Al_2O_3 membrane [162, 198]. Butanol conversion is reported to be 99%, with 100% selectivity towards 1-butene [29]. The subsequent oligomerization is analogous to the second oligomerization, as in Scenario 1. In Scenarios 1 to 5, after the oligomerization, olefins fade to the hydrotreater, similar to the base case scenario. Following hydrotreating, alkanes are directed to the hydro-isomerization reactor where dodecane and octane undergo isomerization reactions with the Pt/AlSBA-15 catalyst at 340 °C and 5 MPa [199].

Table 15. The yield of olefins and alkanes from the oligomerization and isomerization reactions and final recovery after fractionation in ethanol processes

Processes	**Base scenario (Direct ethanol oligomerization)**			**Scenario 1 (Ethanol to butene oligomerization)**				**Scenario 2 (Ethanol to hexene oligomerization)**			
Components	**Oligomerization**	**Isomerization**	**Final jet range**	**Oligomerization 1**	**Oligomerization 2**	**Isomerization**	**Final jet range**	**Oligomerization 1**	**Oligomerization 2**	**Isomerization**	**Final jet range**
nC_4	11.5%	11.0%		81.9%		3.76%				6.46%	
nC_6	19.1%	19.9%		17.7%				93.0%			
nC_8	22.1%	2.45%	4.13%	0.35%	27.0%	3.05%	4.74%	3.50%	10.0%	11.0%	10.7%
iC_8		18.2%	17.0%			20.9%	30.7%			7.54%	6.87%
nC_{10}	18.4%	19.9%	35.5%	0.1%							
nc_{12}	14.4%	15.5%	27.7%		26.0%	26.2%	48.6%	3.50%	85.0%	39.1%	45.9%
iC_{12}										30.9%	39.0%
nC_{14}	7.5%	8.10%	14.4%								
nC_{16}	3.5%	1.78%	1.31%		18.0%	8.54%	16.0%				
iC_{16}		1.75%	0.003%			8.49%	1.77%				
nC_{18}	3.5%	1.21%									
nC_{20}					29.0%	29.1%			5.00%	4.88%	

In Scenarios 4 and 6, fresh iso-butanol serves as the co-feed in a proportionate ratio with butanol coming either from the condensation step or open source to attain the desired isomer content (~40%). In this scenario, iso-butanol (85 wt%) is dehydrated with a γ-Al_2O_3 catalyst at 325 °C, 1 atm, and a WHSV of 1 h^{-1}. The conversion of iso-butanol reaches 95%, with a selectivity of 95.1% towards isobutylene, accompanied by 1.6% 1-butene, 0.5% trans-2-butene, and 1.9% cis-2-butene [159]. Iso-butene undergoes oligomerization in the presence of an Amberlyst 35 catalyst at a temperature of 100 °C and a pressure of 250 psig. The molar selectivity of iso-butene oligomerization results in 20% C_8, 70% C_{12}, and 10% C_{16} [154]. Following the oligomerization of n-butene and iso-butene, the resulting olefins are blended in a mixer and fed to the hydrotreater. In this step, the hydro-isomerization reaction is omitted, as iso-butanol has been directly introduced. After the hydrotreating process, the produced alkanes are separated from hydrogen and directed to the fractionation column to isolate alkanes within the jet range. All the yield data and final composition of jet range alkanes are given in **Table 16** (**Table 24** and **Table 25** in ***Appendix B*** includes the chemical formulas)**.**

Table 16. The yield of olefins and alkanes from the oligomerization and isomerization reactions and final recovery after fractionation in butanol processes

Processes	**Scenario 3, 5 (butene oligomerization)**			**Scenario 4, 6 (butene oligomerization)**		
Components	**Oligomerization**	**Isomerization**	**Final jet range**	**Oligomerization 1**	**Oligomerization 2**	**Final jet range**
nC_4		3.76%				
nC_6						
nC_8	27.0%	3.05%	4.74%	27.0%		19.1%
iC_8		20.9%	30.7%		20.0%	8.77%
nC_{10}						19.9%
nc_{12}	26.0%	26.2%	48.6%	26.0%		
iC_{12}					70.0%	35.5%
nC_{14}						
nC_{16}	18.0%	8.54%	16.0%	18.0%		11.9%
iC_{16}		8.49%	1.77%		10.0%	4.90%
nC_{18}						
nC_{20}				29.0%		

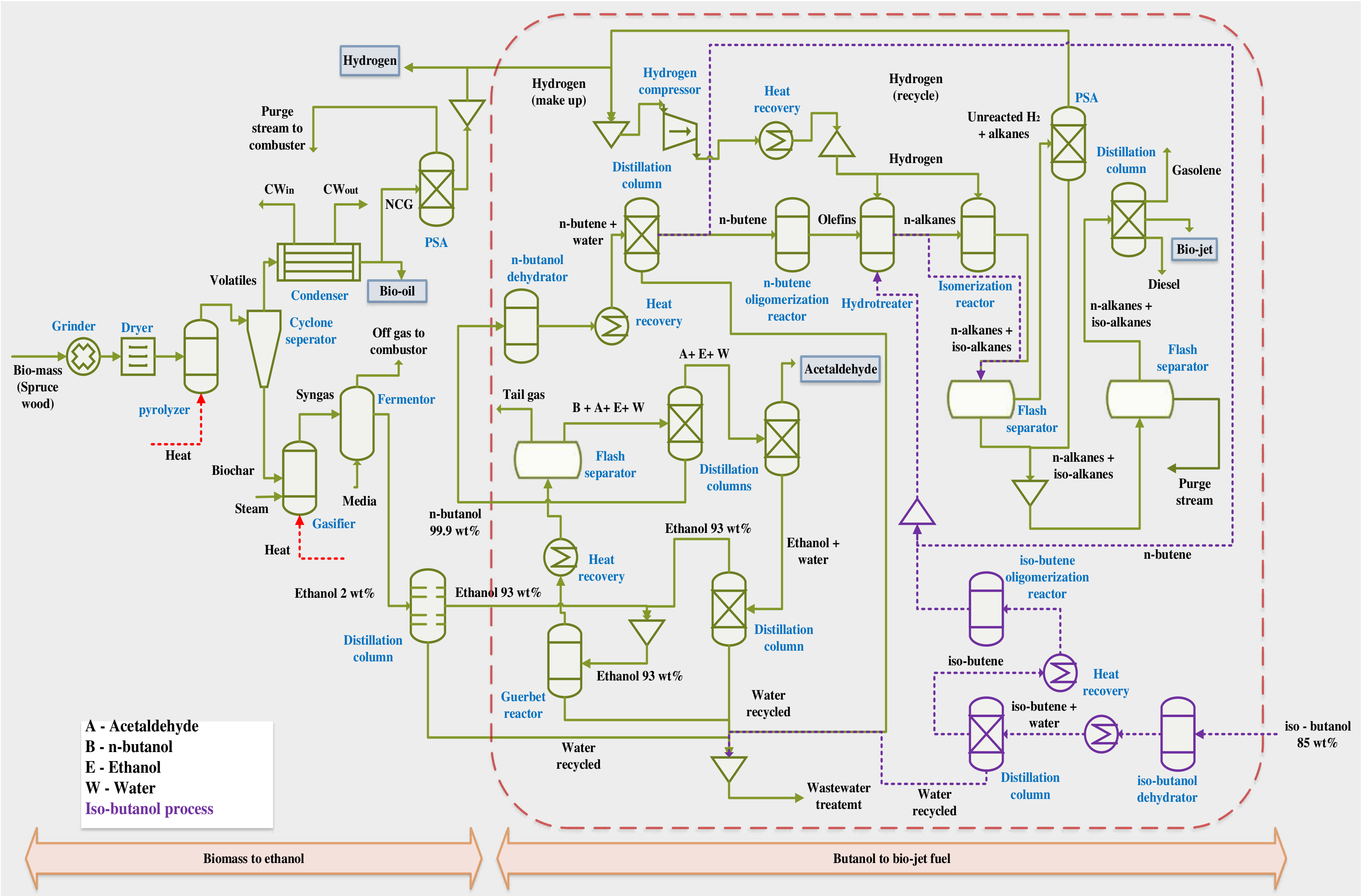

Figure 8. Bio-jet fuel production from butanol.

Note: The dotted line in the figures shows the system boundary which was modeled in this study.

3.5 Development of a techno-economic model

The plant investment cost has two components, the established upstream ethanol process from the fast pyrolysis of spruce wood chips and the downstream alcohol-to-jet processes [29, 36, 187]. In simulation and techno-economic analysis, the pyrolysis plant is assumed to generate ethanol for the jet fuel plant on-site in Calgary, Canada. The profitability assessment for each scenario in this study assumes a 10% internal rate of return (IRR) for 35 years, the minimum return required for a plant to recover its expenses [191]. The costs include both capital (CAPEX) and operating expenditure (OPEX). The critical assumptions for developing the techno-economic model are listed in **Table 17**.

Table 17. Key assumptions for the development of the techno-economic model

Parameter	Value	References
Plant lifetime (years)	35	N/A
IRR	10%	N/A
Base year	2019	N/A
Dollar used	USD	N/A
Location	Calgary, Alberta	N/A
Inflation factor of different[a]	2%	[188, 190, 191]
Plant start-up factor[b]		[200-204]
Year 0	0.7	
Year 1	0.8	
Year 2	0.85	
Spread of construction cost		[200]
Year 3	20%	

[a] (This is the average inflation over 12 years)

[b] These values are assumed based on operating factors reported in earlier studies on biomass handling facilities

N/A: Not applicable (assumed)

The capital cost (CAPEX), including construction, equipment costs, installation, etc., was calculated using Peters and Timmerhaus's method [186, 205]. After finalizing the process model in Aspen Plus, the costs for conventional equipment were calculated using the Aspen Process Economic Analyzer (APEA) [213]. The purchase costs for other non-conventional equipment were obtained from various published sources. In the spreadsheet-based techno-economic model, each piece of equipment is represented and sized according to its specific design parameters. When mapping reactors, a constant aspect ratio defined in Appendix C (L/D = 3) was maintained to ensure optimal and consistent equipment cost [205, 206]. The critical assumptions and formulas for developing the techno-economic model are listed in **Table 18**.

Table 18. Key formulas for the development of the techno-economic model

Parameter	**Value**
Method for estimating CAPEX [205]	
Total purchased equipment cost (TPEC)	**100% TPEC**
Total installed cost (TIC)	**302% TPEC**
Indirect cost (IC)	**89% TPEC**
Total direct and indirect cost (TDIC)	**TIC + IC**
Contingency	**20% TDIC**
Fixed capital investment (FCI)	**TDIC + contingency**
Location factor (LF)	**10% FCI**
Total capital cost (TCI)	**FCI+ LF**
Method for estimating OPEX	
Maintenance cost (M)	**3% TCI**
Operating charges (OC)	**25% of labor cost**
Plant overhead (PO)	**50% (labour cost + maintenance cost)**
Subtotal operating cost	**M + OC + PO + labour cost + raw materials cost + utilities cost**
General and administration (G & A)	**8% of subtotal operating cost**
Total operating cost	**G & A + subtotal operating cost**

To explore the cost allocation of capital expenditures, the principal operational process units for all the scenarios are defined as follows:

- **Dehydration unit** – Dehydration reactor, heat exchangers, heaters and coolers, and separator.
- **Oligomerization unit** – Cooler, filter, compressors, oligomerization reactors, and mixer.
- **Hydrotreating unit** – Heaters and coolers, hydrotreating and isomerization reactors, compressor, mixer, flash separator, and pressure swing adsorption (PSA) unit.
- **Fractionation unit** – Mixer, flash separator, and distillation column.

The plant's capacity and the scale-up facility were evaluated assuming ethanol is sourced from the market. The scale factor, which describes the nonlinear relationship in the cost model, is used to determine CAPEX when transitioning from one capacity to the next [207]. Capital investments are graphically depicted against their respective capacities to derive the scale factor for equipment, units, and the entire plant in each scenario. In the chemical industry, the scale factor averages about 0.6 and can be used for new technology as sufficient information is unavailable [208]. For petrochemical plants, the scale factor found by Mohajerani et al. is usually about 0.7 [207].

Following capital costs, the operating costs are crucial in the analysis and consist of variable and fixed costs. Variable operating costs include expenditures related to feedstock, utilities, wastewater treatment, and raw materials, such as catalysts and their replacement costs (catalyst activity tends to decrease over time) [16]. These costs are evaluated based on the energy and material balances derived from the process model. Fixed operating costs refer to labor, supervision, maintenance, and other general and administrative expenses [16]. In scenarios involving ethanol purchase, feedstock costs include the cost of merchant H_2. Conversely, in ethanol production scenarios, these costs include green H_2 sourced from the upstream process, with the surplus being sold at the same price.

A discounted cash flow model was developed to assess the cost of production of bio-jet derived from the combined CAPEX and OPEX. To estimate the bio-jet fuel cost, it was assumed that the cost is a function of ethanol feed rate and price; ethanol production costs are the same in all the cases for ease of economic comparison. A Morris sensitivity analysis was conducted on several process-sensitive input parameters (except plant lifetime) to see the impact on the bio-jet fuel price, along with the traditional sensitivity analysis with a tornado plot (including plant lifetime). The formal sensitivity analysis ignores the effect of interactions between the input parameters, while the Morris method considers these interactions using the Regression, Uncertainty, and Sensitivity Tool (RUST) [36]. RUST was further used with the parameters of greatest impact to run a Monte Carlo simulation to determine the uncertainty in the profitability of the processes. For the uncertainty analysis, triangular distributions between the minimum and maximum values were used over 30,000 runs to determine the probability distribution of the cost of bio-jet fuel.

Chapter 4. Results and Discussions

4.1 Material balance and production rate

This study explores five hypothetical production scenarios, each featuring two cases that use either merchant ethanol or ethanol from an upstream process. In addition, two single-case scenarios involving butanol are considered. Process yield, relative to biomass and ethanol feed, along with the final recovery after fractionation column loss and isomer content, are assessed through the material balance using Aspen Plus. **Figure 9** illustrates three production parameters. The order of increasing process yield, and final recovery is as follows: Scenario 1 < base scenario < Scenario 3 < Scenario 5 < Scenario 2 < Scenario 4 < Scenario 6. The reported improvement in the process yield is attributed to an increased carbon number in higher olefins [33]. Bio-jet fuel yield hinges on the conversion rate of the oligomerization step, which has been identified as a bottleneck in every pathway. The highest yield, recovery, and isomer content are observed in Scenario 6.

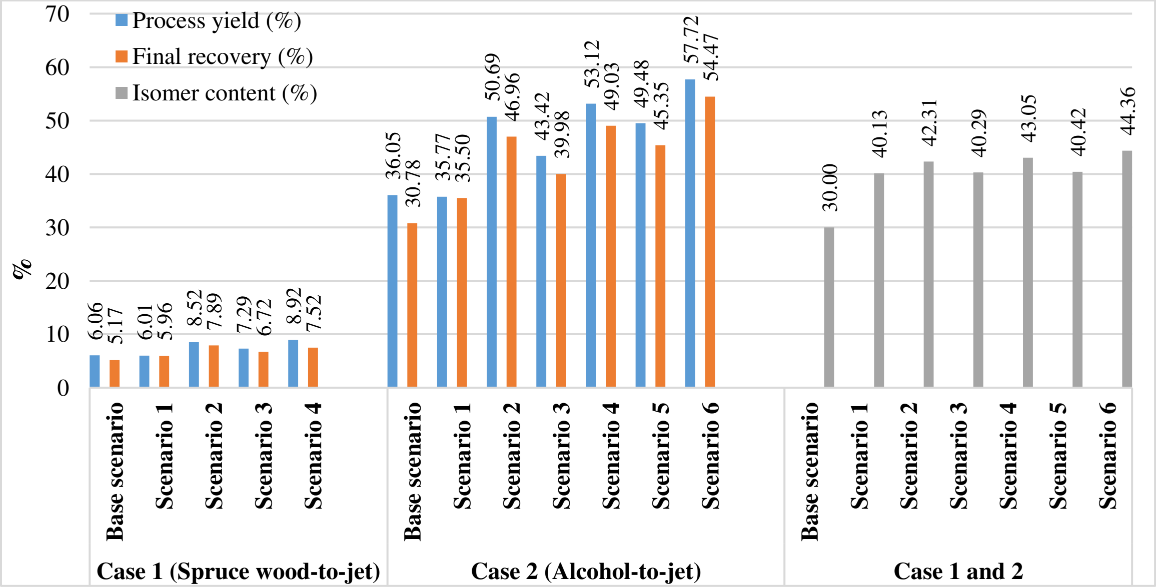

Figure 9. Production rate results in each scenario

4.2 Energy consumption

The energy consumption for the primary process units is consistent in the ATJ refinery section in every scenario because of similar operations (shown in **Figure 10**) and is notably lower than the cradle-to-gate (Case 1) energy demand in the respective scenarios (**Figure 11**).

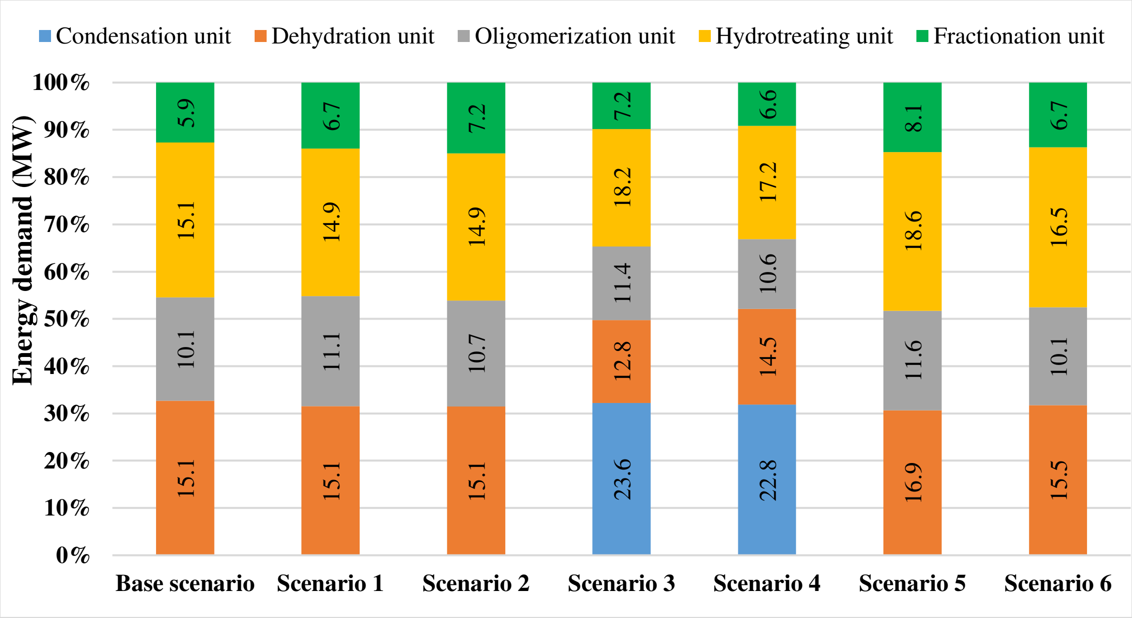

Figure 10. Energy demand in the biorefinery in the alcohol-to-jet (ATJ) pathways (Case 2)

Waste heat recovery heat exchangers were used for energy optimization through heat integration during the simulation. In the cradle-to-gate integrated refinery, there is an additional energy demand in field preparation, feedstock transportation, and the upstream ethanol refinery stages. The contributions of field preparation and feedstock transportation are comparatively lower, ranging from about 3.3% to 5.8% and 5.6% to 9.8%, respectively, than the biorefining stage. [9, 56]. The plant gate was chosen as the endpoint for a consistent comparison.

As with other NER calculations, evaluating the efficiency of a bio-jet fuel production process involves comparing the usable energy output to the total fossil energy input throughout the entire life cycle. A positive NER value signifies that the bio-jet/biofuel plant is energy efficient, generating more usable energy than the total fossil energy demand for its production [36, 209]. **Figure 11** shows the energy sustainability of the proposed pathways, with reasonably high NER ratios.

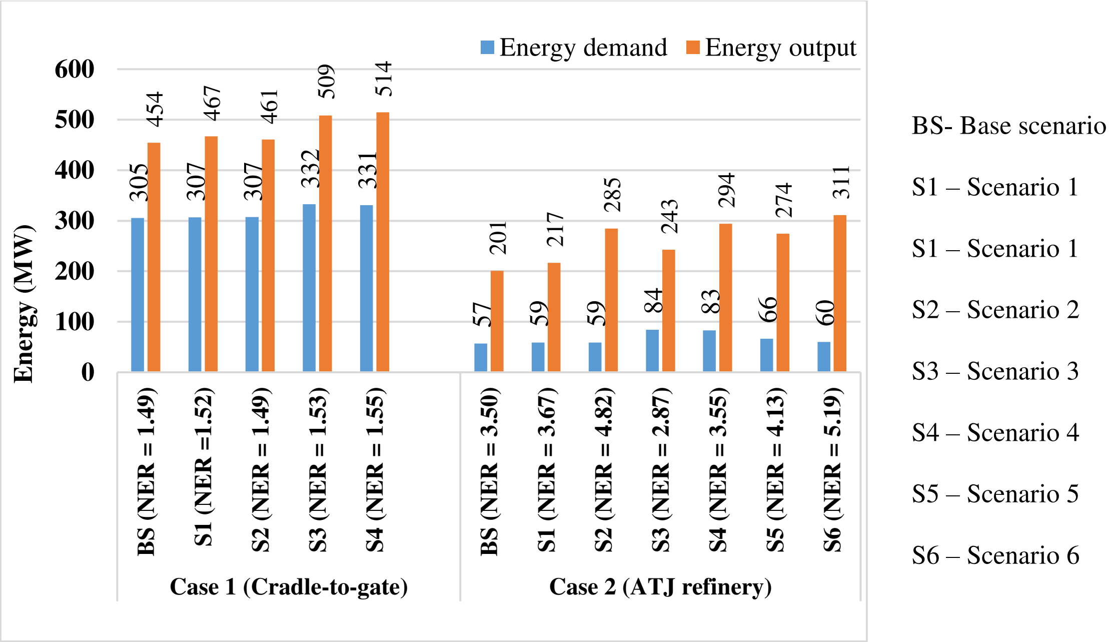

Figure 11. Energy profile comparison (cradle-to-gate integrated refinery, ATJ refinery itself)

4.3 Techno-economic evaluation

4.3.1 Capital cost

Figure 12 shows the overall capital investments (CAPEX) in the scenarios at a baseline capacity in the following order: Scenario 1 > Scenario 2 > base scenario > Scenario 4 > Scenario 5 > Scenario 3 > Scenario 6. Scenario 1 is the most capital-intensive, around 1.21 and 1.85 times higher than Scenario 6 (lowest) and the base case scenario, respectively. The reactors are the primary cost contributors to CAPEX compared to the auxiliary equipment in all the scenarios. **Figure 12** also breaks down capital investments for key units in every scenario, which are estimated from our APEA analysis results and the findings/results from the literature. The oligomerization and hydrotreating units account for a significant portion of CAPEX because of the thermodynamic and operational demands of multiple reactors, larger vessels to accommodate increased volumes, and demand for more auxiliary components than usual.

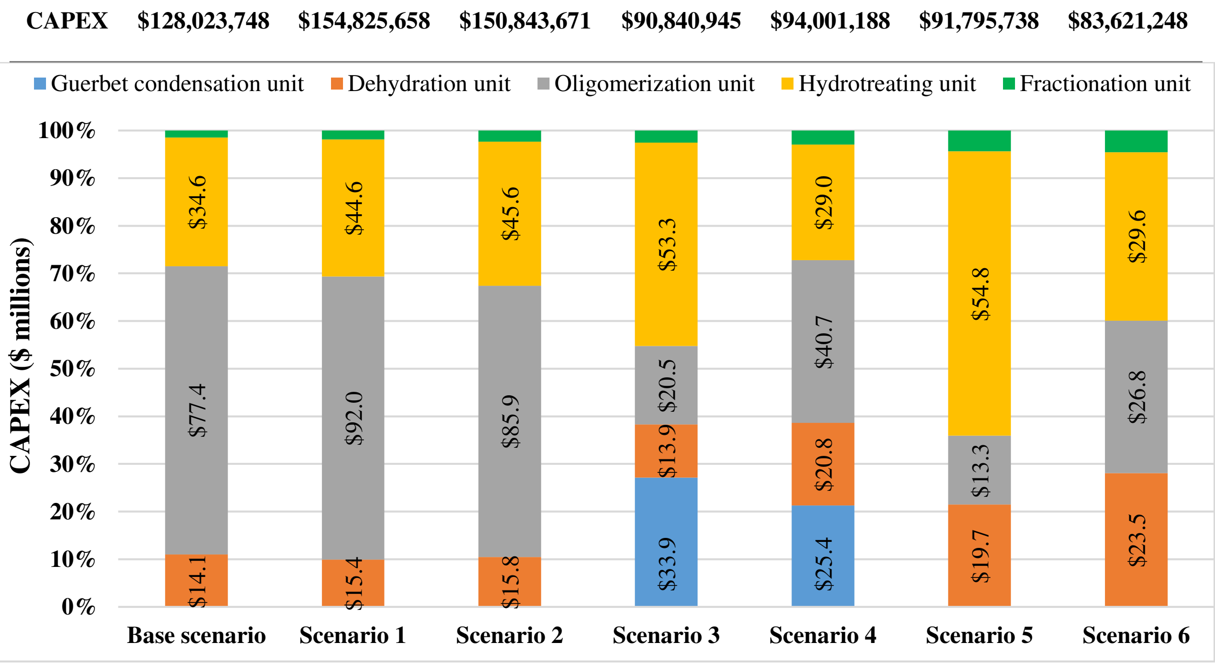

Figure 12. CAPEX of significant units, by scenario (alcohol-to-jet refinery) [67]

4.3.2 Scale factor and economies of scale

The scale factor links capital investment to plant capacity and guides the decision on the most profitable plant size. To evaluate the scale factor for an ATJ refinery, plant capacities were increased hypothetically from 2000 to 50000 kg/hr (as shown in **Figure 13**). The overall scale factor increases in the order of Scenario 6 > Scenario 4 > Scenario 3 > Scenario 5 > Scenario 2>

base scenario > Scenario 1. **Table 19** shows Table 19. The scale factor for individual units, reactors, and overall plants in every scenario as estimated in this study and under assumed conditions. This table also shows the relevant values found in published studies. Regardless of the scenario, similar operations exhibit consistent scale factors also shown in **Figure 12**. However, some reactors exhibit considerably higher scale factors than the overall unit, a discrepancy that is a result of several factors.

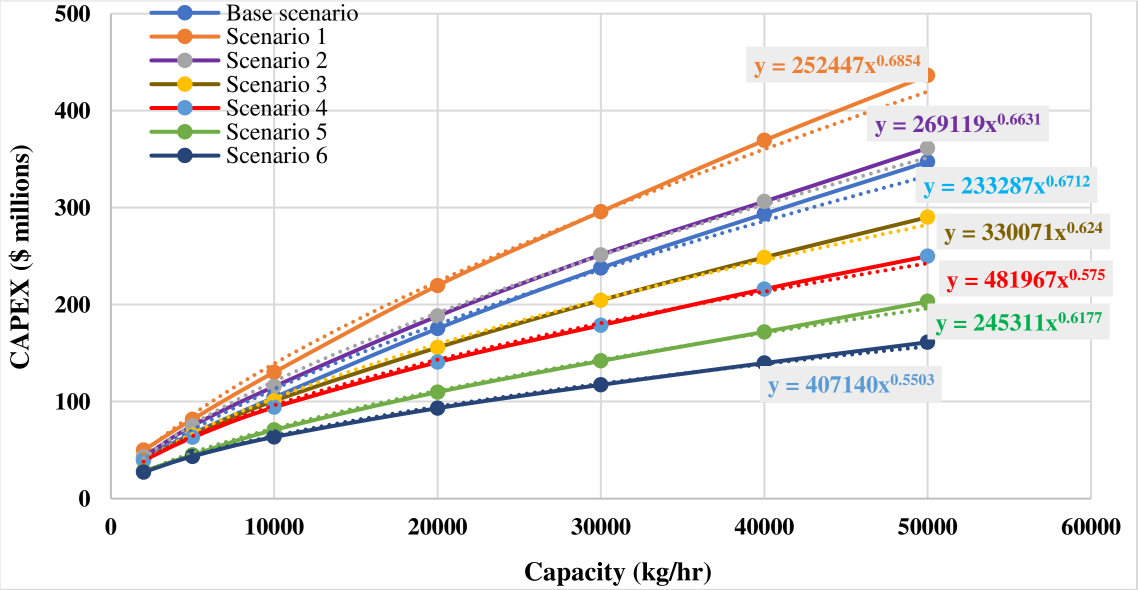

Figure 13. The scale factor for the overall capital investment in every scenario

While mapping the reactors using a constant aspect ratio of 3 in APEA, a limitation was found in that the maximum vessel length becomes a constraint beyond a specific feed volume; moreover, the maximum vessel length varies among reactors too. To address these constraints, the incoming feed is divided into multiple streams, and several identical reactors, each smaller than the total capacity, are considered to estimate equipment costs. Oligomerization reactions with liquid catalysts introduce an additional requirement for a standby reactor to facilitate catalyst regeneration.

Table 19. The scale factor for individual units, reactors, and overall plants in every scenario

Scenario	Scale Factor									
	Condensation unit		Dehydration unit		Oligomerization unit		Hydrotreating unit		Fractionation unit	Overall
Base Scenario	n/a		EU	0.75	EU	0.72	EU	0.55	0.53	0.67
			DR-E	0.80	OR-E	0.82	HDR	0.84		
							HIR	0.78		
Scenario 1	n/a		EU	0.74	EU	0.72	EU	0.62	0.54	0.68
			DR-E	0.80	OR-E	0.82	HDR	0.86		
					OR-N	0.72	HIR	0.79		
Scenario 2	n/a		EU	0.74	EU	0.70	EU	0.60	0.51	0.66
			DR-E	0.80	OR-E	0.82	HDR	0.86		
					OR-H	0.63	HIR	0.78		
Scenario 3	EU	0.60	EU	0.74	EU	0.55	EU	0.62	0.54	0.62
	CR	0.66	DR-E	0.76	OR-N	0.55	HDR	0.79		
							HIR	0.78		
Scenario 4	EU	0.67	EU	0.67	EU	0.57	EU	0.44	0.53	0.58
	CR	0.66	DR-N	0.75	OR-N	0.57	HDR	0.68		
			DR-I	0.72	OR-I	0.59				
Scenario 5	n/a		EU	0.71	EU	0.59	EU	0.60	0.53	0.65
			DR-N	0.75	OR-N	0.59	HDR	0.86		
							HIR	0.75		
Scenario 6	n/a		EU	0.67	EU	0.58	EU	0.43	0.55	0.55
			DR-N	0.75	OR-N	0.58	HDR	0.68		
			DR-I	0.72	OR-I	0.59				
Literature data	n/a		0.65		0.56		0.62		n/a	0.6~0.7
Reference			[69]		[69]		[207]			[207]

EU – Entire unit, CR – Condensation reactor, DR-E – Ethanol dehydration reactor, DR-N – n-butanol dehydration reactor, DR-I – isobutanol dehydration reactor, OR-E – Ethylene oligomerization reactor, OR-N – n-butene oligomerization reactor, OR-H – Hexene oligomerization reactor, OR-I – iso-butene oligomerization reactor, HDR – Hydrotreater, HDI – Hydroisomerization reactor.

The expansion of capacity, considering the aforementioned factors, results in a comparatively higher additional CAPEX with elevated scale factors. The scale factor for the fractionation unit stands out as relatively lower than the other units because of the minimum CAPEX, attributed to the minimal number of pieces of equipment involved. **Figure 14** and **Figure 15** visually represent the relationship between the capital cost of significant units and plant capacity.

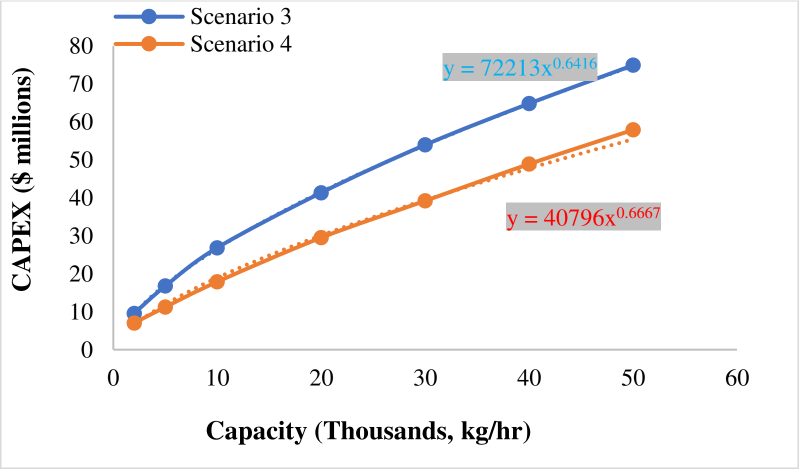

Guerbet condensation

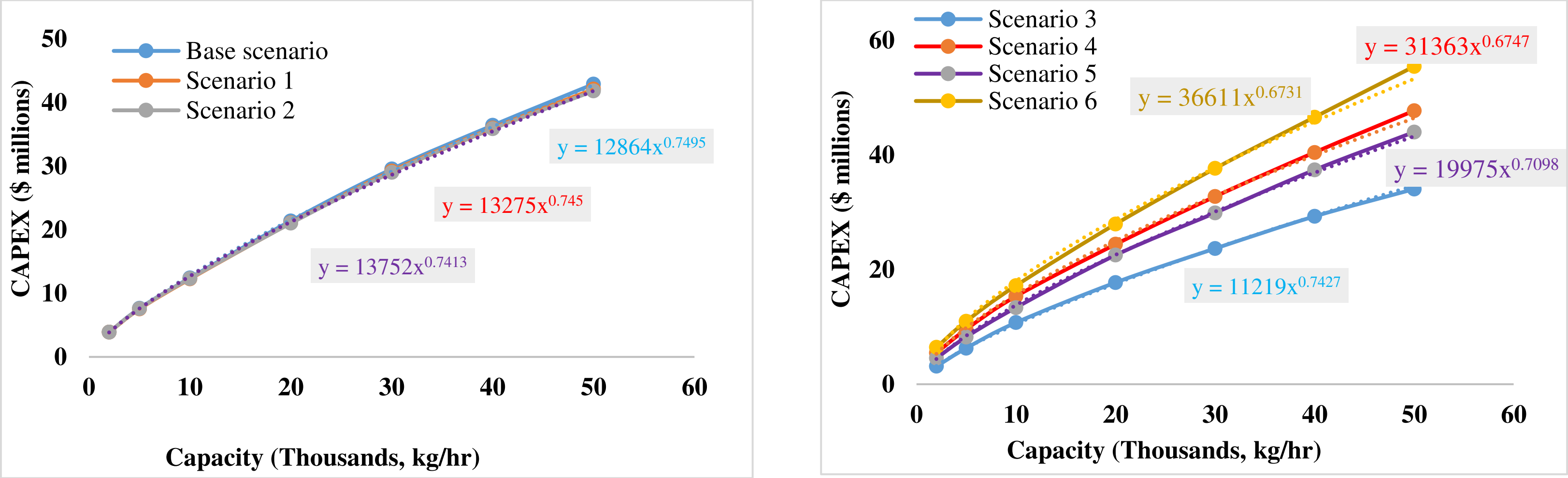

Ethanol dehydration **Butanol dehydration**

Figure 14. The scale factor for the primary unit operations

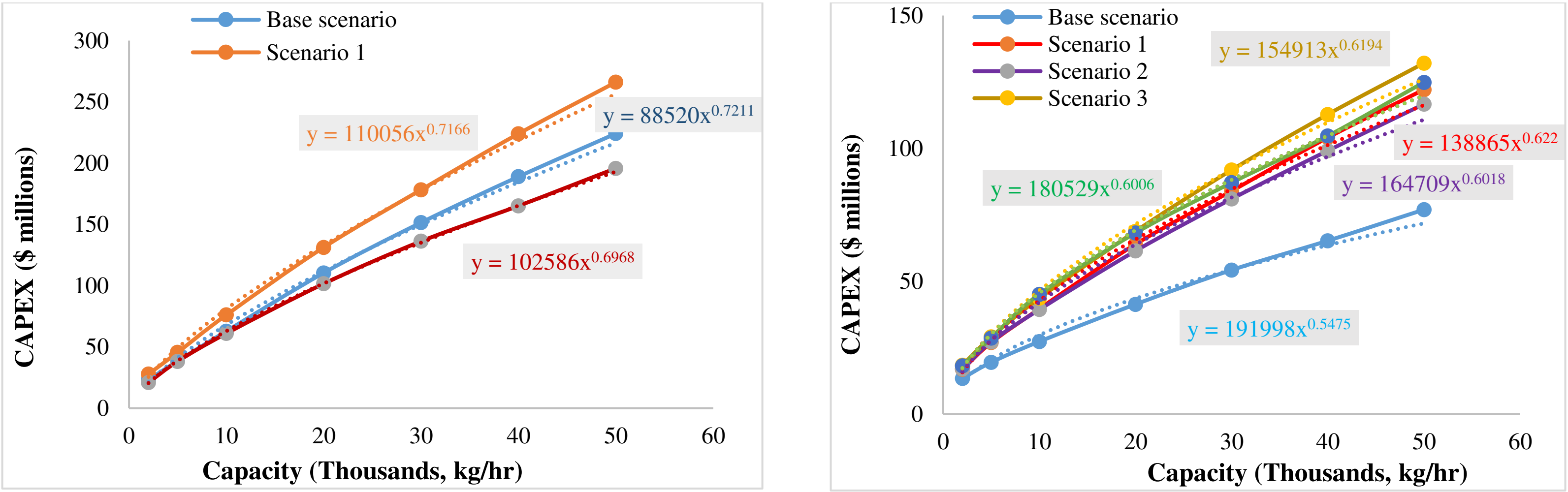

Ethylene oligomerization **Hydroisomerization and hydrotreating**

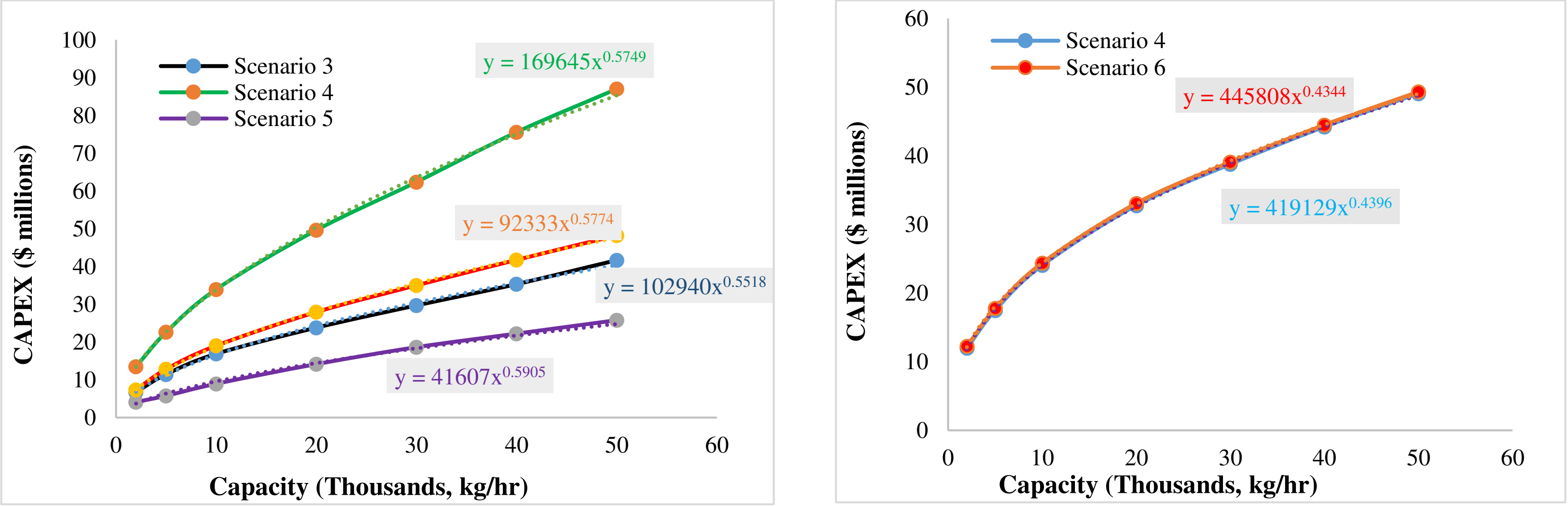

Butene oligomerization **Hydrotreating**

Figure 15. The scale factor for the primary unit operations

This study also examines the impact of plant capacity on the capital investment per unit of processed alcohol, as shown in **Figure 16**. While the total capital cost rises with increasing capacity, a diminishing rate of increase is observed in all cases. This declining trend signifies economies of scale. For instance, if the scale factor is 0.7, a 1% increase in plant size results in a 0.7% increase in capital cost. After an initial sharp decline in the curve for small capacities, the slope of the curve also decreases in every scenario, indicating a diminishing return with additional capacity. This suggests that economies of scale become less significant after the plant reaches a specific higher capacity (50000 kg/hr).

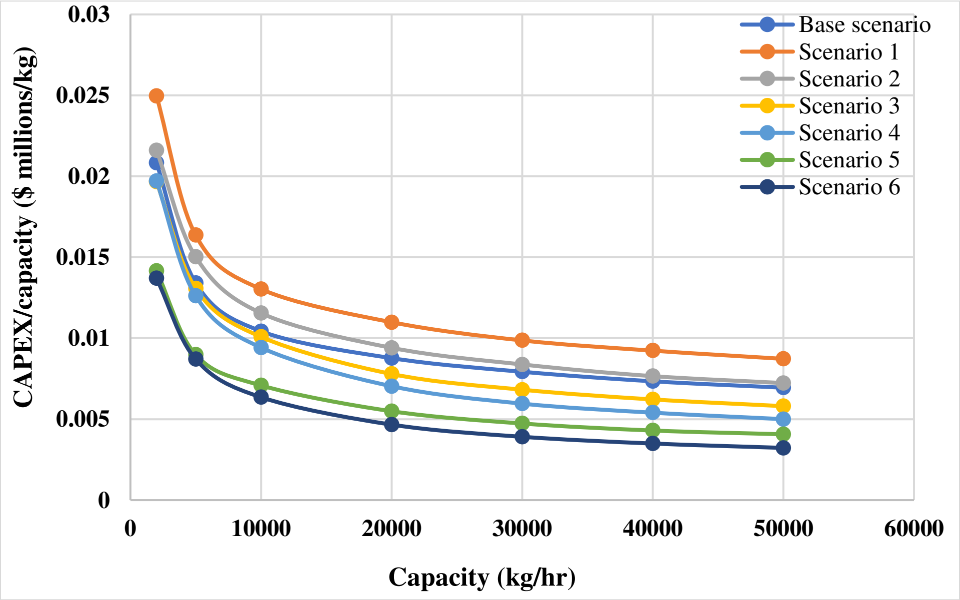

Figure 16. Influence of capacity on capital cost per unit of alcohol processed (Case 2)

4.3.3 Operating cost

The operating cost is established in every scenario using the capital cost. Variable operating costs, derived from utilities, raw materials, and feedstocks, include electricity, steam (medium, high, and low pressure), cooling water, chilled water, and refrigerant. Wastewater generated is sustainably managed through disposal in a wastewater treatment plant and factored into utility costs. Labor costs, based on the total number of labor requirement provided by the APEA process model and considering the average Canadian labor wage, are incorporated. Fixed operating costs are computed using the values in **Table 18**. In the discounted cash flow analysis, operating costs for the initial year and yearly escalations up to the end of the plant's lifetime are considered. The feedstock cost has the highest contribution to the total operating cost in all cases, as shown in **Figure 17**.

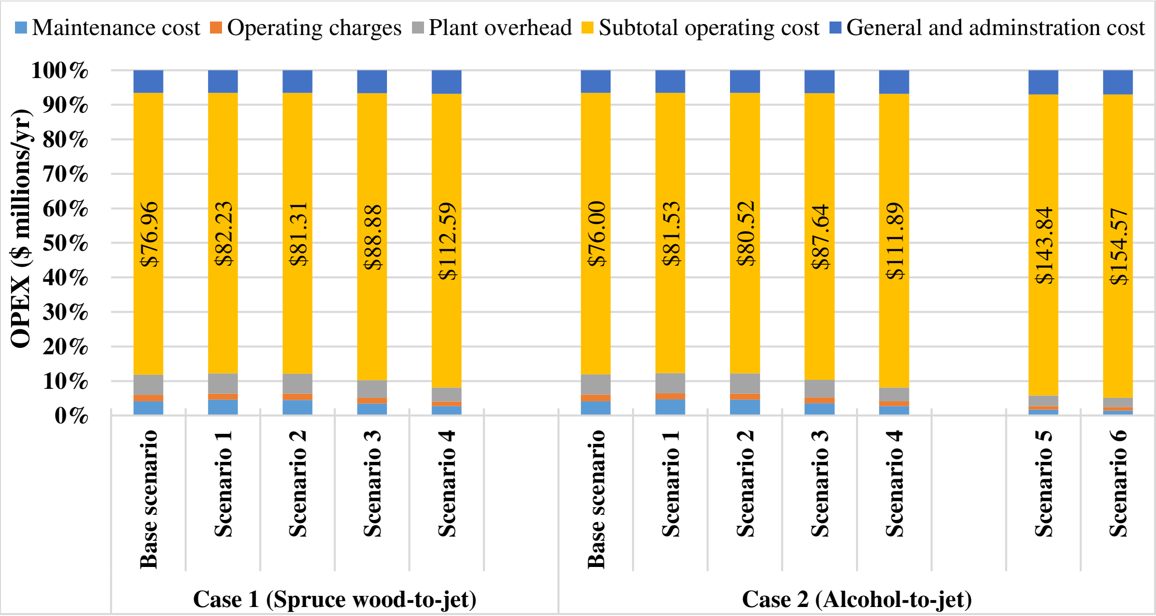

Figure 17. Operating cost distribution in every scenario

In **Figure 18** the cost components are compared for the best and base case scenarios at baseline capacity by highlighting the feedstock cost by percentage shares. Capital cost is the second-highest contributor, at approximately 15-16%. The remaining cost components range from 2% to 10% in every scenario, with the raw materials, specifically catalyst cost, contributing the least. Operating labor costs is relatively low because of the extensive use of automated machinery in the processes.

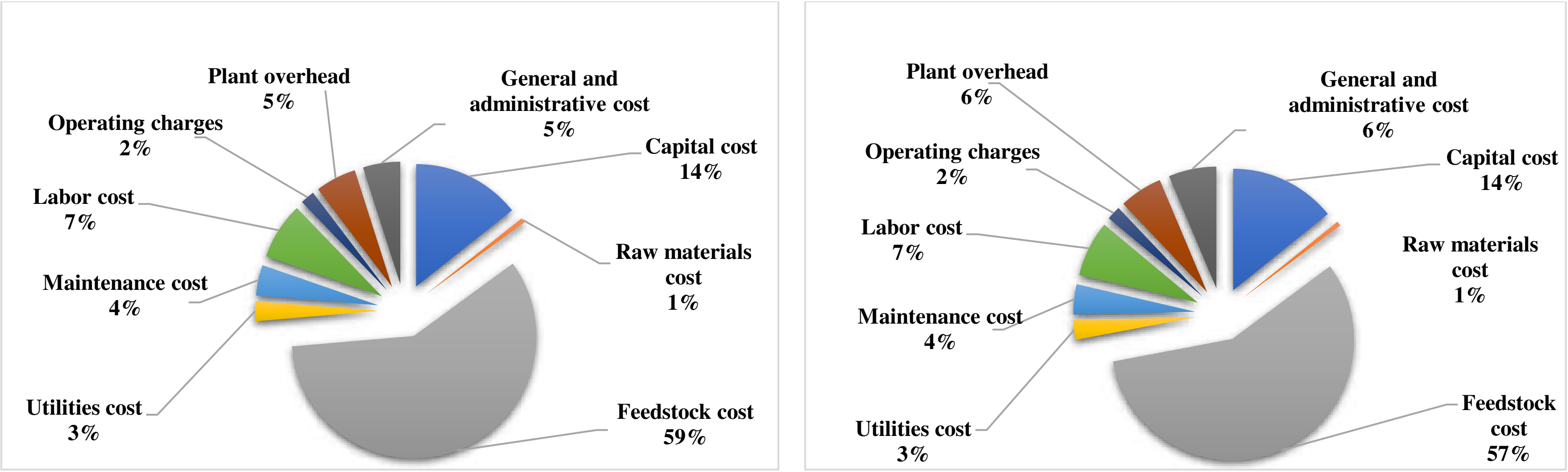

Base scenario, Case 1

Base scenario, Case 2

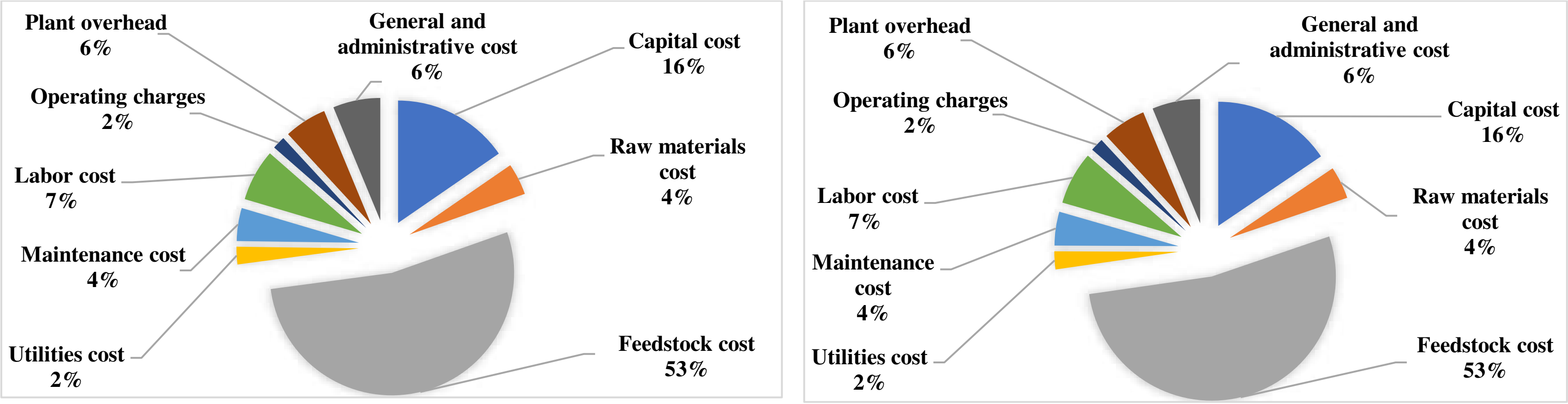

Scenario 2, Case 1

Scenario 2, Case 2

Figure 18. Overall cost comparison of the base and best-case scenarios for the baseline capacity

4.3.4 Process optimization

In Case 1, in every scenario, the feedstock cost ranges from 51% to 64% of the total cost. For ethanol processes in Case 2, the feedstock cost makes up 25% to 60% and increases as the capacity increases, from 2000 kg/hr to 50000 kg/hr. In the butanol process, feedstock cost is from 35% to 80% for the selected range of capacities shown in **Figure 19**. Processes involving butanol offer advantages in terms of production rate, energy sustainability, and capital cost. However, the feedstock cost is notably higher, up to 80% for larger capacities, as shown in **Figure 19**.

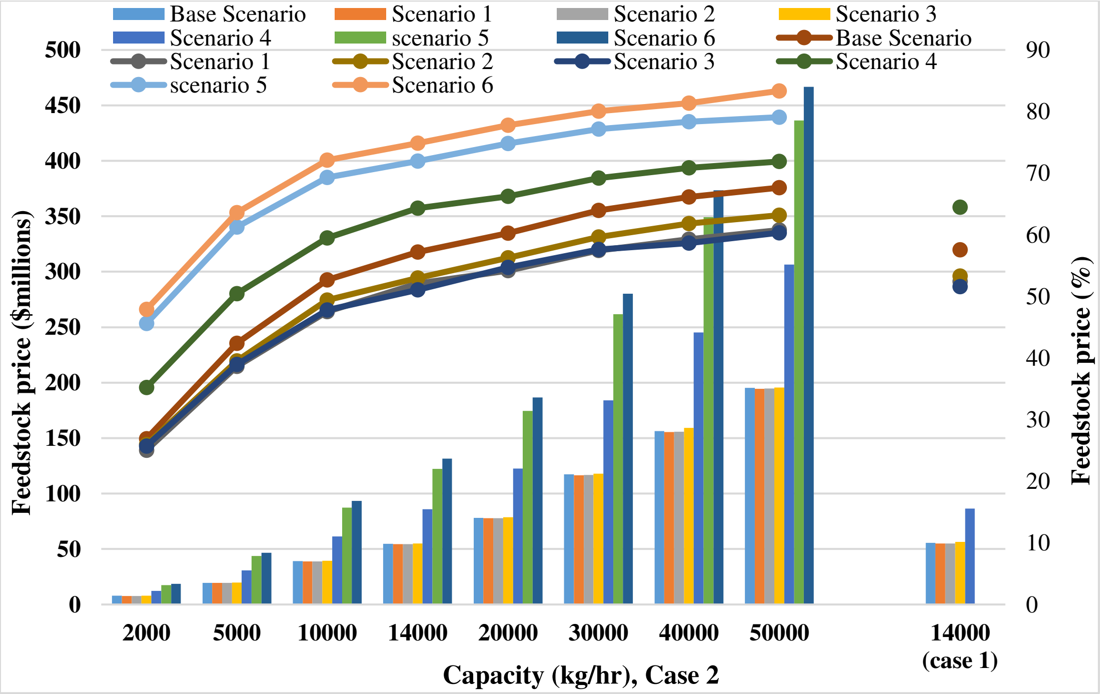

Figure 19. Comparison of feedstock prices of all the scenarios

This results in higher operating costs (shown in **Figure 17**) than ethanol processes. Moreover, Feedstock cost comes from the prices of ethanol, n-butanol, iso-butanol, and hydrogen. Processes involving recycle streams, purge streams, and make-up streams of feeds contribute to the non-uniformity of price variations which is reflected in **Figure 19**. Considering all the factors, Scenario 2 emerges as the most optimized condition.

4.3.5 Cost of production

Figure 20 illustrates the production costs of bio-jet fuel in every scenario and respective cases, while **Table 20** lists values for a capacity of 14000 kg/hr. The calculated cost of production (COP) ranges from \$0.97-\$2.12/L (\$1.43-\$3.27/kg), peaking at 2.26 times the price of conventional jet fuel (\$1.12/L) [69]. This aligns with the results in the literature, where bio-jet costs are 2-6 times higher than traditional jet fuels, depending on factors such as feedstocks and processes [210].

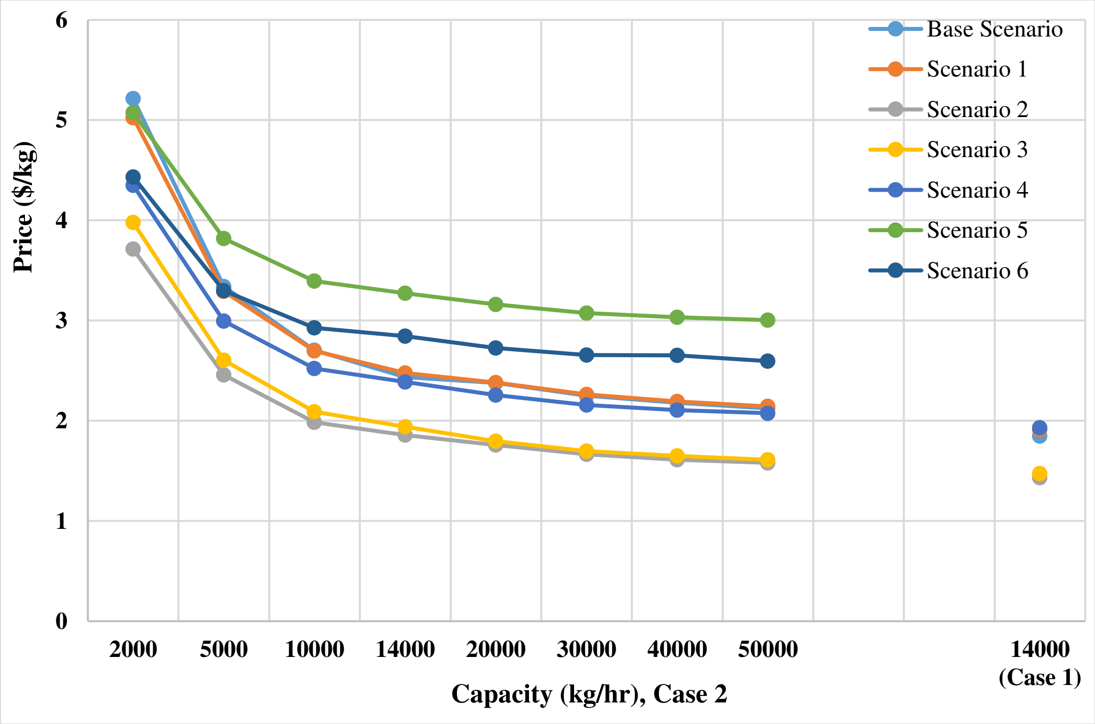

Figure 20. Bio-jet fuel price and indications of economies of scale in every scenario

In every scenario in Case 1, additional revenue is generated from green hydrogen produced in the upstream process along with the bio-jet. Scenarios incorporating Guerbet condensation also benefit a little by producing saleable acetaldehyde as a by-product. Case 1 in Scenario 2 produces bio-jet at the lowest cost; this is attributed to its higher yield, as shown in Table 7, and establishes it as the optimal case.

Table 20. Bio-jet fuel prices in every scenario for the baseline capacity (14000 kg/hr)

Bio-jet price	**Case 1**		**Case 2**			**Bio-jet price**	
Base scenario	$1.17/L	$1.85/kg	$1.85/L	$2.44/kg	**Scenario 5**	$2.12/L	$3.27/kg
Scenario 1	$1.24/L	$1.91/kg	$1.60/L	$2.48/kg	**Scenario 6**	$1.78/L	$2.85/kg
Scenario 2	$0.94/L	$1.43/kg	$1.22/L	$1.86/kg	**Conventional price (fossil jet)**	$1.12/L	
Scenario 3	$0.97/L	$1.47/kg	$1.28/L	$1.94/kg			
Scenario 4	$1.20/L	$1.93/kg	$1.48/L	$2.39/kg			

4.3.7 Sensitivity analysis

A sensitivity analysis was performed for both the base and best case scenarios at a capacity of 14000 kg/hr through Morris sensitivity analysis and tornado plots (as illustrated in **Figure 21** and **Figure 22**). This involved assessing the impact of inputs such as feedstock price, plant lifetime, discount rate and the costs of capital, maintenance, labor, plant overhead, operating charges, general and administration (G&A), utility by varying them by +/- 20% of their default values.

Morris sensitivity analysis randomly changes one parameter at a time by the same relative amount. For each parameter, the mean and standard variation were calculated. The plot's horizontal axis shows the mean change in input parameters and the vertical axis shows the standard deviation, indicating how a parameter relates to others nonlinearly influencing the bio-jet price. The most sensitive parameters are those with the highest mean and standard deviation, while parameters in the lower left corner have an insignificant effect and are excluded from uncertainty analysis.

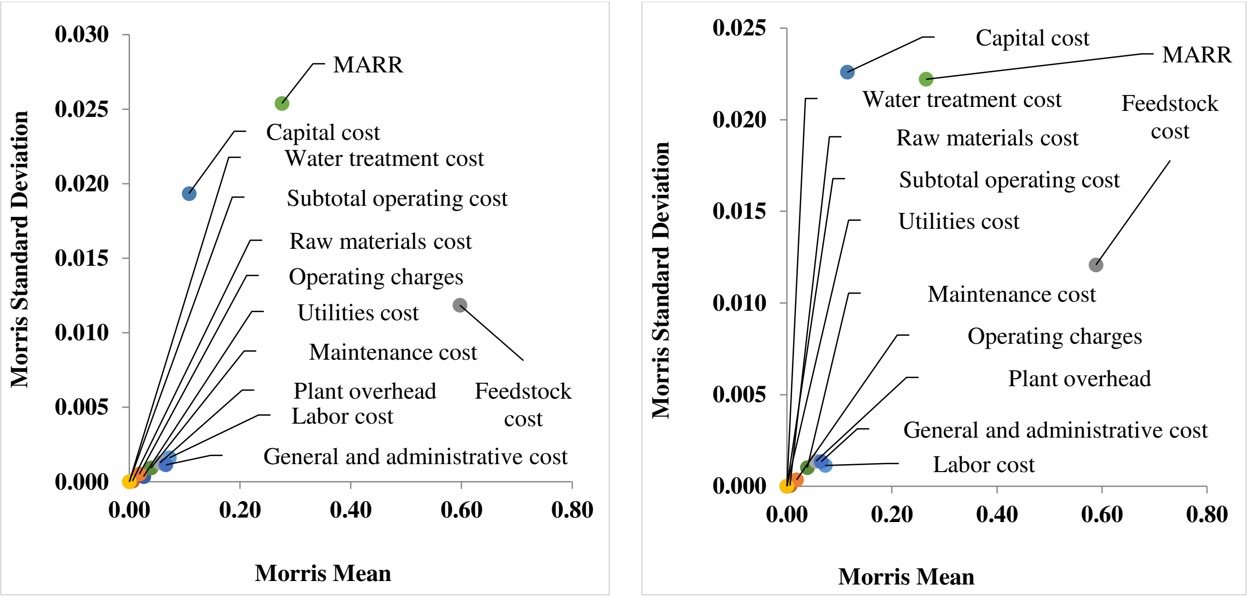

Base scenario, Case 1 **Base scenario, Case 2**

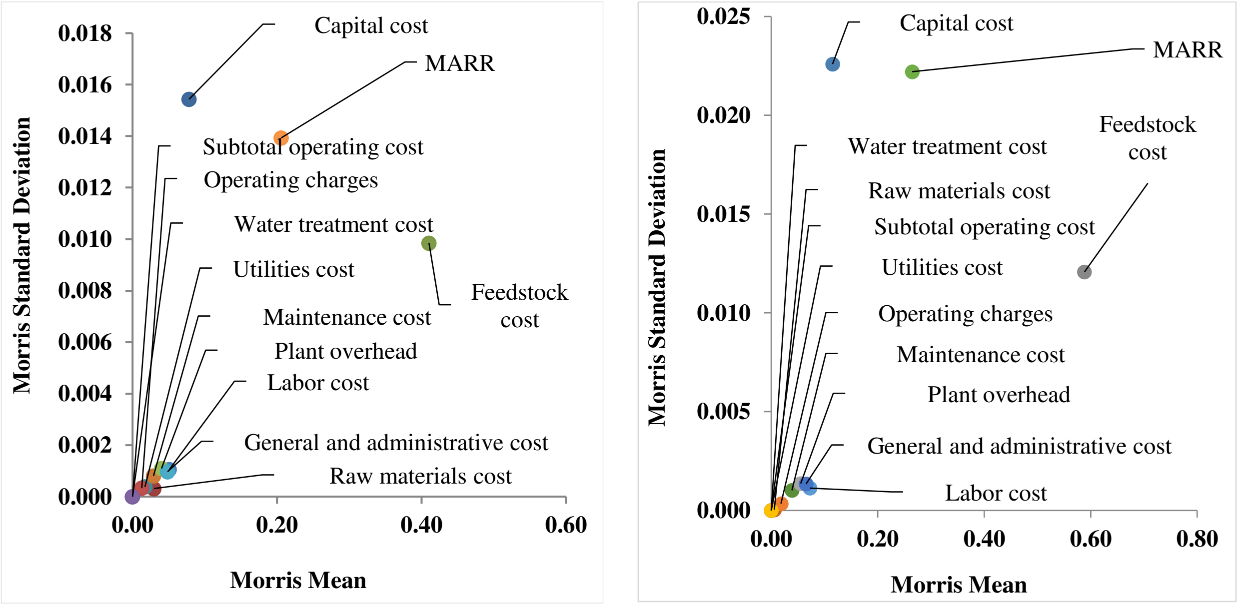

Scenario 2, Case 1 **Scenario 2, Case 2**

Figure 21. Sensitivity analysis (Morris plot) of the base and best-case scenarios for the baseline capacity

The tornado plot specifically features the sensitivity of bio-jet production cost to plant lifetime along with the other parameters considered in the Morris plot. Interestingly, the relationship between the cost of bio-jet and plant lifetime is opposite to that of the other parameters. An increase in plant lifetime leads to a decrease in bio-jet price, and vice versa. According to both the Morris and tornado plots, the parameter that most affects bio-jet price is the feedstock price. When feedstock costs decrease, the cost of production (COP) decreases. COP is also influenced by plant lifetime, discount rate, capital cost, and labor cost for both the base and best-case scenarios.

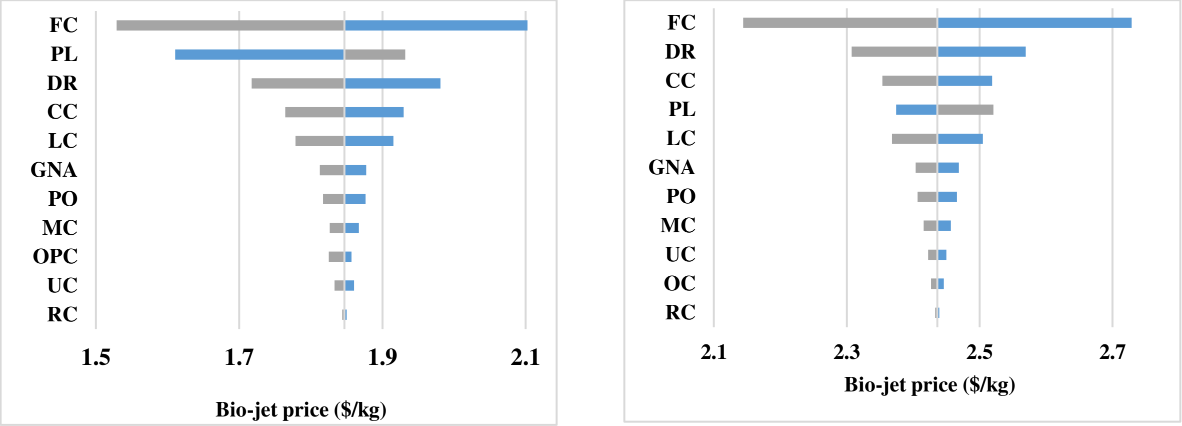

Base scenario, Case 1 **Base scenario, Case 2**

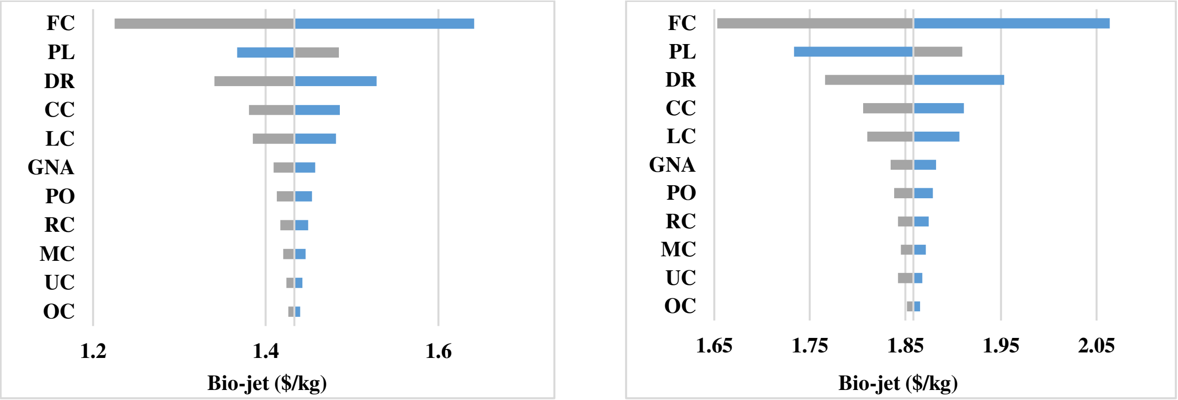

Scenario 2, Case 1 **Scenario 2, Case 2**

Figure 22. Sensitivity analysis (Tornado plot) of the base and best-case scenarios for the baseline capacity

4.3.8 Uncertainty analysis

In sensitivity analysis, one parameter is changed at a time, assuming others remain constant. To better understand the impact of uncertainty and risk on bio-jet production costs, uncertainty analysis was conducted. The Monte Carlo simulation was applied to each case in both the base and best-case scenarios for a 14000 kg/hr capacity plant with a focus on highly volatile cost components, particularly the feedstock price (**Figure 23**). This involved simultaneous variations of multiple parameters to address those highly uncertain and volatile because of the lack of field data. In the Monte Carlo simulation, values were randomly chosen from the entire parameter range and iterated 30,000 times using a probability function to generate a range of production costs. The simulation output provides the mean and the most likely bio-jet costs (**Table 21**). Controlling these parameters is crucial for ensuring the economic viability and competitiveness of this pathway.

Table 21. Production cost ranges from the Monte Carlo simulation

Bio-jet fuel price range ($/kg)		**Most likely**	**Mean**
Base case scenario	Case 1	1.85 ± 0.018	1.91
	Case 2	2.44 ± 0.016	2.51
Scenario 2 (Best case scenario)	Case 1	1.43 ± 0.014	1.47
	Case 2	1.86 ± 0.012	1.83

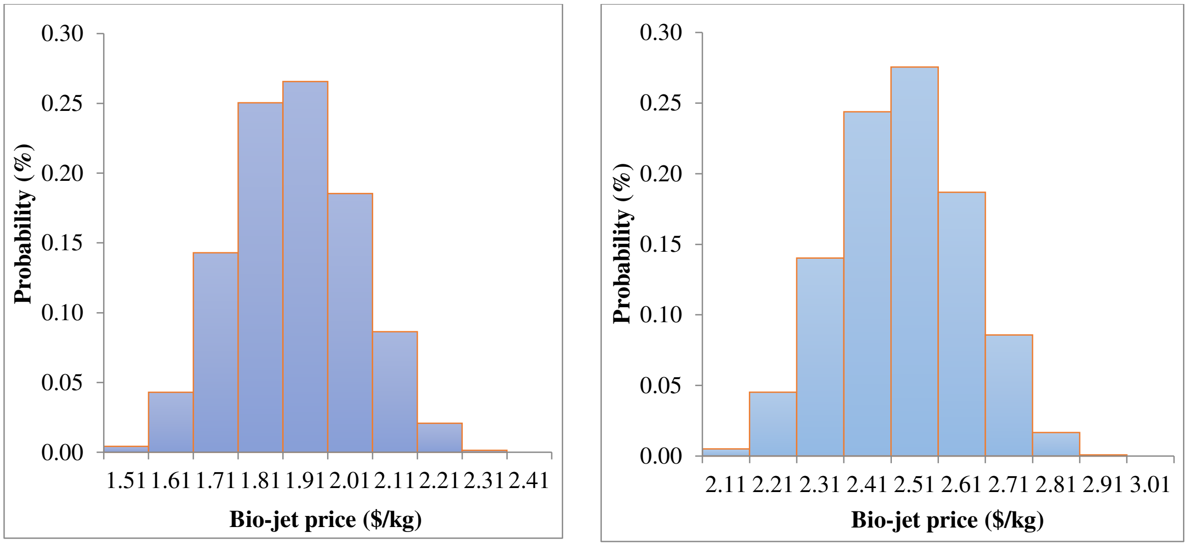

Base scenario, Case 1 **Base scenario, Case 2**

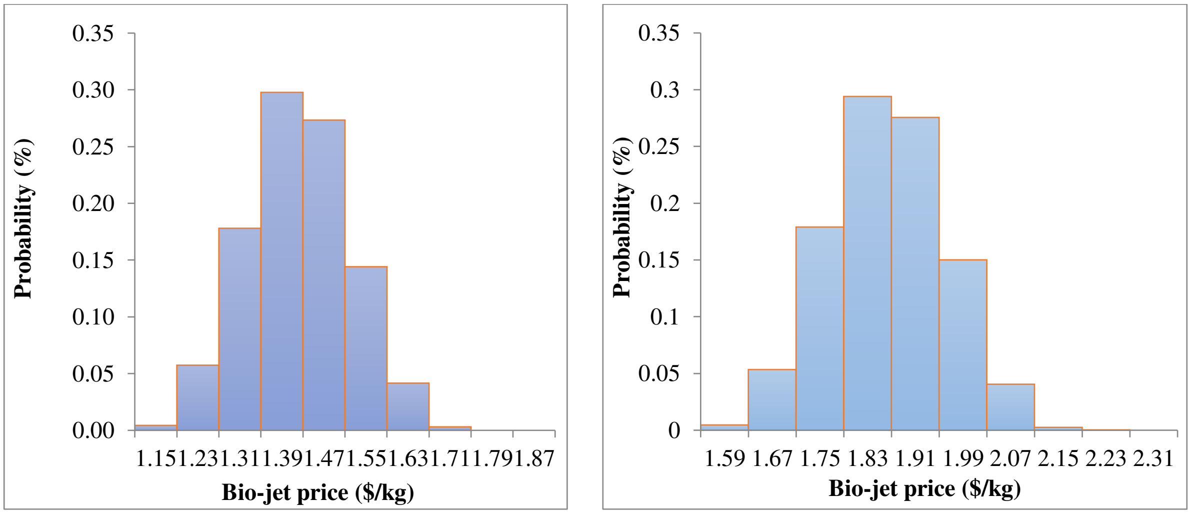

Scenario 2, Case 1 **Scenario 2, Case 2**

Figure 23. Uncertainty analysis of the base and best-case scenarios

Chapter 5. Conclusions and recommendations for future work

5.1 Conclusion

The alcohol-to-jet (ATJ) pathway includes several methods that convert biomass into bio-jet using alcohol intermediates. The methods used to create alcohol platform molecules are more advanced than those used to turn these intermediates into bio-jet fuel. However, jet fuel production pathways that use ethanol and butanol as intermediates are the most advanced ATJ pathways; significant research efforts have been made, and the pathways are certified by ASTM. One of the main areas of current research is using lignocellulosic biomass as feedstock to convert to bio-aviation fuel via the ATJ process. The technical process of producing bio-jet from platform alcohol molecules has been highlighted in this paper, in particular the process chemistry, process conditions, and other features such as temperature, pressure, catalysts, significant milestones during the development of catalysts over the years, reactor type, and other reaction parameters, etc. Over the years, considerable work has been done to develop suitable catalysts and operating conditions to facilitate the individual unit operations to make the entire jet fuel production process energy efficient and economical.

The major findings of this research are compared in **Figure 24** which includes process yield (%), isomer content (%), and bio-jet price ($/L). The yield from the processes varies from 36% to 58% in case 2 (6 ~ 9% in case 1 which is calculated based on the biomass feedstock) while the maximum yield at scenario 6. Apart from the base scenario isomer content is around 40% in all the processes which meets the criteria for commercial grade. calculated cost of production

(COP) or bio-jet price ranges from \$0.97 - \$2.12/L (\$1.43 - \$3.27/kg), peaking at 2.26 times the price of conventional jet fuel (\$1.12/L) with the lowest price at scenario 2. The price range from the scenarios aligns with the results in the literature, where bio-jet costs are 2 - 6 times higher than traditional jet fuels. Scenario 2 was chosen as the most optimum considering the process yield, CAPEX, OPEX, energy requirements, and bio-jet price.

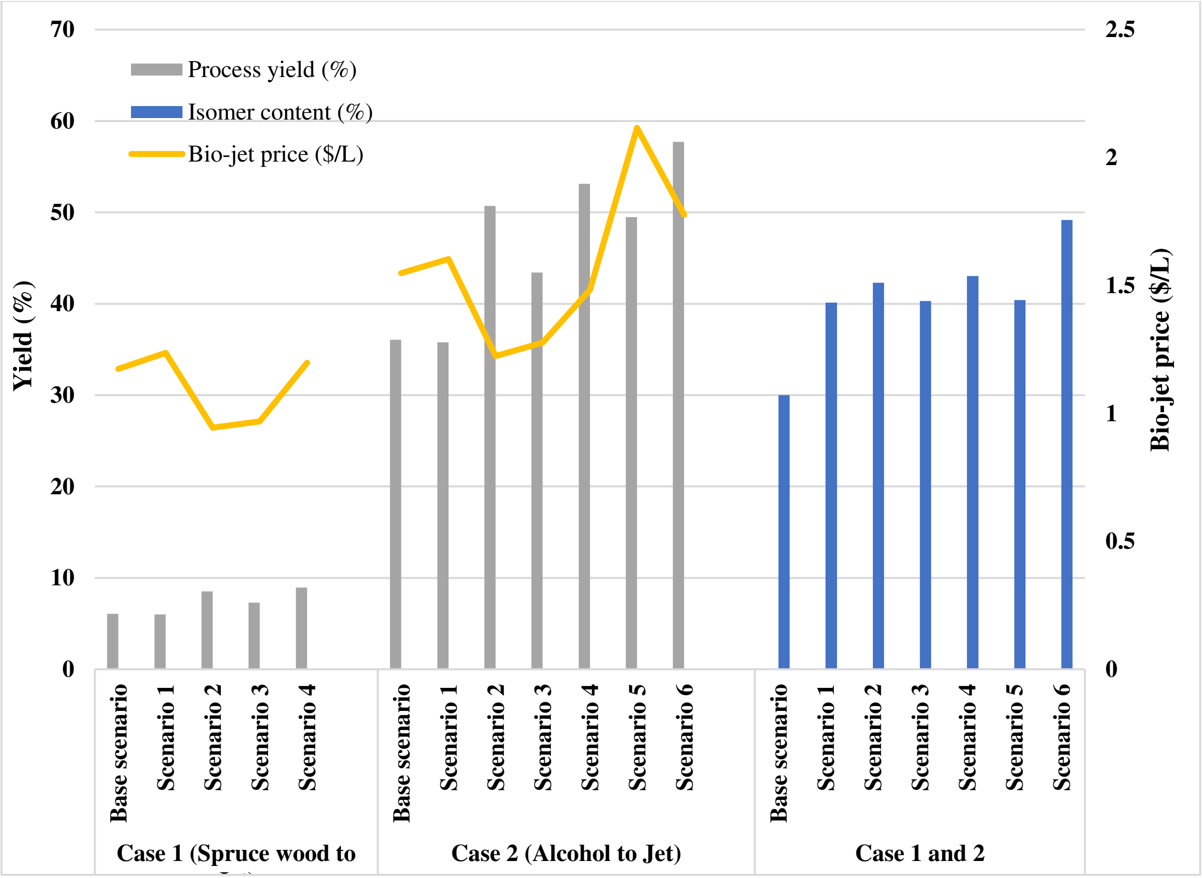

Figure 24. Comparison of production rate and bio-jet price among the scenarios

The status of global research in bio-jet fuel production from a technical viewpoint is also briefly outlined while identifying gaps that need to be filled. The gaps on which future research can be carried out include identifying more suitable feedstocks; conducting a detailed techno-economic analysis of the potential pathways; finding ways to improve the competitiveness for alternative jet fuels, ways to penetrate the air transportation sector market, ways to improve the energy intensity of the processes, and ways to meet emission reduction targets in large-scale production; conducting life cycle analysis; determining the fuel readiness level; and estimating statistics of commercial practices. This stage is necessary to develop and demonstrate an integrated approach, such as a bio-refinery based on biomass-derived intermediates to produce bio-jet.

This techno-economic assessment provides insights into the economic competitiveness of producing bio-jet from lignocellulosic feedstock via fast pyrolysis and syngas fermentation or directly from platform alcohols. Each technology presents its own set of advantages and disadvantages. Simple processes often result in lower yields; enhanced processes generally involve more complex unit operations or sophisticated catalysts, leading to higher yields. In most instances, substantial technology development is still required to achieve commercialization and ultimately attain cost competitiveness.

5.2 Recommendations for future work

Future research opportunities broadly include identifying suitable feedstocks, techno-economic analyses for unexplored pathways, developing approaches to enter the air transportation market with alternative jet fuels, improving the energy efficiency of the processes, meeting emission reduction targets in large-scale, performing life cycle analyses, and compiling statistics on commercial practices. This stage is crucial for developing and demonstrating an integrated approach, such as a bio-refinery based on biomass-derived intermediates, to produce bio-jet fuel. There are some specific recommendations given below.

- Technoeconomic model development from a single biogenic source for multiple alcohols by controlling syngas fermenter.
- From Alcohol-to-jet, the yield, process efficiency, and techno-economic feasibility can be increased with higher alcohols such as hexanol, sorbitol, etc. This could be explored in future work.
- Hydro-processing of bio-oil can also be explored.
- Future research should focus on discovering viable feedstocks and processes; assessing energy and economic efficiency, devising strategies to increase market penetration, achieving emission reduction in large-scale production, conducting LCA, and gathering data on commercial practices.

References

[1] Gutiérrez-Antonio C, Gómez-Castro F, de Lira-Flores J, Hernández S. A review on the production processes of renewable jet fuel. Renewable and Sustainable Energy Reviews. 2017; 79:709-29.

[2] Rossetti I, Compagnoni M, Finocchio E, Ramis G, Di Michele A, Millot Y, et al. Ethylene production via catalytic dehydration of diluted bioethanol: A step towards an integrated biorefinery. Applied Catalysis B: Environmental. 2017; 210:407-20.

[3] Inventory of U.S. Greenhouse Gas Emissions and Sinks. 8-17-2020 https://www.epa.gov/ghgemissions/overview-greenhouse-gases[4] Zhan N, Hu Y, Li H, Yu D, Han Y, Huang H. Lanthanum–phosphorous modified HZSM-5 catalysts in dehydration of ethanol to ethylene: A comparative analysis. Catalysis Communications. 2010; 11:633-7.

[5] Akbari M, Oyedun AO, Gemechu E, Kumar A. Comparative life cycle energy and greenhouse gas footprints of dry and wet torrefaction processes of various biomass feedstocks. Journal of Environmental Chemical Engineering. 2021; 9:105415.

[6] Climate Change: Atmospheric Carbon Dioxide, 8-17-2020
https://www.epa.gov/climate-indicators/greenhouse-gases,

[7] Hoff K. Airplane emissions. 2000. 8-17-2020
https://www.icao.int/environmental-protection/Pages/aircraft-engine-emissions.aspx

[8] Brasseur GP, Gupta M, Anderson BE, Balasubramanian S, Barrett S, Duda D, et al. Impact of aviation on climate: FAA's aviation climate change research initiative (ACCRI) phase II. Bulletin of the American Meteorological Society. 2016; 97:561-83.

[9] Dokurno M, Douglas P. Simulation of an ethylene oligomerization reactor system using ASPEN. The Canadian Journal of Chemical Engineering. 1984; 62:818-24.

[10] Liu G, Yan B, Chen G. Technical review on jet fuel production. Renewable and Sustainable Energy Reviews. 2013; 25:59-70.

[11] Preston H, Lee DS, Hooper PD. The inclusion of the aviation sector within the European Union's Emissions Trading Scheme: What are the prospects for a more sustainable aviation industry? Environmental Development. 2012; 2:48-56.

[12] Jones SB, Valkenburt C, Walton CW, Elliott DC, Holladay JE, Stevens DJ, et al. Production of gasoline and diesel from biomass via fast pyrolysis, hydrotreating and hydrocracking: a design case. Pacific Northwest National Lab (PNNL), Richland, WA (United States); 2009.

[13] Ibarra-Gonzalez P, Rong B-G. A review of the current state of biofuels production from lignocellulosic biomass using thermochemical conversion routes. Chinese Journal of Chemical Engineering. 2019; 27:1523-35.

[14] Khan S, Lup ANK, Qureshi KM, Abnisa F, Daud WMAW, Patah MFA. A review on deoxygenation of triglycerides for jet fuel range hydrocarbons. Journal of Analytical and Applied Pyrolysis. 2019; 140:1-24.

[15] Mawhood R, Gazis E, de Jong S, Hoefnagels R, Slade R. Production pathways for renewable jet fuel: a review of commercialization status and future prospects. Biofuels, Bioproducts and Biorefining. 2016; 10:462-84.

[16] Richter S, Braun-Unkhoff M, Naumann C, Riedel U. Paths to alternative fuels for aviation. CEAS Aeronautical Journal. 2018; 9:389-403.

[17] Wang M, Dewil R, Maniatis K, Wheeldon J, Tan T, Baeyens J, et al. Biomass-derived aviation fuels: Challenges and perspective. Progress in Energy and Combustion Science. 2019;74:31-49.

[18] Wang W-C, Tao L. Bio-jet fuel conversion technologies. Renewable and Sustainable Energy Reviews. 2016; 53:801-22.

[19] Why ESK, Ong HC, Lee HV, Gan YY, Chen W-H, Chong CT. Renewable aviation fuel by advanced hydroprocessing of biomass: Challenges and perspective. Energy Conversion and Management. 2019; 199:112015.

[20] Wei H, Liu W, Chen X, Yang Q, Li J, Chen H. Renewable bio-jet fuel production for aviation: A review. Fuel. 2019; 254:115599.

[21] Blakey S, Rye L, Wilson CW. Aviation gas turbine alternative fuels: A review. Proceedings of the combustion institute. 2011; 33:2863-85.

[22] Hari TK, Yaakob Z, Binitha NN. Aviation biofuel from renewable resources: Routes, opportunities and challenges. Renewable and Sustainable Energy Reviews. 2015; 42:1234-44.

[23] Fivga A, Speranza LG, Branco CM, Ouadi M, Hornung A. A review on the current state of the art for the production of advanced liquid biofuels. Aims Energy. 2019; 7:46-76.

[24] Reksowadojo IK, Duong LH, Pham DN. Review of typical biofuel for aviation alternative fuel purposes. Ng Pham. 2014; 4:20-30.

[25] Overton J. Fact Sheet: The Growth in Greenhouse Gas Emissions from Commercial Aviation. 2019, 2020-04-15

https://www.canada.ca/en/environment-climate-change/services/environmental-indicators/greenhouse-gas-emissions.html

[26] Fuel Efficiency: Everything You Need to Know.

[27] Communication from the commission to the european Parliament, the council, the european economic and social committee and the committee of the regions. 2020., 8.7.2020

https://ec.europa.eu/energy/sites/ener/files/hydrogen_strategy.pdf

[28] Patel M, Kumar A. Production of renewable diesel through the hydroprocessing of lignocellulosic biomass-derived bio-oil: A review. Renewable and Sustainable Energy Reviews. 2016; 58:1293-307.

[29] Brooks K, Snowden-Swan L, Jones S, Butcher M, Lee G-S, Anderson D, et al. Low-carbon aviation fuel through the alcohol to jet pathway. Biofuels for aviation: Elsevier; 2016. p. 109-50.

[30] Zhao X, Taheripour F, Malina R, Staples MD, Tyner WE. Estimating induced land use change emissions for sustainable aviation biofuel pathways. Science of the Total Environment. 2021; 779:146238.

[31] Naik SN, Goud VV, Rout PK, Dalai AK. Production of first and second generation biofuels: a comprehensive review. Renewable and sustainable energy reviews. 2010; 14:578-97.

[32] Li L, Coppola E, Rine J, Miller JL, Walker D. Catalytic hydrothermal conversion of triglycerides to non-ester biofuels. Energy & Fuels. 2010; 24:1305-15.

[33] Pechstein J, Neuling U, Gebauer J, Kaltschmitt M. Alcohol-to-Jet (AtJ). Biokerosene: Springer; 2018. p. 543-74.

[34] Morales M, Quintero J, Conejeros R, Aroca G. Life cycle assessment of lignocellulosic bioethanol: Environmental impacts and energy balance. Renewable and Sustainable Energy Reviews. 2015; 42:1349-61.

[35] Dassanayake GDM, Kumar A. Techno-economic assessment of triticale straw for power generation. Applied energy. 2012; 98:236-45.

[36] Giwa T, Akbari M, Kumar A. Assessment of the greenhouse gas emission footprint of a biorefinery over its life cycle. Energy Conversion and Management. 2022; 271:116327.

[37] Zhang YHP. Reviving the carbohydrate economy via multi-product lignocellulose biorefineries. Journal of Industrial Microbiology and Biotechnology. 2008; 35:367-75.

[38] Zhang YP. Reviving the carbohydrate economy via multi-product lignocellulose biorefineries. Journal of industrial microbiology and biotechnology. 2008; 35:367-75.

[39] Williams CL, Emerson RM, Hernandez S, Klinger JL, Fillerup EP, Thomas BJ. Preprocessing and hybrid biochemical/thermochemical conversion of short rotation woody coppice for biofuels. Frontiers in Energy Research. 2018; 6:74.

[40] What is the difference between slow and fast pyrolysis?, 2024-08-09
https://kindle-tech.com/faqs/what-is-the-difference-between-slow-and-fast-pyrolysis

[41] Patel M, Zhang X, Kumar A. Techno-economic and life cycle assessment on lignocellulosic biomass thermochemical conversion technologies: A review. Renewable and Sustainable Energy Reviews. 2016; 53:1486-99.

[42] Brassard P, Godbout S, Lévesque V, Palacios JH, Raghavan V, Ahmed A, et al. 4 - Biochar for soil amendment. In: Jeguirim M, Limousy L, editors. Char and Carbon Materials Derived from Biomass: Elsevier; 2019. p. 109-46.

[43] Tan X-f, Liu S-b, Liu Y-g, Gu Y-l, Zeng G-m, Hu X-j, et al. Biochar as potential sustainable precursors for activated carbon production: Multiple applications in environmental protection and energy storage. Bioresource Technology. 2017;227:359-72.

[44] Hidalgo P, Navia R, Hunter R, Coronado G, Gonzalez M. Synthesis of carbon nanotubes using biochar as precursor material under microwave irradiation. Journal of Environmental Management. 2019; 244:83-91.

[45] Akbari M, Oyedun AO, Kumar A. Techno-economic assessment of wet and dry torrefaction of biomass feedstock. Energy. 2020; 207:118287.

[46] Barrette J, Paré D, Manka F, Guindon L, Bernier P, Titus B. Forecasting the spatial distribution of logging residues across the Canadian managed forest. Canadian Journal of Forest Research. 2018; 48:1470-81.

[47] Enerkem's patented gasification technology converts waste into sustainable products.,
2023-07-12
https://enerkem.com/solution/technology

[48] Hileman JI, Ortiz DS, Bartis JT, Wong HM, Donohoo PE, Weiss MA, et al. Near-term feasibility of alternative jet fuels. Rand Corporation; 2009.

[49] Kumari D, Singh R. Pretreatment of lignocellulosic wastes for biofuel production: a critical review. Renewable and Sustainable Energy Reviews. 2018; 90:877-91.

[50] Milbrandt A, Kinchin C, McCormick R. Feasibility of Producing and Using Biomass-Based Diesel and Jet Fuel in the United States. National Renewable Energy Lab (NREL), Golden, CO (United States); 2013.

[51] Gonçalves FA, Ruiz HA, dos Santos ES, Teixeira JA, de Macedo GR. Bioethanol production from coconuts and cactus pretreated by autohydrolysis. Industrial Crops and Products. 2015; 77:1-12.

[52] Kumar M, Gayen K. Developments in biobutanol production: new insights. Applied Energy. 2011; 88:1999-2012.

[53] Bastian S, Liu X, Meyerowitz JT, Snow CD, Chen MM, Arnold FH. Engineered ketol-acid reductoisomerase and alcohol dehydrogenase enable anaerobic 2-methylpropan-1-ol production at theoretical yield in Escherichia coli. Metabolic engineering. 2011; 13:345-52.

[54] Pang Z-W, Lu W, Zhang H, Liang Z-W, Liang J-J, Du L-W, et al. Butanol production employing fed-batch fermentation by Clostridium acetobutylicum GX01 using alkali-pretreated

sugarcane bagasse hydrolysed by enzymes from Thermoascus aurantiacus QS 7-2-4. Bioresource technology. 2016; 212:82-91.

[55] Chiaramonti D, Prussi M, Buffi M, Tacconi D. Sustainable bio kerosene: Process routes and industrial demonstration activities in aviation biofuels. Applied Energy. 2014; 136:767-74.

[56] Güell BM, Bugge M, Kempegowda RS, George A, Paap SM. Benchmark of conversion and production technologies for synthetic biofuels for aviation. Norway: SINTEF Energy Research. 2012.

[57] Wollrab A. Organische chemie: Springer; 2009.

[58] Baliban RC, Elia JA, Floudas CA, Xiao X, Zhang Z, Li J, et al. Thermochemical conversion of duckweed biomass to gasoline, diesel, and jet fuel: process synthesis and global optimization. Industrial & Engineering Chemistry Research. 2013; 52:11436-50.

[59] Breitmaier E, Jung G. Organische Chemie: Grundlagen, Stoffklassen, Reaktionen, Konzepte, Molekülstrukturen; 129 Tabellen: Georg Thieme Verlag; 2005.

[60] Zhang X, Lei H, Zhu L, Wei Y, Liu Y, Yadavalli G, et al. Production of renewable jet fuel range alkanes and aromatics via integrated catalytic processes of intact biomass. Fuel. 2015; 160:375-85.

[61] Sikarwar VS, Zhao M, Fennell PS, Shah N, Anthony EJ. Progress in biofuel production from gasification. Progress in Energy and Combustion Science. 2017; 61:189-248.

[62] Ghavipour M, Behbahani RM, Moradi GR, Soleimanimehr A. Methanol dehydration over alkali-modified H-ZSM-5; effect of temperature and water dilution on products distribution. Fuel. 2013; 113:310-7.

[63] Bradin D. Process for producing renewable jet fuel compositions. Google Patents; 2018.

[64] Zhang X. Essential scientific mapping of the value chain of thermochemically converted second-generation bio-fuels. Green Chemistry. 2016; 18:5086-117.

[65] Nesterenko N, Minoux D, Van Donk S, Dath J-P. Method for distillate production by means of catalytic oligomerization of olefins in the presence of methanol and/or dimethyl ether. Google Patents; 2012.

[66] Ramasamy KK, Wang Y. Catalyst activity comparison of alcohols over zeolites. Journal of energy chemistry. 2013; 22:65-71.

[67] Kalnenieks U, Pappas KM, Bettenbrock K. Zymomonas mobilis metabolism: Novel tools and targets for its rational engineering. Advances in Microbial Physiology: Elsevier; 2020. p. 37-88.

[68] Harvey BG, Meylemans HA. The role of butanol in the development of sustainable fuel technologies. Journal of Chemical Technology & Biotechnology. 2011; 86:2-9.

[69] Tao L, Markham JN, Haq Z, Biddy MJ. Techno-economic analysis for upgrading the biomass-derived ethanol-to-jet blendstocks. Green Chemistry. 2017; 19:1082-101.

[70] Le Van Mao R, Nguyen TM, McLaughlin GP. The bioethanol-to-ethylene (BETE) process. Applied catalysis. 1989; 48:265-77.

[71] Ouyang J, Kong F, Su G, Hu Y, Song Q. Catalytic conversion of bio-ethanol to ethylene over La-modified HZSM-5 catalysts in a bioreactor. Catalysis letters. 2009; 132:64-74.

[72] Chen Y, Wu Y, Tao L, Dai B, Yang M, Chen Z, et al. Dehydration reaction of bio-ethanol to ethylene over modified SAPO catalysts. Journal of Industrial and Engineering Chemistry. 2010; 16:717-22.

[73] Gołąbek K, Tarach KA, Filek U, Góra-Marek K. Ethylene formation by dehydration of ethanol over medium pore zeolites. Spectrochimica Acta Part A: Molecular and Biomolecular Spectroscopy. 2018; 192:464-72.

[74] Zhang M, Yu Y. Dehydration of ethanol to ethylene. Industrial & Engineering Chemistry Research. 2013;52:9505-14.

[75] Noller H, Thomke K. Transition states of catalytic dehydration and dehydrogenation of alcohols. Journal of Molecular Catalysis. 1979; 6:375-92.

[76] Froment G. Fixed bed catalytic reactors' current design status. Industrial & Engineering Chemistry. 1967; 59:18-27.

[77] Froment GF, Bischoff KB, De Wilde J. Chemical reactor analysis and design: Wiley New York; 1990.

[78] Zhang W. A review of techniques for the process intensification of fluidized bed reactors. Chinese Journal of Chemical Engineering. 2009; 17:688-702.

[79] Pearson DE, Tanner RD, Picciotto ID, Sawyer JS, Cleveland Jr JH. Phosphoric acid systems. Catalytic conversion of fermentation ethanol to ethylene. Industrial & Engineering Chemistry Product Research and Development. 1981; 20:734-40.

[80] Mostafa M, Youssef A, Hassan S. Conversion of ethanol and isopropanol on alumina, titania and alumina-titania catalysts. Materials letters. 1991; 12:207-13.

[81] Zaki T. Catalytic dehydration of ethanol using transition metal oxide catalysts. Journal of colloid and Interface Science. 2005; 284:606-13.

[82] Wang Y, Li C, Gu C, SUN L, SUN B. Recent developments in heteropoly acid and their supported catalysts. Industrial Catalysis. 2007; 15:1-4.

[83] Mizuno N, Misono M. Heteropolyacid catalysts. Current opinion in solid state and materials science. 1997; 2:84-9.

[84] Xu R, Pang W, Yu J, Huo Q, Chen J. Chemistry of zeolites and related porous materials: synthesis and structure: John Wiley & Sons; 2009.

[85] LI Y, JIN Z, YANG W. Research status of dehydration of ethanol into ethylene over zeolite. Chemical Industry and Engineering Progress. 2009; 1.

[86] Argauer RJ, Landolt GR. Crystalline zeolite ZSM-5 and method of preparing the same. Google Patents; 1972.

[87] Dwyer FG, Jenkins EE. Crystalline silicates and method of preparing the same. Google Patents; 1976.

[88] Olson D, Kokotailo G, Lawton S, Meier W. Crystal structure and structure-related properties of ZSM-5. The Journal of Physical Chemistry. 1981; 85:2238-43.

[89] ZSM-5 - Zeolite Socony Mobil–5. Jul 24, 2019.

[90] Van Koningsveld H, Jansen J, Van Bekkum H. The monoclinic framework structure of zeolite H-ZSM-5. Comparison with the orthorhombic framework of as-synthesized ZSM-5. Zeolites. 1990; 10:235-42.

[91] Gayubo AG, Alonso A, Valle B, Aguayo AT, Bilbao J. Kinetic model for the transformation of bioethanol into olefins over a HZSM-5 zeolite treated with alkali. Industrial & engineering chemistry research. 2010; 49:10836-44.

[92] Narula CK, Li Z, Casbeer EM, Geiger RA, Moses-Debusk M, Keller M, et al. Heterobimetallic zeolite, InV-ZSM-5, enables efficient conversion of biomass-derived ethanol to renewable hydrocarbons. Scientific reports. 2015; 5:16039.

[93] Zhang D, Wang R, Yang X. Effect of P content on the catalytic performance of P-modified HZSM-5 catalysts in dehydration of ethanol to ethylene. Catalysis Letters. 2008; 124:384-91.

[94] Zhang X, Wang R, Yang X, Zhang F. Comparison of four catalysts in the catalytic dehydration of ethanol to ethylene. Microporous and Mesoporous Materials. 2008; 116:210-5.

[95] Phung TK, Lagazzo A, Crespo MÁR, Escribano VS, Busca G. A study of commercial transition aluminas and of their catalytic activity in the dehydration of ethanol. Journal of catalysis. 2014; 311:102-13.

[96] Jing X. Development of High Selectivity Catalysts for Preparing Ethylene from Ethanol Dehydration [J]. Chemical Reaction Engineering and Technology. 2011;1.

[97] Ezzo E, El-Shobaky G, Selim M. Catalytic conversion of alcohols on Al_2O_3-Cr_2O_3 catalysts I: The catalytic decomposition of ethanol. Surface Technology. 1980; 10:47-54.

[98] Ezzo E, Yousef N, Mazhar H. Studies of the mixed oxide catalyst Al_2O_3-Cr_2O_3 II: The catalytic conversion of ethanol. Surface Technology. 1981; 14:65-72.

[99] Riad M, Sobhi Z, Mikhail S. Catalytic dehydration reaction of ethanol over transition metal catalysts. Journal of Engineering and applied science-cairo-. 2002; 49:195-208.

[100] Doheim M, Hanafy S, El-Shobaky G. Catalytic conversion of ethanol and isopropanol over the Mn_2O_3/Al_2O_3 system doped with Na_2O. Materials letters. 2002; 55:304-11.

[101] El-Shobaky G, Doheim M, Ghozza A, El-Boohy H. Catalytic conversion of ethanol over Co_3O_4/MgO system treated with γ-irradiation. Materials letters. 2002; 57:525-31.

[102] Doheim M, El-Shobaky H. Catalytic conversion of ethanol and iso-propanol over ZnO-treated Co_3O_4/Al_2O_3 solids. Colloids and surfaces A: Physicochemical and engineering aspects. 2002; 204:169-74.

[103] El-Katatny EA, Halawy SA, Mohamed MA, Zaki MI. Recovery of ethene-selective FeO_x/Al_2O_3 ethanol dehydration catalyst from industrial chemical wastes. Applied Catalysis A: General. 2000; 199:83-92.

[104] Chen G, Li S, Jiao F, Yuan Q. Catalytic dehydration of bioethanol to ethylene over TiO_2/γ-Al_2O_3 catalysts in microchannel reactors. Catalysis Today. 2007; 125:111-9.

[105] Yu Y, Liu B. Research and production of NC1301 type catalyst for ethanol dehydration to produce ethylene. J Chem Ind Eng. 1995; 16:8-10.

[106] Li Y, Chen X-c, Sun W, Liu S, Hou W. Experimental study of the catalytic dehydration of ethanol to ethylene on a gamma-Al_2O_3 catalyst. Journal-beijing university of chemical technology natural science edition. 2007; 34:449.

[107] Phung TK, Hernández LP, Busca G. Conversion of ethanol over transition metal oxide catalysts: effect of tungsta addition on catalytic behaviour of titania and zirconia. Applied Catalysis A: General. 2015; 489:180-7.

[108] Varisli D, Dogu T, Dogu G. Ethylene and diethyl-ether production by dehydration reaction of ethanol over different hetero-polyacid catalysts. Chemical Engineering Science. 2007; 62:5349-52.

[109] Haber J, Pamin K, Matachowski L, Napruszewska B, Połtowicz J. Potassium and silver salts of tungstophosphoric acid as catalysts in dehydration of ethanol and hydration of ethylene. Journal of Catalysis. 2002; 207:296-306.

[110] Bokade VV, Yadav GD. Heteropolyacid supported on montmorillonite catalyst for dehydration of dilute bio-ethanol. Applied Clay Science. 2011; 53:263-71.

[111] Varisli D, Dogu T, Dogu G. Petrochemicals from ethanol over a W–Si-based nanocomposite bidisperse solid acid catalyst. Chemical engineering science. 2010; 65:153-9.

[112] Clemente MCH, Martins GAV, de Freitas EF, Dias JA, Dias SC. Ethylene production via catalytic ethanol dehydration by 12-tungstophosphoric acid@ ceria-zirconia. Fuel. 2019; 239:491-501.

[113] Filek U, Kirpsza A, Micek-Ilnicka A, Lalik E, Bielański A. Ethanol conversion over cesium-doped mono-and bi-cationic aluminum and gallium $H_3PW_{12}O_{40}$ salts. Journal of Molecular Catalysis A: Chemical. 2015; 407:152-62.

[114] Almohalla M, Rodríguez-Ramos I, Guerrero-Ruiz A. Comparative study of three heteropolyacids supported on carbon materials as catalysts for ethylene production from bioethanol. Catalysis Science & Technology. 2017; 7:1892-901.

[115] Hao T. Dehydration of dilute aqueous solution of ethanol into ethylene over ZSM-5 zeolite catalysts. Petrochem Technol. 1985; 14:92-3.

[116] Phillips CB, Datta R. Production of ethylene from hydrous ethanol on H-ZSM-5 under mild conditions. Industrial & engineering chemistry research. 1997; 36:4466-75.

[117] Le Van Mao R, Dao LH. Ethylene light olefins from ethanol. Google Patents; 1987.

[118] Bun S, Nishiyama S, Tsuruya S, Masai M. Ethanol conversion over ion-exchanged ZSM-5 zeolites. Applied catalysis. 1990; 59:13-29.

[119] Takahara I, Saito M, Inaba M, Murata K. Dehydration of ethanol into ethylene over solid acid catalysts. Catalysis Letters. 2005; 105:249-52.

[120] Moon S, Chae H-J, Park MB. Dehydration of Bioethanol to Ethylene over H-ZSM-5 Catalysts: A Scale-Up Study. Catalysts. 2019; 9:186.

[121] Sheng Q, Ling K, Li Z, Zhao L. Effect of steam treatment on catalytic performance of HZSM-5 catalyst for ethanol dehydration to ethylene. Fuel processing technology. 2013; 110:73-8.

[122] Bi J, Guo X, Liu M, Wang X. High effective dehydration of bio-ethanol into ethylene over nanoscale HZSM-5 zeolite catalysts. Catalysis Today. 2010; 149:143-7.

[123] de Oliveira TKR, Rosset M, Perez-Lopez OW. Ethanol dehydration to diethyl ether over Cu-Fe/ZSM-5 catalysts. Catalysis Communications. 2018; 104:32-6.

[124] Ramesh K, Hui LM, Han Y-F, Borgna A. Structure and reactivity of phosphorous modified H-ZSM-5 catalysts for ethanol dehydration. Catalysis Communications. 2009; 10:567-71.

[125] Wu C-Y, Wu H-S. Ethylene formation from ethanol dehydration using ZSM-5 catalyst. ACS omega. 2017; 2:4287-96.

[126] Li X, Rezaei F, Ludlow DK, Rownaghi AA. Synthesis of SAPO-34@ ZSM-5 and SAPO-34@ Silicalite-1 core-shell zeolite composites for ethanol dehydration. Industrial & Engineering Chemistry Research. 2018; 57:1446-53.

[127] Babu BH, Lee M, Hwang DW, Kim Y, Chae H-J. An integrated process for production of jet-fuel range olefins from ethylene using Ni-AlSBA-15 and Amberlyst-35 catalysts. Applied Catalysis A: General. 2017; 530:48-55.

[128] Jiang P, Wu X, Zhu L, Jin F, Liu J, Xia T, et al. Production of jet fuel range paraffins by low temperature polymerization of gaseous light olefins using ionic liquid. Energy Conversion and Management. 2016; 120:338-45.

[129] Shin M, Jeong H, Park M-J, Suh Y-W. Benefits of the SiO_2-supported nickel phosphide catalyst on ethylene oligomerization. Applied Catalysis A: General. 2020; 591:117376.

[130] Andrei RD, Popa MI, Fajula F, Hulea V. Heterogeneous oligomerization of ethylene over highly active and stable Ni-AlSBA-15 mesoporous catalysts. Journal of Catalysis. 2015; 323:76-84.

[131] Goetjen TA, Zhang X, Liu J, Hupp JT, Farha OK. Metal-Organic Framework supported single site chromium (III) catalyst for ethylene oligomerization at low pressure and temperature. ACS Sustainable Chemistry & Engineering. 2019; 7:2553-7.

[132] Lee M, Yoon JW, Kim Y, Yoon JS, Chae H-J, Han Y-H, et al. Ni/SIRAL-30 as a heterogeneous catalyst for ethylene oligomerization. Applied Catalysis A: General. 2018; 562:87-93.

[133] Kwon M-H, Yoon JS, Lee M, Hwang DW, Kim Y, Park MB, et al. One-pot cascade ethylene oligomerization using Ni/Siral-30 and H-ZSM-5 catalysts. Applied Catalysis A: General. 2019; 572:226-31.

[134] Jan O, Song K, Dichiara A, Resende FL. Oligomerization of supercritical ethylene over nickel-based silica-alumina catalysts. Chemical Engineering Science. 2019; 197:212-22.

[135] Panpian P, Tran TTV, Kongparakul S, Attanatho L, Thanmongkhon Y, Wang P, et al. Production of bio-jet fuel through ethylene oligomerization using NiAlKIT-6 as a highly efficient catalyst. Fuel. 2021; 287:119831.

[136] Attanatho L, Lao-ubol S, Suemanotham A, Prasongthum N, Khowattana P, Laosombut T, et al. Jet fuel range hydrocarbon synthesis through ethylene oligomerization over platelet Ni-AlSBA-15 catalyst. SN Applied Sciences. 2020; 2:1-12.

[137] Liu Y. Catalytic ethylene oligomerization over Ni/Al-HMS: A key step in conversion of bio-ethanol to higher olefins. Catalysts. 2018; 8:537.

[138] Yoon JS, Park MB, Kim Y, Hwang DW, Chae H-J. Effect of Metal Oxide–Support Interactions on Ethylene Oligomerization over Nickel Oxide/Silica–Alumina Catalysts. Catalysts. 2019; 9:933.

[139] Chen L, Li G, Wang Z, Li S, Zhang M, Li X. Ethylene Oligomerization over Nickel Supported Silica-Alumina Catalysts with High Selectivity for C_{10+} Products. Catalysts. 2020; 10:180.

[140] Harvey BG, Meylemans HA. 1-Hexene: a renewable C_6 platform for full-performance jet and diesel fuels. Green Chemistry. 2014; 16:770-6.

[141] Goto D, Harada Y, Furumoto Y, Takahashi A, Fujitani T, Oumi Y, et al. Conversion of ethanol to propylene over HZSM-5 type zeolites containing alkaline earth metals. Applied Catalysis A: General. 2010; 383:89-95.

[142] Inoue K, Inaba M, Takahara I, Murata K. Conversion of ethanol to propylene by H-ZSM-5 with Si/Al 2 ratio of 280. Catalysis letters. 2010; 136:14-9.

[143] Iwamoto M. One-step formation of propene from ethene or ethanol through metathesis on nickel ion-loaded silica. Molecules. 2011; 16:7844-63.

[144] Gabriëls D, Hernández WY, Sels B, Van Der Voort P, Verberckmoes A. Review of catalytic systems and thermodynamics for the Guerbet condensation reaction and challenges for biomass valorization. Catalysis Science & Technology. 2015; 5:3876-902.

[145] Dowson GR, Haddow MF, Lee J, Wingad RL, Wass DF. Catalytic conversion of ethanol into an advanced biofuel: unprecedented selectivity for n-butanol. Angewandte Chemie International Edition. 2013; 52:9005-8.

[146] Strömberg N, Loren A, Lind L, Bioproducts P. An inventory and comparison of swedish biobutanol projects relative global biobutanol production, research and development.

[147] Kozlowski JT, Davis RJ. Heterogeneous catalysts for the guerbet coupling of alcohols. Acs Catalysis. 2013; 3:1588-600.

[148] Scalbert J, Thibault-Starzyk F, Jacquot R, Morvan D, Meunier F. Ethanol condensation to butanol at high temperatures over a basic heterogeneous catalyst: How relevant is acetaldehyde self-aldolization? Journal of catalysis. 2014; 311:28-32.

[149] Pospech J, Fleischer I, Franke R, Buchholz S, Beller M. Alternative metals for homogeneous catalyzed hydroformylation reactions. Angewandte Chemie International Edition. 2013; 52:2852-72.

[150] Hulea V, Fajula F. Ni-exchanged AlMCM-41-An efficient bifunctional catalyst for ethylene oligomerization. Journal of Catalysis. 2004; 225:213-22.

[151] Mahdaviani SH, Soudbar D, Parvari M. Selective ethylene dimerization toward 1-butene by a new highly efficient catalyst system and determination of its optimum operating conditions in a buchi reactor. International Journal of Chemical Engineering and Applications. 2010; 1:276.

[152] Chang CD, Rodewald PG. Propylene oligomerization over silica-modified zeolites. Google Patents; 1991.

[153] Yi-Nong L. Investigation of Propene Oligomerization Catalyzed by Phosphootungstic Acid Catalysts. China Petroleum Processing & Petrochemical Technology. 2012; 14:10.

[154] Geleynse S, Brandt K, Garcia-Perez M, Wolcott M, Zhang X. The Alcohol-to-Jet Conversion Pathway for Drop-In Biofuels: Techno-Economic Evaluation. Chem Sus Chem. 2018; 11:3728-41.

[155] Busto M, Lovato ME, Vera CR, Shimizu K, Grau JM. Silica-supported tungsta-zirconia catalysts for hydroisomerization–cracking of long alkanes. Applied Catalysis A: General. 2009; 355:123-31.

[156] Akbari M, Oyedun AO, Jain S, Kumar A. Options for the conversion of pulp and paper mill by-products in Western Canada. Sustainable Energy Technologies and Assessments. 2018; 26:83-92.

[157] Pham V, Holtzapple M, El-Halwagi M. Techno-economic analysis of biomass to fuel conversion via the MixAlco process. Journal of Industrial Microbiology and Biotechnology. 2010; 37:1157-68.

[158] Atsonios K, Kougioumtzis M-A, Panopoulos KD, Kakaras E. Alternative thermochemical routes for aviation biofuels via alcohols synthesis: process modeling, techno-economic assessment and comparison. Applied Energy. 2015; 138:346-66.

[159] Taylor JD, Jenni MM, Peters MW. Dehydration of fermented isobutanol for the production of renewable chemicals and fuels. Topics in Catalysis. 2010; 53:1224-30.

[160] Makarova M, Williams C, Thomas J, Zamaraev K. Dehydration of n-butanol on HNa-ZSM-5. Catalysis letters. 1990; 4:261-3.

[161] Lee IC, St Clair JG, Gamson AS. Catalytic Oxidative Dehydration of Butanol Isomers: 1-Butanol, 2-Butanol, and Isobutanol. Army research lab adelphi md sensors and electron devices directorate; 2011.

[162] Lu M, Xiong G, Zhao H, Cui W, Gu J, Bauser H. Dehydration of 1-butanol over γ-$A1_2O_3$ catalytic membrane. Catalysis today. 1995; 25:339-44.

[163] Jeong S, Kim H, Bae J-h, Kim DH, Peden CH, Park Y-K, et al. Synthesis of butenes through 2-butanol dehydration over mesoporous materials produced from ferrierite. Catalysis today. 2012; 185:191-7.

[164] Wright ME, Harvey BG, Quintana RL. Highly efficient zirconium-catalyzed batch conversion of 1-butene: a new route to jet fuels. Energy & fuels. 2008; 22:3299-302.

[165] Harvey BG, Quintana RL. Synthesis of renewable jet and diesel fuels from 2-ethyl-1-hexene. Energy & Environmental Science. 2010; 3:352-7.

[166] Wright ME, Harvey BG, Quintana RL. Diesel and jet fuels based on the oligomerization of butene. Google Patents; 2013.

[167] Bond JQ, Alonso DM, Wang D, West RM, Dumesic JA. Integrated catalytic conversion of γ-valerolactone to liquid alkenes for transportation fuels. Science. 2010; 327:1110-4.

[168] Gruber PR, Peters MW, Griffith JM, Al Obaidi Y, Manzer LE, Taylor JD, et al. Renewable compositions. Google Patents; 2012.

[169] Park DH, Kim S-S, Pinnavaia TJ, Tzompantzi F, Prince J, Valente JS. Selective isobutene oligomerization by mesoporous MSU-SBEA catalysts. The Journal of Physical Chemistry C. 2011; 115:5809-16.

[170] Coelho A, Caeiro G, Lemos M, Lemos F, Ribeiro FR. 1-Butene oligomerization over ZSM-5 zeolite: Part 1–Effect of reaction conditions. Fuel. 2013; 111:449-60.

[171] Lavrenov A, Duplyakin V. Oligomerization of butenes on borate-containing alumina. Kinetics and Catalysis. 2009; 50:235-40.

[172] Yoon JW, Chang J-S, Lee H-D, Kim T-J, Jhung SH. Trimerization of isobutene over cation exchange resins: Effect of physical properties of the resins and reaction conditions. Journal of Molecular Catalysis A: Chemical. 2006; 260:181-6.

[173] Sakuneka TM, de Klerk A, Nel RJ, Pienaar AD. Synthetic jet fuel production by combined propene oligomerization and aromatic alkylation over solid phosphoric acid. Industrial & engineering chemistry research. 2008; 47:1828-34.

[174] Li Z, Pan L, Nie G, Xie J, Xie J, Zhang X, et al. Synthesis of high-performance jet fuel blends from biomass-derived 4-ethylphenol and phenylmethanol. Chemical Engineering Science. 2018; 191:343-9.

[175] Wang T, Qiu S, Weng Y, Chen L, Liu Q, Long J, et al. Liquid fuel production by aqueous phase catalytic transformation of biomass for aviation. Applied Energy. 2015; 160:329-35.

[176] Gabriel CB, Canhaci SJ, Borges LE, Fraga MA. Aviation biofuel range cycloalkane from renewables: Liquid-phase catalytic conversion of menthol on niobium-supported catalysts. Fuel. 2020; 277:118288.

[177] Sheng X, Li N, Li G, Wang W, Yang J, Cong Y, et al. Synthesis of high-density aviation fuel with cyclopentanol derived from lignocellulose. Scientific reports. 2015; 5:1-4.

[178] Chen F, Li N, Li S, Li G, Wang A, Cong Y, et al. Synthesis of jet fuel range cycloalkanes with diacetone alcohol from lignocellulose. Green Chemistry. 2016; 18:5751-5.

[179] Zhang H, Fang Y, Wang M, Appels L, Deng Y. Prospects and perspectives foster enhanced research on bio-aviation fuels. Journal of Environmental Management. 2020; 274:111214.

[180] EU, Levels GTR. Horizon 2020—Work Programme 2014–2015: General Annexes. European Commission Brussels, Belgium; 2014.

[181] Technology readiness levels., 2023-07-09

https://www.beyonddiscovery.org/reactor-design/vessel-design-and-aspect-ratio.html

[182] IATA I. International Air Transport Association. Annual Review. 2017;2017., https://www.faa.gov/regulations_policies/policy_guidance/envir_policy/media/contrails.pdf

[183] Jenkins R, Sutton A, Robichaud D. Pyrolysis of Biomass for Aviation Fuel. Biofuels for Aviation: Elsevier; 2016. p. 191-215.

[184] Sinha A, Anand M, Farooqui S. Aviation Biofuels Through Lipid Hydroprocessing. Biofuels for Aviation: Elsevier; 2016. p. 85-108.

[185] Landau MV, Hos T, Vidruk Nehemya R, Nomikos G, Herskowitz M. Eco-friendly and sustainable process for converting hydrous bioethanol to butanol. Catalysts. 2021; 11:498.

[186] Patel M, Oyedun AO, Kumar A, Gupta R. A techno-economic assessment of renewable diesel and gasoline production from aspen hardwood. Waste and Biomass Valorization. 2019; 10:2745-60.

[187] de Medeiros EM, Posada JA, Noorman H, Osseweijer P, Maciel Filho R. Hydrous bioethanol production from sugarcane bagasse via energy self-sufficient gasification-fermentation hybrid route: simulation and financial analysis. Journal of cleaner production. 2017; 168:1625-35.

[188] Canadian Ethanol Plants. 2023-07-09.
https://ethanolproducer.com/plants/listplants/Canada/Operational/All

[189] Azeotrope., 2024-08-09
https://www.newworldencyclopedia.org/entry/Azeotrope

[190] Pearson DE. Process for catalytic dehydration of ethanol vapor to ethylene. Google Patents; 1983.

[191] Giwa T. Techno-economic assessment of an integrated biorefinery producing bio-oil, 1 ethanol, and hydrogen.

[192] Hu Y, Zhan N, Dou C, Huang H, Han Y, Yu D, et al. Selective dehydration of bio-ethanol to ethylene catalyzed by lanthanum-phosphorous-modified HZSM-5: Influence of the fusel. Wiley Online Library; 2010.

[193] Dokurno M, Douglas P. Simulation of an ethylene oligomerization reactor system using aspen. Canadian journal of chemical engineering. 1983; 62:818-24.

[194] Al-Jarallah A, Anabtawi J, Siddiqui M, Aitani A, Al-Sa'doun A. Ethylene dimerization and oligomerization to butene-1 and linear α-olefins: A review of catalytic systems and processes. Catalysis today. 1992; 14:1-121.

[195] Jaroszewska K, Masalska A, Grzechowiak JR. Hydroisomerization of long-chain bio-derived n-alkanes into monobranched high cetane isomers via a dual-component catalyst bed. Fuel. 2020; 268:117239.

[196] Kang Y, Rao X, Yuan P, Wang C, Wang T, Yue Y. Al-functionalized mesoporous SBA-15 with enhanced acidity for hydroisomerization of n-octane. Fuel Processing Technology. 2021; 215:106765.

[197] Banu A-M, Friedrich D, Brandani S, Düren T. A multiscale study of MOFs as adsorbents in H2 PSA purification. Industrial & Engineering Chemistry Research. 2013; 52:9946-57.

[198] Zhang X, Zhong J, Wang J, Zhang L, Gao J, Liu A. Catalytic performance and characterization of Ni-doped HZSM-5 catalysts for selective trimerization of n-butene. Fuel processing technology. 2009; 90:863-70.

[199] Nie C, Huang L, Zhao D, Li Q. Performance of Pt/Al-SBA-15 catalysts in hydroisomerization of n-dodecane. Catalysis letters. 2001; 71:117-25.

[200] Miller P, Kumar A. Techno-economic assessment of hydrogenation-derived renewable diesel production from canola and camelina. Sustainable Energy Technologies and Assessments. 2014; 6:105-15.

[201] Gunaseelan VN. Anaerobic digestion of biomass for methane production: a review. Biomass and bioenergy. 1997; 13:83-114.

[202] Shahrukh H, Oyedun AO, Kumar A, Ghiasi B, Kumar L, Sokhansanj S. Techno-economic assessment of pellets produced from steam pretreated biomass feedstock. Biomass and Bioenergy. 2016; 87:131-43.

[203] Kumar A, Cameron JB, Flynn PC. Biomass power cost and optimum plant size in western Canada. Biomass and Bioenergy. 2003; 24:445-64.

[204] Sultana A, Kumar A, Harfield D. Development of agri-pellet production cost and optimum size. Bioresource technology. 2010; 101:5609-21.

[205] Peters MS, Timmerhaus KD. Plant design and economics for chemical engineers: McGraw-Hill International; 2018.

[206] Vessel Design And Aspect Ratio. 2023-07-09. https://www.beyonddiscovery.org/reactor-design/vessel-design-and-aspect-ratio.html

[207] Mohajerani S, Kumar A, Oni AO. A techno-economic assessment of gas-to-liquid and coal-to-liquid plants through the development of scale factors. Energy. 2018; 150:681-93.

[208] Tribe M, Alpine R. Scale economies and the "0.6 rule". Engineering Costs and Production Economics. 1986; 10:271-8.

[209] Patel M, Oyedun AO, Kumar A, Gupta R. What is the production cost of renewable diesel from woody biomass and agricultural residue based on experimentation? A comparative assessment. Fuel Processing Technology. 2019; 191:79-92.

[210] Hong Y, Cui H, Dai J, Ge Q. Estimating the Cost of Biofuel Use to Mitigate International Air Transport Emissions: A Case Study in Palau and Seychelles. Sustainability. 2019; 11:3545.

[211] Larson ED, Jin H, Celik FE. Gasification-based fuels and electricity production from biomass, without and with carbon capture and storage. Princeton Environmental Institute, Princeton University. 2005.

[212] Aspen Plus®: Jump start: getting started with Aspen Plus® V10,
Accessed Sept 2020

[213] Aspentech: Aspen process economic analyzer.
https ://www.aspen tech.com/Compa ny/About -Aspen Tech/ (2014). Accessed Sept 2020

Appendices

Appendix A

Table 1. Process conditions to validate the simulation of the base case scenario and scenarios 1 and 2

Processes / Conditions	Dehydration	Oligomerization		Hydrotreating	Hydroisomerization
	- Catalyst - Density of catalyst - WHSV - Temperature & pressure - Catalyst lifetime - Catalyst cost - Reactor	- Catalyst - Density of catalyst - WHSV - Temperature & pressure - Catalyst lifetime - Catalyst cost - Reactor		- Catalyst - Density of catalyst - WHSV - Temperature & pressure - Catalyst lifetime - Catalyst cost - Reactor	- Catalyst -Density of catalyst - WHSV - Temperature & pressure - Catalyst lifetime - Catalyst cost - Reactor
Base scenario (Direct ethanol oligomerization)	- 0.5% LaHZSM-5 - 897.03 kgm^{-3} [69] - 2 h^{-1} - 240 °C, 1 atm - 3 years [69] - $145.51/kg [69] - Fixed-bed reactor, simulated with RStoic reactor (aspect ratio 3)	- Triethylaluminum (Ziegler catalyst) - 832.96 kgm^{-3} [69] - 1.9 h^{-1} - 250 °C, 100 bar - 1 year [69] - $24.25/kg [69] - Tubular reactor, simulated with RYield reactor (aspect ratio 3)		- Cobalt molybdenum (CoMo) - 3155.64 kgm-3 [69] - 3 h-1 - 340 °C, 6 MPa - 3 years [69] - $41.88/kg [69] - Fixed-bed reactor, simulated with RStoic reactor (aspect ratio 3)	- Pt/AlSBA-15 - 550 kgm^{-3} [115] - 1.5 h^{-1} - 340 °C, 5 MPa - 3 years (approximately) [69] - $60/kg [115] - Fixed-bed microreactor, simulated with RStoic reactor (aspect ratio 3)
Scenario 1 (Ethanol to butene oligomerization)		**Step 1** - Triethylaluminum (Ziegler Catalyst) - 832.96 kgm^{-3} [69] - 1.9 h^{-1} - 55 °C, 30 bar - 1 year [69] - $24.25/year [69] - Tubular reactor, simulated with RYield reactor (aspect ratio 3)	**Step 2** - Zirconium-based methyl aluminoxane (Cp_2ZrCl_2/MAO) - 6730 kgm^{-3} [115] - 2 h^{-1} - 25 °C, 1 atm - 4 years (approximately) [69] - $3800/kg (approximately) [70] - Stainless steel Parr reactor, simulated with RYield reactor (aspect ratio 3)		
Scenario 2 (Ethanol to hexene oligomerization)		**Step 1** - Chromium salt with triethyl aluminum (TEA) and ethyl aluminum dichloride (EADC) - 6730 kgm^{-3} [115] - 1.9 h^{-1} - 100 °C, 40 bar - 4 years (approximately) [69] - $3800/kg [70] - simulated with RYield reactor (aspect ratio 3)			

Table 2. Process conditions to validate the simulation for scenarios 3-6

Processes / **Conditions**	**Condensation**	**Dehydration**	**Oligomerization**	**Hydrotreating**	**Hydroisomerization**
	- Catalyst - Density of catalyst - WHSV - Temperature & pressure - Catalyst lifetime - Catalyst cost - Reactor	- Catalyst - Density of catalyst - WHSV - Temperature & pressure - Catalyst lifetime - Catalyst cost - Reactor	- Catalyst - Density of catalyst - WHSV - Temperature & pressure - Catalyst lifetime - Catalyst cost - Reactor	- Catalyst - Density of catalyst - WHSV - Temperature & pressure - Catalyst lifetime - Catalyst cost - Reactor	- Catalyst - Density of catalyst - WHSV - Temperature & pressure - Catalyst lifetime - Catalyst cost - Reactor
Scenario 3 (Guerbet condensation; n-butanol to jet)	C-HAP - 3076 kgm^{-3} [70] - 1 h^{-1} - 400 °C, 1 atm - 1 year [185] - $13/kg [70] - Fixed-bed reactor, simulated with RStoic reactor (aspect ratio 3)	For n-butanol – γ-Al$_2$O$_3$ - 780 kgm^{-3} [90] - 2 h-1 - 300 °C, 1 atm - 3 years approximately - $35/kg [70] - Membrane reactor, simulated with RStoic reactor (aspect ratio 3)	For n-butene, Zirconium-based methyl aluminoxane (Cp$_2$ZrCl$_2$/MAO) - 6730 kgm^{-3} [115] - 2 h^{-1} - 25 °C, 1 atm - 4 years (approximately) [69] - $3800/kg [70] - Stainless steel Parr reactor, simulated with RYield reactor (aspect ratio 3)	- Cobalt molybdenum (CoMo) - 3155.64 kgm^{-3} [69] - 3 h^{-1} - 340 °C, 6 MPa - 3 years [69] - $41.88/kg [69] - Fixed-bed reactor, simulated with RStoic reactor (aspect ratio 3)	- Pt/AlSBA-15 - 550 kgm^{-3} [115] - 1.5 h^{-1} - 340 °C, 5 MPa - 3 years (approximately) [69] - $60/kg [115] - Fixed-bed microreactor, simulated with RStoic reactor (aspect ratio 3)
Scenario 5 (n-butanol to jet)	n/a				
Scenario 4 (Guerbet condensation; n-butanol and isobutanol to jet)	C-HAP - 3076 kgm^{-3} [70] - 1 h^{-1} - 400 °C, 1 atm - 1 year [185] - $13/kg [70] - Fixed-bed reactor, simulated with RStoic reactor (aspect ratio 3)	For isobutanol - γ-Al$_2$O$_3$ - 780 kgm^{-3} [90] - 1 h^{-1} - 325 °C, 1 atm - 3 years (approximately) - $35/kg - Fixed-bed reactor, simulated with RStoic reactor (aspect ratio 3)	For iso-butene, Amberlyst-35 - 1200 kgm^{-3} [70] - 2 h^{-1} - 100 °C, 250 psig - 1 year (approximately) - $50/kg - Fixed-bed reactor, simulated with RYield reactor (aspect ratio 3)		n/a
Scenario 6 (n-butanol and isobutanol to jet)	n/a				

Aspect ratio, $\frac{L}{D}$ = 3; The aspect ratio (AR) is the ratio between the distance along the sidewall (vessel's tangent to tangent length) and its diameter, crucial for determining the vessel's agitation requirements. Typically, it ranges from 1.2 to 5.

Appendix B

Table 3. The alkanes used in the simulation of the process scenarios

n-alkanes					
Alkanes	**Name**	**Formula**	**Alkanes**	**Name**	**Formula**
nC_4	n-butane	C_4H_{10}	nC_{14}	n-tetradecane	$C_{14}H_{32}$
nC_6	n-hexane	C_6H_{14}	nC_{16}	n-hexadecane	$C_{16}H_{34}$
nC_8	n-octane	C_8H_{18}	nC_{18}	n-octadecane	$C_{18}H_{38}$
nC_{10}	n-decane	$C_{10}H_{22}$	nC_{20}	n-eicosane	$C_{20}H_{42}$
nc_{12}	n-dodecane	$C_{12}H_{26}$			

Table 4. The iso-alkanes used in the simulation of the process scenarios

Iso-alkanes					
Alkanes	**Formula**	**Name**	**Alkanes**	**Formula**	**Name**
iC_8	C_8H_{18}	2-methylheptane	iC_{16}	$C_{16}H_{34}$	3-ethyltetradecane
		2,2-dimethylhexane			2-methylpentadecane
		2,2,4-trimethylpentane			Tetra-decane,2,3-dimethyl
ic_{12}	$C_{12}H_{26}$	2,3-dimethyldecane			2,6,11-trimethyltridecane
		5-methylundecane			2-methylpentadecane

Equations involved in production

$$\text{Process yield \%} = \frac{\text{Jet range alkanes produced}}{\text{Amount of fresh feed}}$$

$$\text{Final recovery of jet \%} = \frac{\text{Jet range alkanes recovered after the final fractionation stage}}{\text{Amount of ethanol feed}}$$

$$\text{Isomer content \%} = \frac{\text{Jet range alkane isomers recovered after the fractionation stage}}{\text{Jet range alkanes produced}}$$

Scale factor, $C_r = C_b \left(\frac{c_r}{c_b}\right)^f$, where C_r is the required capacity, C_b is the base capacity, c_b is the cost of the base case capacity, c_r is the cost of the necessary size, and f is the scale factor [211].